FOG

Freiberg Online Geology

FOG is an electronic journal registered under **ISSN 1434-7512**

2009, VOL 23

Daniel Steinbrückner

Quantification of submarine degassing of Panarea Volcano in the Aeolian archipelago, Italy

113 pages, 32 figures, 21 tables, 68 references

Diploma thesis

Quantification of submarine degassing of Panarea Volcano in the Aeolian archipelago, Italy

Daniel Steinbrückner

Technische Universität Bergakademie Freiberg
Faculty of Geosciences, Geo-Engineering and Mining
Department of Geology
Chair for Hydrogeology

Supervisors: Prof. Dr. Broder Merkel (TUBA Freiberg)
Dipl.-Geoökol. Mandy Schipek (TUBA Freiberg)
Dr. Francesco Italiano (INGV Palermo)

Freiberg, 30.06.2009

Statutory declaration

I hereby assure that I wrote this actual scientific work without the inadmissible help of others and without the use of aids other than the ones declared. Thoughts directly and indirectly taken from sources are indicated as such.

.....

Freiberg, 30.06.2009 Daniel Steinbrückner

Acknowledgement

First of all, I thank my supervisors for the preparation of this theme, for their support on scientific work during and after the dives as well as for their helpful tips. I also thank all of the members of the Scientific Diving Group for realising the campaigns and supporting for my work in the field as well as afterwards in Freiberg.

For my stay in Italy I thank Dr. Francesco Italiano and his colleagues of the INGV who gave me very interesting insights into the geochemical analysis of volcanic gas and water samples. Thank you for the great residence in Palermo and the unforgettable trip to Mt. Etna.

Furthermore, I want to thank Dr. N.-A. Kummer and Dipl.-Chem. H.-J. Peter for their help for the gas and water analysis as well as for the answers to my questions. I thank Dipl.-Ing. (FH) Sabine Starke for the GC analysis, although I can't use the results.

I also thank Johannes Kleutges for providing me the results of his gas flow measurements and for detailed information I ask several times.

Further thanks to Maike Hamel and Robert Sieland for the joint work in Italy as well as in Freiberg. A special thank to Robert for the numerous constructive discussions and for the help to finish this thesis successfully.

I further want to thank Sebastian Kloss for his tips to improve the text.

Finally, I thank my parents and grandparents for their support both financially and mental.

Index of contents

Index of figures

Index of tables

Abbreviations

a.s.l.	above sea level
b.s.l	below sea level
CA	Calc-alkaline
DIVA	Data-Interpolating Variational analysis
EC	Electrical conductivity
e.g.	exempli gratia (for example)
FID	Flame ionisation detector
FSVG	Flowmeter for Submarine Volcanic Gas emission
GC	Gas chromatography
GPS	Global Positioning System
HKCA	High-potassium calc-alkaline
IC	Ion chromatography
ICP-MS	Inductive coupled plasma mass spectrometer
i.e.	id est (that is)
INGV	Istituto Nazionale di Geofisica e Vulcanologia
IR	infrared
M	Magnitude
ODV	Ocean Data Viewer
OI	Optimal Interpolation
PDB	*Belemnitella americana* from the Cretaceous Peedee formation
PE	Polyethylene
PTFE	Polytetrafluorethylene (Teflon)
PVF	Polyvinyl fluoride
SATP	Standard ambient temperature and pressure
SSW	Standard seawater
std	standard deviation
STP	Standard temperature and pressure
TDS	Total dissolved solids
TIC	Total inorganic carbon
TISAB	Total ionic strength adjustment buffer
TUBA Freiberg	TU Bergakademie Freiberg
UV	ultraviolet

VCDT	Canyon Diablo Triolith
VIM	Variational Inverse Method
WISTAU	Scientific Diving Group, TU Bergakademie Freiberg

Abstract

The submarine hydrothermal system to the east of Panarea Island (Aeolian Islands, Italy) was investigated with regard to the geochemistry and rate of emission of the gases discharging on the seafloor. During two campaigns in May and September 2008 the sampling of fluids and measurements on the seafloor were carried out by scuba diving at 6 different sites within a shallow marine fumarolic field, in depths between 8 and 30 m. The gases were analysed for CO_2, H_2S, CO, CH_4, light alkanes and elemental composition, thermal waters for on-line parameters, TIC, S-species and halogens (Cl-, F- and Br-). For evaluation of the gas composition and its responsible processes external data were used, too. The quantification of submarine degassing was carried out by both measurements and estimations of gas flow rates.

The CO_2-rich gases are encountered partial dissolution as well as mixing with atmospheric compounds saturated in seawater during their migration towards the seafloor. An input of deep magmatic gases is provided by isotopic ratios. Distinctive physico-chemical parameters of the Black Point fluid discharges in comparison to the other sites may reveal a contribution of acid magmatic gases. The dissolution of discharged gases in seawater causes a decrease of pH and increase of TIC in vicinity of the emission points.

The total gas output of the investigation area is $2.3 * 10^7$ L/day, which is 2 to 3 orders of magnitude lower than the degassing rate at the submarine gas eruption occurred in November 2002. But, the system seems to have achieved again a state of constant degassing, although a new submarine gas eruption in the future can not be excluded.

The determined gas output equals the emission of 52.7 t CO_2 per day which is marginal compared to subaerial volcanoes like Mt. Etna. Again, the global CO_2 emission by subaerial volcanoes is trivial against the anthropogenic CO_2 release.

1. Introduction and objectives

1.1 Fundamentals and state of research

1.1.1 Geothermal/hydrothermal systems

Geothermal systems are found throughout the world in a range of geological settings. These different types have a heat source at few kilometres depth in common which sets water in the upper Earth's crust into convection. High-temperature geothermal reservoirs are typical settings around plate margins such as subduction zones, spreading ridges, and rift zones and within orogenic belts. They are often volcanogenic with heat provided by intrusive masses of magma that drive the geothermal convection system (Nicholson, 1993, Herzig and Hannington, 2006).
Traditionally, the research of hydrothermal systems has been divided into deep-sea hydrothermal systems (mid-ocean ridges) and sub-aerial hydrothermal or geothermal systems. Only recently a third type of hydrothermal system found in marine shallow water near-shore environments or on the tops of seamounts has been receiving consideration (Pichler, 2005).

The major source for the composition of the formed hydrothermal fluids are water-rock reactions (Nicholson, 1993). Phase separation and subsequent mixing of the brines with more dilute hydrothermal fluids during the ascent to the seafloor, the interactions with sediments in the upflow as well as the contribution of a degassing magma may dramatically modify the initial fluid chemistry (Herzig and Hannington, 2006).
In the case of mid-ocean ridges (MOR) seawater penetrates deeply into the crust along cracks and fissures, then, is heated and in a reaction zone situated close to the top of the subaxial magma chamber (Herzig and Hannington, 2006). It reacts with basalts and is converted into a highly corrosive and metal-bearing hydrothermal fluid. The major physical and chemical changes to seawater include increasing temperature, decreasing pH, and decreasing redox potential (Eh) as well as the typical enrichment in elements such as chloride (Cl), lithium (Li), potassium (K), calcium (Ca), manganese (Mn), iron (Fe) etc., and the depletion in magnesium (Mg) and sulphate (SO_4) (Herzig and Hannington, 2006, Nicholson, 1993).
Due to its buoyancy at high temperatures, the hydrothermal fluid rises to the seafloor. Mostly during the ascent, when the hydrothermal fluid intersect the two-phase curve of seawater, it undergoes boiling, a process that separates a low-salinity, vapour-rich phase from the liquid phase. Phase separation is one of the most important processes controlling chemistry of liquid

and vapour hydrothermal discharges (Herzig and Hannington, 2006, Nicholson, 1993). At temperatures and pressures higher than the critical point of seawater (407 °C and 298 bars), supercritical phase separation involves the condensation of a small amount of high salinity brine, which may accumulates to a metal-rich brine (Herzig and Hannington, 2006).
At the seafloor the hydrothermal fluids discharge along geological faults, particularly where these intersect (Dando et al., 1999, Herzig and Hannington, 2006, Italiano and Nuccio, 1991). The vapours may migrate to the seafloor independently of the liquid phase and mainly discharge as fumaroles (Nicholson, 1993). Gases such as carbon dioxide (CO_2), hydrogen sulphide (H_2S), nitrogen (N_2), hydrogen (H_2), methane (CH_4), carbon monoxide (CO) as well as steam (H_2O) are typical components in hydrothermal vapour discharges.
The flux of volatiles in volcanic arc and back-arc hydrothermal systems release is likely much greater than that of mid-ocean ridges, because of both degassing of the subducted slab and the mantle (Dando et al., 1999, Herzig and Hannington, 2006). Additionally, the direct contribution of magmatic gases, such as carbon dioxide (CO_2), sulphur dioxide (SO_2) and hydrogen chloride (HCl), to the hydrothermal systems can result in highly acidic hydrothermal fluids with pH < 2 (Gamo et al., 2006, Herzig and Hannington, 2006).

Hydrothermalism in the Mediterranean Sea results from the collision of the African and European plates, with the subduction of the oceanic part of the African plate below Europe. High heat flows in the resulting volcanic arcs and back-arc extensional areas have set up hydrothermal convection systems (Dando et al., 1999). Most of the known submarine hydrothermal venting in the Mediterranean is from shallow water (< 200 m depth) (Dando et al., 1999).

1.1.2 The hydrothermal system of Panarea

Submarine hydrothermal exhalations, both shallow and deep, occur off the coasts of all the Aeolian Islands, Italy (Gugliandolo et al., 2006, Italiano and Nuccio, 1991). Thereby, the hydrothermal system located to the east of Panarea Island showed the most active submarine emissions at shallow depths (Gugliandolo et al., 2006). Although, the Panarea hydrothermal system has been known since the Roman age detailed scientific investigations of the discharging fluids at sea bottom were firstly carried out in the mid 1980s by Italiano and Nuccio (1991).

This study was focused on the fumarolic area of La Calcara on the island of Panarea, but mainly on the submarine hydrothermal manifestation east of the coast. The authors identified 23 fields of submarine gas and thermal water discharges in a 4 km^2 wide area along the main regional tectonic alignments (NE-SW, NW-SE and N-S). The gas exhalations, with an evaluated total gas output of 9 * 10^6 litres per day, were dominated by CO_2 (> 92 vol.%) and H_2S (0 – 6.5 vol.%), with relatively low amounts of atmospheric species, CH_4, H_2 and traces of CO (Italiano and Nuccio, 1991).

Based on the chemical and isotopic composition of the gas and water discharges as well as gaseous and liquid phase geothermometry Italiano and Nuccio (1991) created a semi-quantitative stratified model for the geothermal system of Panarea (Fig. 1). It was hypothesised that magmatic fluids have been intruded in recent times, probably derived from a cooling magma body, are the thermal source for the system. The deep geothermal reservoir at temperatures more than 270 °C is feeding a relative large main geothermal body, recharged by marine waters circulating at depth. Ascending fluids reach two different shallow submarine hydrothermal systems, one partially recharged by continental waters from Panarea Island and the other one by marine waters. Both systems have temperatures of about 170 – 210 °C and feed the hydrothermal emissions at the seafloor.

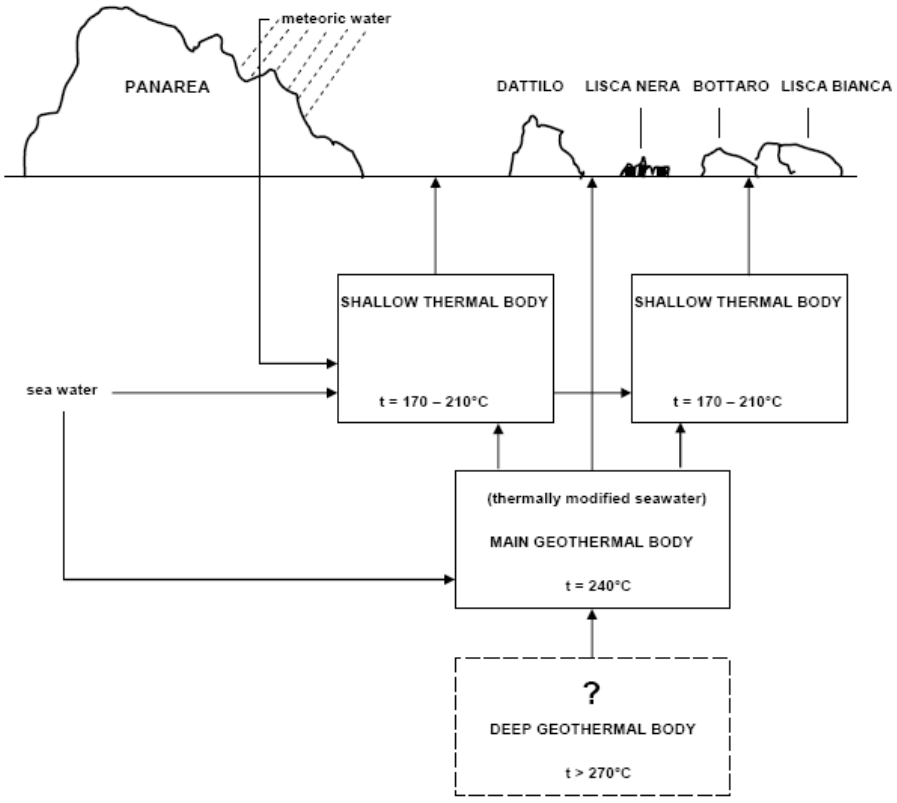

Fig. 1. Schematic representation of the geothermal system of Panarea (modified from Italiano and Nuccio (1991)).

1.1.3 The submarine gas eruption of 2002

Before November 2002 the submarine hydrothermal activity was limited to weak gas bubbling that could only be seen on the surface when the sea was very calm and the volcanic activity of the Panarea volcano complex was considered to be quiescent (Caliro et al., 2004) (Dolfi et al., 2007). However, there are historical reports of intensive gas discharges in this area, so-called “bollitore”, which were described as boiling of seawater with death of fishes (Anzidei et al., 2005, Caliro et al., 2004, Dolfi et al., 2007, Esposito et al., 2006, Italiano and Nuccio, 1991). Moreover, hundreds of craters on the seafloor were identified suggesting that the seafloor in this area was the site of gas eruptions in the past (Esposito et al., 2006).

During the night between November, 2nd and 3rd 2002 a submarine gas burst started offshore about 2.5 km east of Panarea Island. The anomalous release of gas together with intense sulphurous smell, death of thousands of fishes and the whitening of the sea surface due to dispersed fine-grained sediments and colloidal sulphur, was first observed by some local fishermen. Three huge plumes of gas bubbles several metres in diameter could be seen on the

sea surface. They originated from gas vents have been explosive at the onset of the event which produced large craters (Esposito et al., 2006). The crater of the main active exhalative centre with an extent of 35 m * 25 m and a depth of 7 m could be related to a sediment removal of $3 * 10^3$ m^3 (Esposito et al., 2006).

Although, a seismic event of minor magnitude (M < 1.8) was recorded between 2nd and 3rd November 2002 (Esposito et al., 2006) the submarine gas eruption occurred suddenly, without a significant geophysical precursory signal (Anzidei et al., 2005, Caracausi et al., 2005b). However, the event followed near the end of a prolonged seismotectonic paroxysmal period in southern Italy, with a strong earthquake (M = 5.6) in the southern Tyrrhenian Sea on the 6th of September and the onset of the strongest Mount Etna eruption in the last decades on the 27th of October (Dolfi et al., 2007, Esposito et al., 2006, Tassi et al., 2009). Furthermore, it preceded the paroxysmal eruption at Stromboli that started on the 28th of December (Dolfi et al., 2007, Esposito et al., 2006). The generated landslides at the north-west flank of the volcano caused two tsunamis on the December, 30th which attacked the coast of Stromboli and other Aeolian Islands like Panarea (Tinti et al., 2005).

Geochemical investigation of the hydrothermal fluids revealed a very rapid evolution of the shallow-water hydrothermal system, both in time and space. The hydrothermal gas output suddenly increased by two to three orders of magnitude with respect to the conditions before the crisis and progressively decreased again in the following weeks and month towards steady state levels, still higher than the pre-crisis conditions (Caliro et al., 2004, Caracausi et al., 2005b). Also the composition of the gas emissions changed significantly compared to the period prior November 2002 (Capaccioni et al., 2007, Caracausi et al., 2005a, Chiodini et al., 2006, Italiano and Nuccio, 1991).

The event of anomalous gas release was likely due to an increase in the feeding rate of deep magmatic fluids into the hydrothermal reservoir (Caliro et al., 2004, Capaccioni et al., 2007, Caracausi et al., 2005a, Chiodini et al., 2006). Therefore, two models compatible with the chemical and isotopic data of the discharging hydrothermal fluids were established by Chiodini et al. (2006).

On one hand, the submarine explosion would have been generated by a gaseous phase that was separated at depth through the increased input of high-temperature magmatic fluids. The calculated temperatures ranged from 350 to 450 °C in the hydrothermal system which was either partially or even totally vaporised (Caliro et al., 2004). The rising gases lost their volcanic acid species due to condensation and interaction with seawater.

On the other hand, the input of magmatic fluids in the system caused atypical redox conditions, more oxidising than expected compared to normal hydrothermal environments (Capaccioni et al., 2007, Chiodini et al., 2006). Thus, the explosive event of November, 3rd would have been caused by the achievement of a critical state of overpressure through continuous addition of gas and energy from the magmatic source. In this case, temperatures up to 340 °C and steam pressures of about 140 bar were calculated (Caliro et al., 2004).
Esposito et al. (2006) assumed as well that the November 2002 gas eruption was due to the sudden release of pressurised gas accumulated at shallow depths, whereas the tensile strength of the confining country rock may be periodically overcome, also by means of hydraulic fracturing through the micro-seismic event before the eruption. In contrast, Caracausi et al. (2005b) supposed that the open, widely fractured hydrothermal system is capable of preventing significant overpressure.

For the future the most hazardous scenario is related to phreatic explosive eruptions that may occur offshore and also on the inhabited island of Panarea, densely populated particularly during summer season (Caracausi et al., 2005b, Esposito et al., 2006). Such an event can cause massive releases of toxic gases which are relevant as hazards for fishers, divers and boat tourists, who spend time in the area. Although, anomalous waves can reasonably be excluded since the energy involved of events like the one in 2002 is much lower than that typical for formation of tsunami waves, more energetic episodes in the future due to more intense gas releases or a more direct involvement of magma cannot be excluded (Caracausi et al., 2005b).

1.2 Fundamentals about carbon dioxide and global biogeochemical processes

CO_2 is a very important specie for assessing volcanic activity. It is degassing early from the ascending magmas because of its low solubility in silica melts (Aiuppa et al., 2006b) and thus, becomes the most abundant component of volcanic gases, aside from water vapour (H_2O). With respect to magmatic SO_2, carbon dioxide is less reactive and behaves conservatively during gas-water-rock interaction within the volcanic edifice and upon emission into the atmosphere and is thus a far more promising target specie for providing deeper geochemical insights and early eruption forewarnings based on its emission data than e.g. volcanic SO_2 (Aiuppa et al., 2006b, Burton et al., 2000, De Rosa et al., 2007, McGonigle et al., 2008).

In general, CO_2 is also the most important component of exchange within the global carbon cycle.

1.2.1 The global carbon cycle

The global cycle of carbon involves reactions within and the exchange among the major global reservoirs: geosphere (crust and mantle), hydrosphere, biosphere and atmosphere. The mantle is rarely connected to the combined near-surface system (Bahlburg and Breitkreuz, 2004). The atmosphere and biosphere are the smallest reservoirs for carbon in contrast to, for instance the global content of total dissolved inorganic carbon (DIC) in the oceans (Table 1). But, most of the carbon in the near-surface cycle is concentrated in the Earth crust, in sedimentary rocks including their metamorphic derivates. It is estimated that about 18 % of the total carbon is bound as organic carbon in the sedimentary rocks, whereas 82 % occurs as carbonate (Bahlburg and Breitkreuz, 2004). Within the near-surface compartments carbon is moving in the global carbon cycle and can be divided into a long-term and short-term cycle (Berner, 2004, Emerson and Hedges, 2008).

Table 1. Global carbon reservoirs excluding terrestrial rocks other than coal (according to Emerson and Hedges (2008)).

Reservoirs		Carbon storage [Gt C]
Atmosphere: CO_2	(288ppm in 1850)	612
	(369 ppm in 2000)	784
Biosphere:	Oceans	1 - 2
	Terrestrial	600
Oceans:	DOC	700
	DIC	38,000
	Organic C in sediments (1 m)	1000
Terrestrial:	Fossil fuels (identified reserves)	3574
	Soil humus (1 m)	1500

The short-term cycle, having larger fluxes than the long-term cycle, represents the relatively rapid transfers among the exogenous systems, in the range from days to tens of thousands of years, which is short on a geological time scale. It is primarily controlled by the processes of photosynthesis and respiration (Fig. 2). Upon death of living material decomposition by micro-organisms produces CO_2, which is exchanged between the oceans and the atmosphere as well as organic matter is carried in solution by rivers from soils to the sea.

The long-term cycle (Fig. 2), on one hand, represents the transfer of carbon from the atmosphere to rocks by means of weathering of silicates and carbonates as well as marine carbonate sedimentation. The principal restoring process is the degassing of CO_2 to the atmosphere and oceans through decarbonation via volcanism, metamorphism, and diagenesis, described as the silicate-carbonate subcycle. These processes are taking place over several million years. Another long-term subcycle is the organic cycle representing the burial of organic matter into sediments and the reverse processes of oxidative weathering of organic matter in shales and other sedimentary rocks and the microbial or thermal decomposition of organic matter.

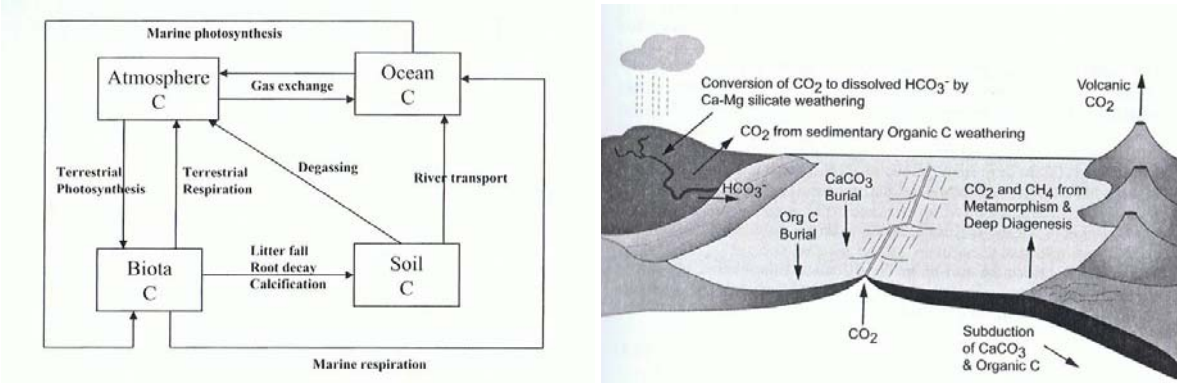

Fig. 2. The global carbon cycle can be divided into a short-term cycle (left) and a long-term cycle (right) (Berner, 2004).

1.2.2 CO_2 in the atmosphere

Although, CO_2 is only an atmospheric trace component, it is of global importance for the climate of the planet. Through the feature of absorbing infra-red (IR) radiation emitted from the earth, CO_2 is one of the major greenhouse gases and significantly contribute to the natural greenhouse effect. However, the global atmospheric concentration of carbon dioxide has increased from a pre-industrial value of about 280 ppm to 379 ppm in 2005 and is still increasing by an average growth rate of 1.9 ppm per year (IPCC, 2007). This is due to anthropogenic processes, primarily the burning of fossil fuels (currently about 26.4 Gt CO_2 per year) (IPCC, 2007).

Volcanic degassing is the primary mechanism for the transfer of mantle-derived CO_2 to the Earth's surface and thus, is one form of CO_2 reflux to the atmosphere in the long-term carbon cycle (Gerlach, 1991). This natural contribution to the atmospheric CO_2 concentration is

assumed to be significant for climatic changes at geological time-scale (million of years) (Morner and Etiope, 2002). At smaller time-scale, the carbon gas output from the solid Earth is considered negligible with respect to the biological and anthropogenic fluxes (Morner and Etiope, 2002). A conservative estimate of the global CO_2 emission of all subaerial and submarine volcanoes was made by Gerlach (1991) with 0.13 – 0.175 Gt per year, whereas Morner and Etiope (2002) assumed that 0.3 Gt CO_2 per year is only the lower limit for all subaerial volcanoes.

Beside the gaseous emission, including the principal components of H_2O, CO_2, SO_2, HCl, HF, HBr, H_2, H_2S and CO, volcanoes emit aerosols to the atmosphere, both during and between eruptions.

Aerosols are suspensions of solid and liquid particles in a gas with a size in the range between about 1 nm and 100 µm (Graedel and Crutzen, 1994, Poschl, 2005). They are formed by a number of processes, and have widely differing origins and also different chemical compositions. Aerosols can act as nuclei for condensation processes and as sites for heterogeneous chemical reactions in the atmosphere. Furthermore, they have a direct impact on the Earth's climate by scattering and absorption of sun and IR radiation, respectively (Graedel and Crutzen, 1994, Highwood and Stevenson, 2003).

Volcanic aerosols include ash (silicates), chlorides, sulphates and trace elements (Allen et al., 2000, Fulignati et al., 2006).

1.2.3 CO_2 in seawater:

About 30 - 40 % of the CO_2 injected into the atmosphere as a result of anthropogenic emissions over the last century has been absorbed by the oceans (Wei et al., 2009), representing the particular role of interaction between the atmosphere and the oceans within the global carbon cycle.

Because of the unique bonding that occurs among water molecules, the heat capacity of water is among the highest of all known substances (Garison 1996). This means that water can absorb or release large amounts of heat while changing relative little in temperature. The amount of energy required to raise the temperature of a unit of mass by 1 K is quantified by the specific heat capacity c_p at constant pressure. For seawater (density of 35 g/kg, 20 °C and 1 atm) c_p is 3.993 kJ * kg^{-1} * K^{-1} (Hill, 1971). The specific heat capacity (at 0 °C and 1 atm) of air is c_p = 1.01 kJ * kg^{-1} * K^{-1} and for CO_2 c_p = 0.85 kJ * kg^{-1} * K^{-1} (Becker et al., 1994).

After transformation into a volumetric specific heat capacity and assuming the same volume of 1 L of seawater, air and CO_2 at 20 °C the heat capacity C results in $C_{seawater}$ = 4.073 kJ * K^{-1}, C_{air} = 1.216 kJ * K^{-1} and C_{CO2} = 1.554 kJ * K^{-1}, respectively. Thus, seawater can store heat about 3 times as much as air and about 2.5 times as much as CO_2.
For a hydrothermal system this may mean that ascending hot gases heat the seawater beneath the seafloor. When the gases discharge they cool more rapid through the contact with colder seawater than the discharging waters which might assumed to be geothermal modified waters.

The surface seawater of the oceans is in equilibrium with the atmosphere. The solubility of gases at thermodynamic equilibrium are described by Henry's law, which states that at constant T, the solubility of a gas in a liquid is proportional to its partial pressure (p_G) (Langmuir, 1997):

$$\mathbf{p_G = K_G * c_G} \qquad \mathbf{(1)}$$

with c_G = concentration in solvent, K_G = Henry's law constant

Obviously, the larger K_G the more soluble is the gas. Beside increasing pressure, the solubility of a gas in seawater also increases with decreasing temperature and salinity. However, Henry's Law can only be applied for pressures up to approximately 50 bar, for dilute solution with small partial pressures and for conservative components, unlike the reactive carbon dioxide in seawater (Chester, 2003). If interactions of molecules with each other diminish the reactivity of an individual gas slightly the fugacity *f* has to be used, an effective partial pressure for real gases (Emerson and Hedges, 2008). At atmospheric pressure (1 atm = 101.325 kPa) the fugacitiy of CO_2 is about 99.6 to 99.7 % of the partial pressure over the range of 0 and 30 °C (Zeebe and Wolf-Gladrow, 2001). The solubility of CO_2 in water and seawater is listed in Table 2 in comparison with other gases.

Table 2. Henry's law constants (K_G [mol * L^{-1} * atm^{-1}]) of several gases for water and seawater. Values characterise the solubility of the gases in the solvents at 1 atm and 20 °C.

gas	water*	seawater** (S = 35)
SO_2	1.76E+00	
H_2S	1.15E-01	
CO_2	3.92E-02	3.30E-02
CH_4		1.23E-03
O_2	1.38E-03	1.12E-03
N_2	6.89E-04	5.62E-04
He		3.36E-04

* *(Langmuir, 1997)*
** *(Emerson and Hedges, 2008)*

The dissolution of CO_2 increases the content of total dissolved inorganic carbon (DIC) in seawater. The carbonate system (equation 2), comprising the components CO_2, HCO_3^- and CO_3^{2-}, is one of the most important chemical equilibria in the ocean and is largely responsible for buffering the pH of seawater (Fabry et al., 2008, Zeebe and Wolf-Gladrow, 2001). Seawater in equilibrium with atmospheric CO_2 is slightly alkaline, with pH of around 8.1 - 8.3 (Brown et al., 1995).

$$\mathbf{H_2O + CO_2 \leftrightarrow H_2CO_3 \leftrightarrow HCO_3^- + H^+ \leftrightarrow CO_3^{2-} + H^+} \qquad \mathbf{(2)}$$

With Ca^{2+} there is formed calcium carbonate ($CaCO_3$) which is supersaturated nearly everywhere in ocean's surface waters, but undersaturated everywhere in deep ocean waters (Brown et al., 1995). The decreasing saturation of calcium carbonate with increasing depth is due to an increasing solubility mainly through the increase of hydrostatic pressure as well as the better solubility in colder water.

However, the increase of the CO_2 concentration in the surface ocean through the anthropogenic CO_2 invasion from the atmosphere has lead to a slight ocean acidification with an seawater pH about 0.1 units lower than the pre-industrial value (Fabry et al., 2008). It may further drop by up to 0.4 units until 2100 (IPCC, 2007). In consequence, the calcium carbonate saturation state in surface seawater will reduce making it more difficult for marine calcifying organisms to form biogenic $CaCO_3$ (Orr et al., 2005). Calcification rates in marine organisms, coccolithophorids and in particular corals, have been found to be extremely sensitive to the increasing CO_2 concentration and the level of carbonate saturation (Hall-Spencer et al., 2008, Wei et al., 2009).

The maximum acidification which is theoretically possible only by increasing the CO_2 concentration in an aquatic solution is upon a pH of about 4.3. In this case, all dissolved inorganic carbon is existent as CO_2. For a further decrease of the pH stronger acids, such as hydrogen chloride (HCl) and sulphuric acid (H_2SO_4), have to be added to the solution.

1.3. Objectives

The aim of the thesis is the evaluation of the hydrothermal gas discharges. Which processes can be inferred by the chemical gas composition and are there indications for the input of magmatic fluids into the hydrothermal system? By this means, the attempt was made to evaluate the current state of the system with regard to the submarine gas eruptions occurred in 2002.

Since the discharging gases predominantly consists of CO_2 the effects on the ambient seawater is examined. Furthermore, the rate of submarine degassing is quantified including the comparison with other CO_2 emitters.

2. Description of the investigation site

2.1 The Aeolian volcanic arc

Several seamounts and seven islands (Alicudi, Filicudi, Salina, Lipari, Vulcano, Panarea and Stromboli belong to the Aeolian archipelago, representing a ring-shaped volcanic arc in the south-eastern Tyrrhenian Sea, Italy (Capaccioni et al., 2005, Esposito et al., 2006, Gabbianelli et al., 1990, Gugliandolo et al., 2006). The Aeolian volcanic arc, with a length of approximately 200 km, is associated with the Preloritanian-Calabrian orogenic belt to the east and is bordered by the abyssal Marsili basin to the west (Capaccioni et al., 2005, Esposito et al., 2006, Gabbianelli et al., 1990) (Fig. 3).

The origin of Aeolian volcanism, most authors agree, is due to active subduction of the Ionian plate beneath the Calabrian Arc (Calanchi et al., 2002, Capaccioni et al., 2005, Caracausi et al., 2005a, Dolfi et al., 2007). Such microplates have been formed in the Mediterranean based on convergence of the African and Eurasian plates (Dando et al., 1999). Some authors suggest that subduction stagnated about 1 million years, since when a general uplift associated with extensional tectonics has affected both the Calabrian Arc and the Aeolian Islands in the last 0.5 – 0.7 million years (Dolfi et al., 2007, FavalliM et al., 2005). Consequently, a heat flow anomaly occurs in relation to slab detachment beneath the Calabrian Arc (Dolfi et al., 2007).
The volcanic activity took place almost entirely during the Quaternary, starting about 400,000 years and is still presently existent (Calanchi et al., 2002, Gugliandolo et al., 2006). Magmatic products belong to calc-alkaline (CA), high-potassium calc-alkaline (HKCA), shoshonite and potassic-alkaline associations (Chiodini et al., 2006, FavalliM et al., 2005).

The Aeolian volcanic arc can divided into three sections. The western part, comprising the islands of Alicudi and Filicudi, is located along a WNW – ESE fault system (Esposito et al., 2006, FavalliM et al., 2005). The central sector includes Salina, Lipari and Vulcano Island and is identified by evolution through the major discontinuity crossing the Aeolian Islands, the NNW – SSE strike-slip Tindari-Letojanni fault system (FavalliM et al., 2005) (Fig. 3). Panarea and Stromboli constitute the eastern sector. Both Islands are arranged along NE – SW trending extensional faults (Esposito et al., 2006).

The eastern branch of the Aeolian volcanic arc is being affected by deep-focus seismicity, representing a narrow NW-dipping Benioff-Wadati plane (Calanchi et al., 2002, Chiodini et al., 2006).

Currently, the Aeolian volcanic arc is characterised by still active volcanoes, Stromboli and Vulcano. The latter one is in a state of solphataric activity as well as hydrothermalism (Gugliandolo et al., 2006). Submarine gas emissions occur in the neighbourhood of many of the Aeolian Islands, such as Salina, Lipari, Vulcano, Stromboli and Panarea (Chiodini et al., 2006). The most active submarine fumarolic system at shallow depths is present off the eastern coast of Panarea, representing the investigation area for this study (Gugliandolo et al., 2006).

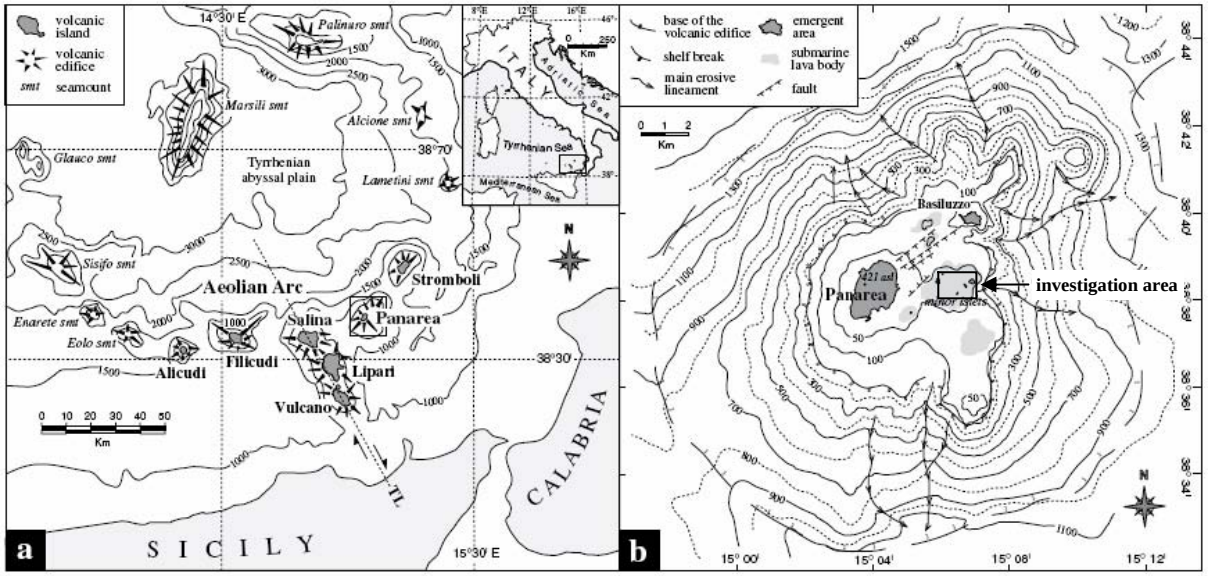

Fig. 3: a) Bathymetry of the Southern Tyrrhenian Sea and location of volcanic edifices of the Aeolian Arc, b) morphological sketch map of Panarea volcanic complex and the investigation area to the East of Panarae Island; coordinates conform to Gauss-Boaga-System, depth contour lines in m b.s.l. (modified from Lucchi et al. (2007)).

2.2 Panarea

Panarea, with 3.3 km^2, is the smallest island of the Aeolian archipelago (Gabbianelli et al., 1990). It is the emergent part of a wide stratovolcano rises from a depth of about 1200 – 1700 m b.s.l. up to 421 m a.s.l. (Calanchi et al., 2002, Gabbianelli et al., 1990). The vast volcanic complex sizes at its base 23 km in diameter and covers an area of 460 km^2 (Gabbianelli et al., 1990). The submerged summit has an broad and almost flat surface reaching about 50 km^2 at a depth of about 100 – 150 m b.s.l. (Calanchi et al., 2002, Chiodini et al., 2006).

The evolution of the Panarea volcanic structure can be described as a result of three different stages of activity (Gabbianelli et al., 1990). The oldest period was characterised by growth of the central apparatus with formation of the island and submarine surroundings. Then, the volcanic structure was enlarged to east, whereas volcanic activity was regulated by a NE-SW oriented fault system. The main island, and likely the minor islets, developed in a relatively short time span between about 150 and 100 ka (Capaccioni et al., 2005, Lucchi et al., 2007). After 50 ka of quiescence the volcanic activity resumed with emplacement of the endogenous dome of Basiluzzo (NE of Panarea Island) (Capaccioni et al., 2005). Recent stage of evolution created a huge caldera in the central part of the complex, which is associated with a positive gravimetric anomaly due to a magmatic intrusion (Gabbianelli et al., 1990, Italiano and Nuccio, 1991).

Panarea is predominantly formed by andesitic and dacitic lava domes, flows and pyroclastica (Calanchi et al., 2002, FavalliM et al., 2005, Gabbianelli et al., 1990). Rocks show a dominant HKCA petrochemical affinity, some shoshonite and a few CA rocks, as late scoria fall, also occur (Calanchi et al., 2002).

Presently, Panarea volcano is characterised by local subsidence and degassing from several fumarolic areas, both inland and offshore. A rapid sink of that still collapsing area in historical time is proven by the discovery of old Roman ruins at 8 - 14 m water depth, located about 200 m to the west of Lisca Bianca islet (Gabbianelli et al., 1990, Italiano and Nuccio, 1991) (Fig. 4).

2.3 The submarine hydrothermal area

The investigation area is located approximately 2.5 km to the east of Panarea Island. It is a shallow submarine subcircular field of about 2.3 km^2 (Esposito et al., 2006) with a maximum water depth of about 30 m and is surrounded by the islets of Datillo, Panarelli, Lisca Bianca, Bottaro and Lisca Nera. Those islets are remnants of lava domes, subaerial ruins of an old volcanic centre (Capaccioni et al., 2007, Gabbianelli et al., 1990). An area of about 4 km^2 to the east offshore of Panarea is affected by widespread exhalative and hydrothermal activity at the sea floor (Italiano and Nuccio, 1991), whereas main vents of CO_2-rich gases as well as thermal water discharges are located approximately in the central portion between the islets. The seafloor is completely covered by loose-to-partly consolidated Holocene sands and

conglomerates, originated from marine erosion of the emerging islets (Capaccioni et al., 2007). These conglomerates lay on porphyritic basaltic-andesite lavas.

Generally, the discharging fluids escape from open rock fractures, but also several areas with diffuse permeation of gases and thermal waters through the sand on the seafloor occur (Gugliandolo et al., 2006). Emissions are normally marked by white bacterial mats appearing as a white film of colloidal sulphur deposits containing numerous filaments of colourless bacteria (Gugliandolo et al., 2006). They are of the genus *Thiothrix*, being sulphur-oxidising, chemoautotrophic bacteria which are supported due to the fact that hydrothermal vent fluids are commonly rich in reduced sulphur compounds (Gugliandolo et al., 2006). However, the vicinity of vent outlets is generally impoverished in flora and fauna due to acid discharges.

The spatial distribution of fumarolic discharges is dominantly regulated by NE-SW oriented fault systems (Esposito et al., 2006, Gabbianelli et al., 1990). A large number of the hydrothermal discharges are distributed on exhalative fields covering generally about a few hundred square meters. More than 20 exhalative fields were identified by Italiano and Nuccio (1991). The submarine sites investigated in May and September 2008 (Fig. 4) will be defined in detail in the following.

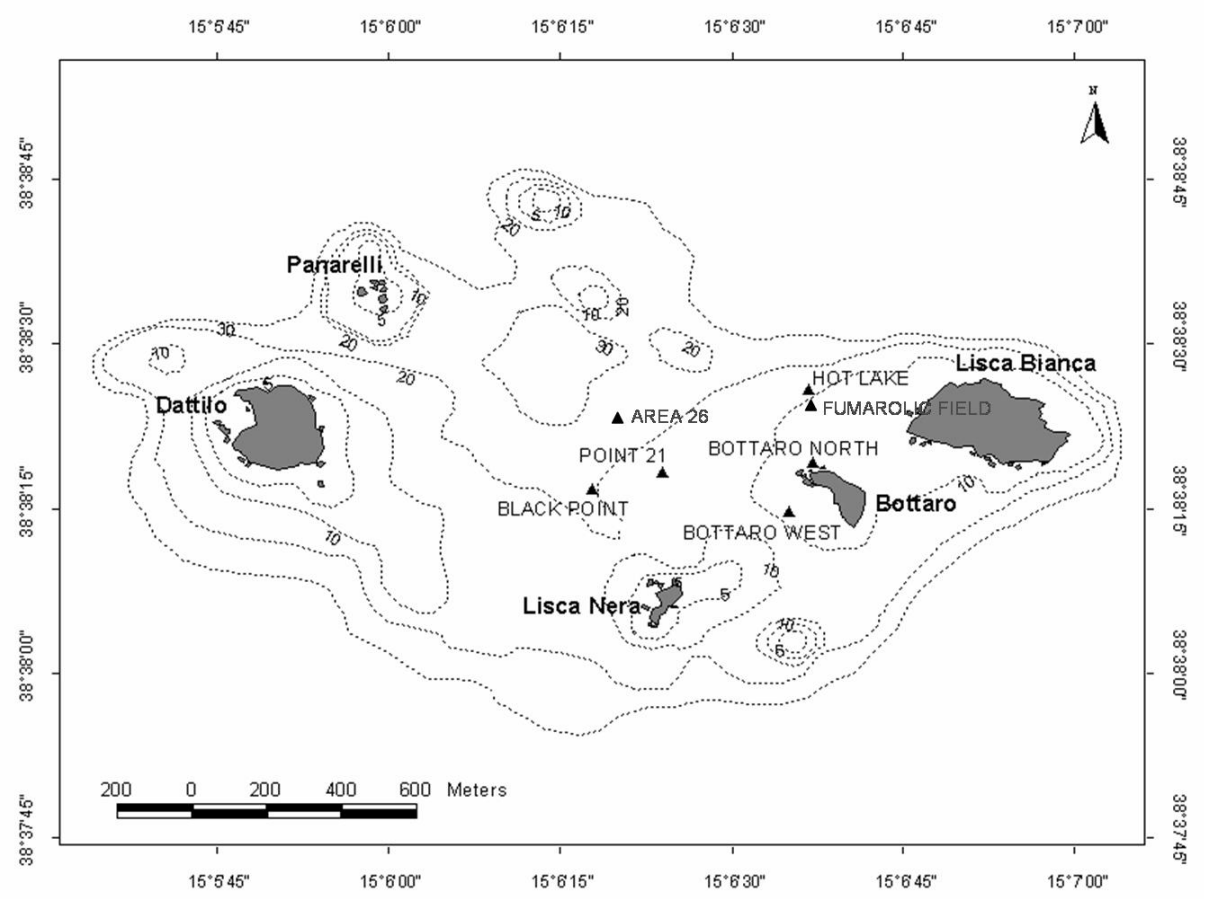

Fig. 4. Investigated sites (triangles) in the hydrothermal system east of Panarea Island. The shallow submarine area is surrounded by the islets of Dattilo, Panarelli, Lisca Bianca, Bottaro and Lisca Nera (modified from Rohland (2007)).

Table 3. Geographical coordinates of the different sites. Values are expressed as "degree" "arc minute" "arc second" [x° x′ x.x″], reference system: WGS 84

Location	Northing	Easting
Bottaro West*	38° 38′ 14.4″	15° 06′ 34.1″
Bottaro North*	38° 38′ 19.2″	15° 06′ 36.4″
Hot Lake*	38° 38′ 24.5″	15° 06′ 35.0″
Fumarolic Field*	38° 38′ 24.1″	15° 06′ 35.8″
Point 21*	38° 38′ 18.1″	15° 06′ 24.4″
Area 26**	38° 38′ 21.2″	15° 06′ 18.5″
Black Point*	38° 38′ 16.7″	15° 06′ 17.1″
Panarea North**	38° 38′ 42.4″	15° 04′ 40.7″

* *modified from (Rohland, 2007)*
** *modified from (WISTAU, 2008)*

2.3.1 Bottaro West

The investigation site Bottaro West is located approximately 30 m to the western margin of the islet Bottaro (for geographical coordinates see Table 3). The submarine structure was formed at the gas burst event in November 2002, representing the most active exhalation centre (see section 1.1.3). The original size of the formed ellipsoidal crater (Esposito et al., 2006) has decreased until September 2008 due to refilling with sediments and rock debris resulting in a 2.5 m thick cover. So, actually the crater is a flat gravel field in a depth of 12 - 12.5 m b.s.l. with an extent of about 12 m in the NW-SE axis and about 10 m in the NE-SW axis. It is enclosed to the south by a more or less steep slope of subcircular shape and up to 4 m high (Appendix 1).

The location features hydrothermal discharges in terms of fumaroles emitting predominantly in the gas phase. At clam days the submarine gas emissions can be noticed olfactorily at the sea surface through the significant smell of hydrogen sulphur (H_2S). The south-western part of the crater is separated from residual part by a 60° striking sediment edge of about 50 cm height. This sector is characterised by diffusive gas exhalations in a field of almost circular shape and a diameter of 5.5 m (Fig. 5a). Within the slope to SE of the sector a wall composed of conglomerates is exposed (approximately 7 m long and 1.5 m high). In front of that, in vicinity of several boulders, some fumaroles exist, where the highest fluid temperatures were determined in situ (Appendix 1). In the NW the residual sector of the crater is characterised by several fumaroles of varying intensities, primarily distributed at the crater rim and within the slopes. All fumaroles are marked by more or less big whitish mats of sulphur deposits and bacteria. Except for the mentioned fumaroles, the outlet temperatures did not distinctively differ from the ambient water temperature (about 27 °C).

2.3.2 Bottaro North

Some meters from the northern cape of Bottaro the very shallow submarine site, defined as Bottaro North, is located (for geographical coordinates see Table 3). At a maximum depth of about 9 m several fumaroles between large boulders occur. Due to some very intensive exhaling vents together with the low water depth strong gas bubbling is clearly visible at sea surface with no waves. Besides this, the smell of hydrogen sulphur at the sea surface is significant during calm days. The location is characterised by a central gravel field

surrounded by large boulders up to several meters in diameter. To the south of that field the sea bottom steeply rises up to the islet of Bottaro.

There are five very intensive exhaling vents; one is located at the gravel field, the residual ones between boulders to the south and east of the field (Fig. 5b). Many smaller vents of varying intensities are located between the boulder deposits. In the north several exhalations are situated on a line-like fracture zone of a couple of metres from west to east (Rohland, 2007). The fluid temperature measured in these vents ranged between 27.9 and 45.7 °C, in the large fumarole, located directly at the gravel field, a temperature of 56 °C was measured (Appendix 2). Beside the Bottaro West site that area was one of the main exhaling centres at the gas burst in November 2002, and was likely formed by this event (Capaccioni et al., 2005, Tassi et al., 2009).

2.3.3 Hot Lake

The investigation site Hot Lake is located approximately 300 m to the north of Bottaro islet (for geographical coordinates see Table 3). At about 18 m b.s.l. a submarine depression having an extent of about 10 m in the NE-SW oriented main axis and about 6.5 m in minor axis is embedded in the sea floor (Fig. 5c). The basin is enclosed by vertical and overhanging sinters of less than 1 m height in the north-eastern part and up to about 2 m in the south-west. To the north-east the basin extended farther eastward. Overhanging walls covered by whitish bacteria layers form small caves in the southern part. The bottom of the basin, in a water depth of approximately 19.5 m, is covered by sediments and a thick layer of dead *Posidonia*, both coated by whitish bacteria deposits. The basin features diffusive thermal water discharges. Since only some small gas bubbles appear from time to time the release of gases in the basin is marginal. Some scattered fumaroles of varying intensities are emplaced at the surrounding sea floor, loaded by pyroclastic rocks. Over five diving campaigns from 2006 to 2008 a progressive subsidence of the basin was noticeable. The discharging thermal waters are characterised by a temperature of about 96 °C (WISTAU, 2008) and very high salinity (Fig. 13).

2.3.4 Fumarolic Field

In the vicinity of Hot Lake, about 50 m course of 150° from Hot Lake (for geographical coordinates see Table 3), there is a plane field characterised by numerous exhaling fumaroles.

It has an almost square shape with an estimated length of 30 m (E-W) and width of 20 m (N-S) and is located about 15 – 17 m b.s.l. (Appendix 3). To the north-west there is an almost plain northward extension towards a smaller gravel field some meters off the central field. The field is covered by fine- to coarse-grained gravel loaded by several boulders in the centre. Rocky slopes enclose the gravel field, steeper rising at the western margin than at the others. The slopes are characterised by scattered fumaroles of varying intensities between boulders and few *Posidonia* fields, the latter ones being located predominantly at the northern slope. Most intensively exhaling fumaroles are situated at the slope some meters to the south-west of the central field (Appendix 3). The majority of gas exhalations discharge in the gravel field, many are diffusely discharging while others are arranged along lineaments clearly marked by white-yellow sulphur deposits and bacteria. Three almost parallel line-like structures, some meters distant to each other and striking 195°, 170° and 160°, respectively, were observed in September 2008 (WISTAU, 2008) (Fig. 5d). Along the westernmost lineament distinctive increased outlet temperatures were measured ranging from 39.7 °C up to 59.1 °C in contrast to the ambient water temperature of about 27 °C (WISTAU, 2008).

2.3.5 Point 21

The investigation site defined as Point 21 is located approximately 300 m to the north-east of Black Point along the route from Black Point to the location of Hot Lake (for GPS coordinates see Table 3). It is distinguished by a submarine depression of about 20 m in NW-SE and about 10 m in NE-SW extension bordered at the south-west by a vertical wall of more than 10 m length from about 17 to 22 m b.s.l. (Appendix 4). Both the wall and the depression situated in front strike approximately 140°. Surrounding area, extensively covered by seaweed (*Posidonia*) and many fumaroles of varying intensities, gradually rising up to the ambient depth of about 17 – 18 m b.s.l..

The site is characterised by five fumaroles emitting massive amounts of gases associated with the discharge of thermal water, whereas it is not clear whether the water is of hydrothermal origin or just heated seawater by the ascending hot gases (see section 1.2.3). Two of these fumaroles are located in the northern, two in the southern part of the depression in front of the wall between rock debris (Fig. 5e). The residual vent is situated directly in the porous rocky wall, about 2 m above the bottom of the depression (Fig. 5e). Coatings of white and yellowish deposits of elemental sulphur can be seen on the wall. All vents are marked by whitish sulphur precipitation and bacterial mats. In situ measurements of fluid discharge temperatures

revealed that most fumaroles of the entire site are characterised by outlet temperatures almost equal to ambient seawater expect for the large vents (Appendix 4). The location of Point 21 already existed before the gas burst 2002, since it was reported by Italiano and Nuccio (1991) as a major gas exhaling field.

2.3.6 Area 26

Gas and water samples which were taken at this site were named “Area 26”, since the water depth is about 26 m. It is located to the north-east of Point 21, tracking the extension of the vertical wall in 300° direction for approximately 100 m (for GPS coordinates see Table 3). The site is characterised by two distinct sediment fields which together span an area of more than 50 m in each direction (WISTAU, 2008). The seafloor is covered by sediment made up of grain sizes from coarse sands to fine gravels and crossed by several exposed conglomerate bodies which are overgrown by vegetation (Becke, 2009). Gas exhalations are widespread over the entire site with fumaroles being scattered over the fields or arranged along a lineament as well as diffusely escaping gas bubbles from the sediments (WISTAU, 2008) (Fig. 5f). Exhalations were sensed as hot and aggressive to divers (WISTAU, 2008). Larger exhalations are marked by conspicuous white sulphur deposits and bacterial mats. Along the line-like structure (striking 320°) about 20 gas exhalations were distributed (Becke, 2009).
Since that location was investigated for the first time by only two dives at the end of the diving campaign in September 2008 no further characterisations or a map can quoted here.

2.3.7 Black Point

The investigation site Black Point is located approximately in the middle between the islets of Dattilo and Bottaro (for geographical coordinates see Table 3). It is a submarine crater lying at a water depth of about 23.5 m and sizes about 25 m in the north-south axis and about 20 m in the east-west axis. The sea bottom is covered by gravel of different grain sizes. Formed ripples by the current were observed during the diving campaign in September 2007, but not in 2008. Many fumaroles of low intensities are diffusely exhaling within the crater, but some are also arranged along line-like structures marked by white deposits of sulphur bacteria (Fig. 5g). Surrounding flanks exhibits an extensive cover of *Posidonia* and a lot of single fumaroles

of varying intensities. Some stronger hydrothermal discharges are emplaced in the south-west and north outside the crater.

The location is named after a black sinter body sticking out morphologically in the SE of the crater (Fig. 5h). It is a porous conglomerate body (2.7 m long, at maximum 1 m wide and 0.5 m high) having a blackish incrustation (Becke, 2009). In the north-eastern part of the body massive hydrothermal gases and waters discharge out of a vent, about 10 cm in diameter. These hydrothermal discharges are accompanied by metallic precipitations that cause a whitish-grey fume. This unique phenomenon has also previously been mentioned by other authors who named that location “Black Smoke” (Esposito et al., 2006, Tassi et al., 2009).

Few metres to the east of the black sinter body there is an area comprising another smaller body showing analogous hydrothermal incrustations and further active hydrothermal discharges with recent mineral precipitation. In this region and of course in the vent of the main sinter body the highest temperatures of 124.5 °C and 134.8 °C, respectively, were measured (Fig. 6). But also fluid temperatures of fumaroles measured in the northern and western part of the location showed significantly increased temperatures in contrast to surrounding sea water.

2.3.8 Lisca Nera

To obtain reference values for the composition of seawater, minor influenced by hydrothermal discharges, water samples were also taken close to the islet of Lisca Nera (Fig. 3).

2.3.9 Panarea North (La Calcara)

Beside the submarine hydrothermal discharges to the east of Panarea, several subaerial fumaroles occur at the north-eastern shoreline of the island (Fig. 5i). The location is called La Calcara. No gas samples were taken by the author of this study, therefore external data from these exhalations were used instead.

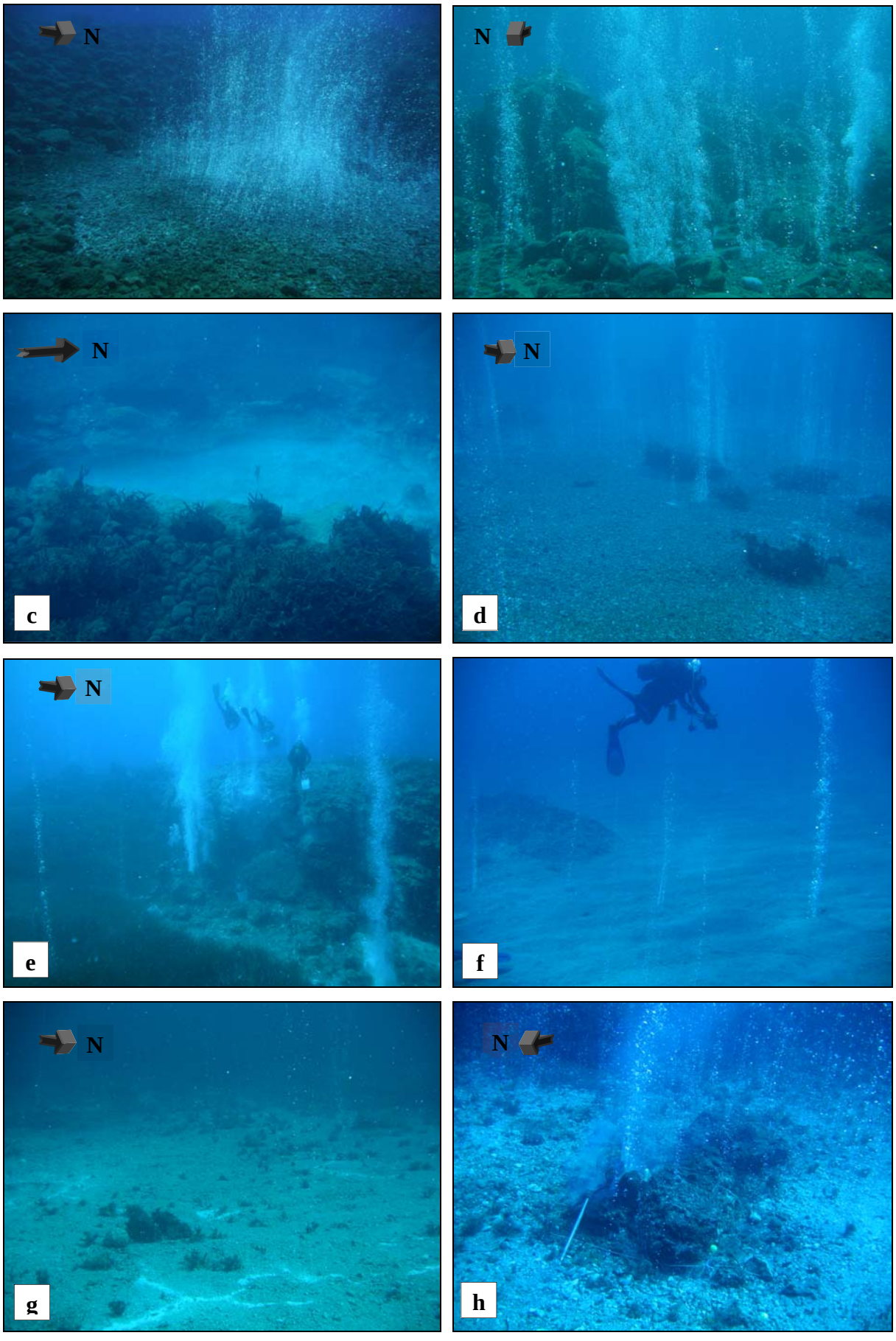
N
N
N
N
c
d
N
N
e
f
N
N
g
h

Fig. 5a. The field of diffuse gas exhalations at Bottaro West site, b) large fumaroles between boulders at the very shallow site of Bottaro North, c) Hot Lake, d) Fumarolic Field with diffusive exhalations as well as fumaroles located along lineaments, e) large fumaroles in front of a vertical wall at Point 21 site, f) gas exhalations discharging from huge sediment fields at Area 26 site, g) whitish marked lineaments of exhalations in the crater of Black Point site, h) the black sinter body at Black Point, i) subaerial fumaroles at La Calcara on Panarea Island (WISTAU, 2007, WISTAU, 2008).

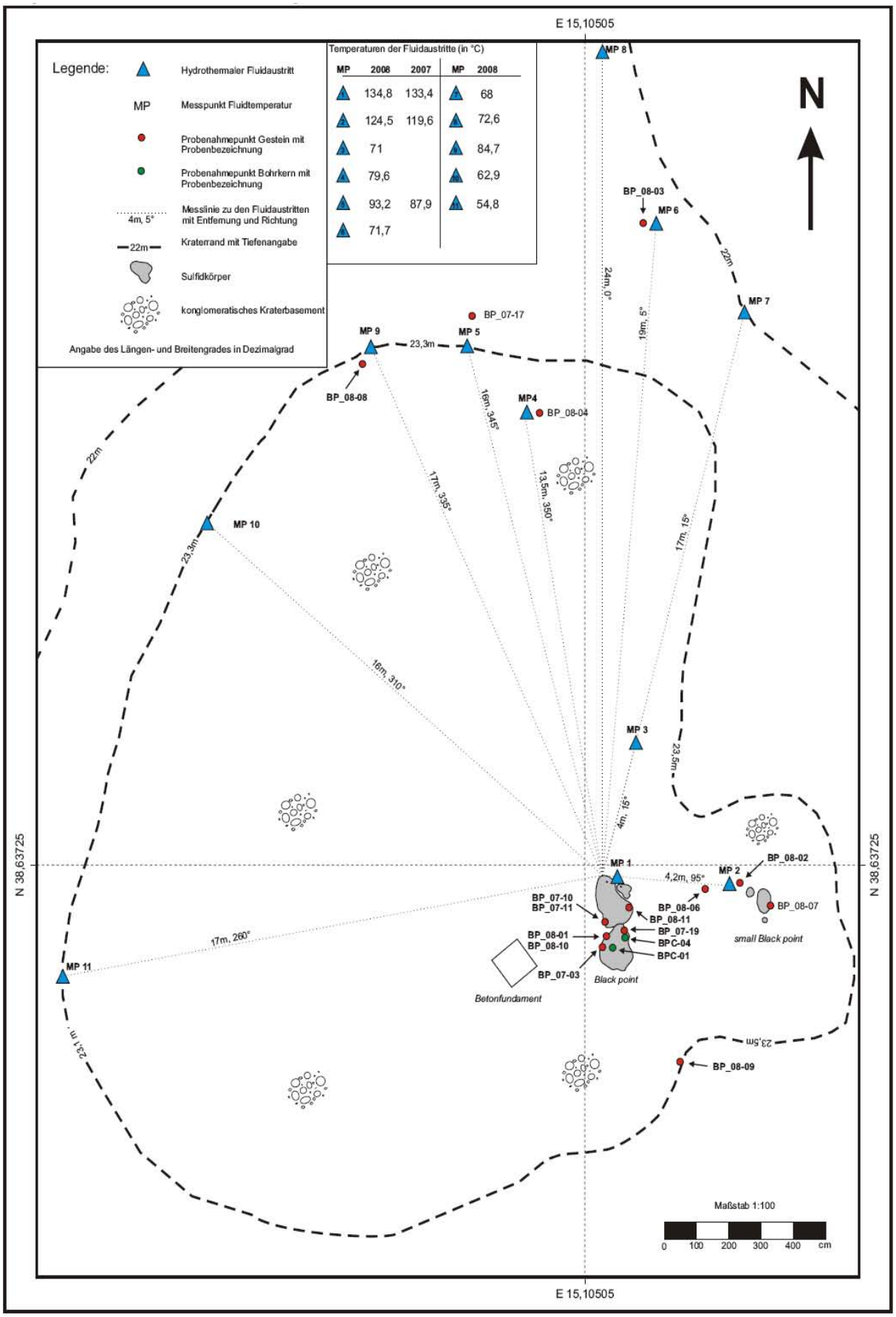

Fig. 6. Sketch map of the Black Point site including measured temperatures of fluid discharges (modified from Becke (2009)).

3. Methodology

Investigations of the submarine hydrothermal fluid emissions at the seafloor were performed by scuba diving. This took place during two diving campaigns in the investigation area near the island of Panarea (see section 2.3). First period lasted from May, 12th to May, 18th 2008. The second campaign, from August, 30th till September, 10th 2008, was performed in the framework of the annual diving excursion to Panarea Island of the scientific diving research group of the TU Bergakademie Freiberg.

To characterise the discharging gases and waters samples were taken. Beside that, measurements were carried out directly at the emission points. The performance under water had been adapted for the prevailing conditions. In addition to common problems confronted with on scientific working during dives, e.g. buoyancy effects of equipment and the limited time for each trip, the acid waters and gases aggressive to metallic matter necessitated the utilisation of rustproof materials.

3.1 Sampling procedures

Escaping gases from the seafloor were sampled by means of a funnel made of stainless steel. The funnel was placed directly over the emission point. In a chamber above the funnel the collected gas was accumulating until seawater was completely displaced through a bypass. A Teflon hose of 50 m length was joined to the funnel by a self-sealing-coupling. Due to buoyancy the gas ran to sea surface onto the boat. Because of the self-locking effect of the self-sealing-couplings only very little water was infiltrated into the Teflon hose. It was removed by the ascending gas for 2 to 5 minutes on the boat, depending on the depth the gases were sampled. When dry gas was escaping from the hose the end was joined via a 250 ml water trap (PTFE) to a gas bag of 16 L volume made of Tedlar polyvinyl fluoride (PVF) (DuPont). Before each sampling the bag was flushed with fresh air to remove the previous gas sample. The time to fill the 16 L gas bag was dependent on the water depth at the sampling point.

Subsequently, the hose was connected via the 250 ml water trap and 2 filters (200 and 25 nm) with washing bottles (PTFE with PTFE Raschig ringes), one filled with 100 ml sodium hypo chloride (NaOCl) solution (NaOCl, dilution 1:10 by bidest water). In the NaOCl solution, a strong oxidation agent, the gas constituents were trapped. The filters were firstly utilised in September 2008 in order to limit the trapping of gases and aerosols < 25 nm. Both the time

for trapping and the time for filling the 16 L gas bag was noted in order to calculate the trapped volume of gas (Appendix 5).

For water sampling two kinds of syringes were applied (100 ml or 450 ml). A flexible Teflon tube was fixed on top of the syringes. The tube was inserted into the sediment or rock fractures at the fluid emission points as deep as possible to avoid dilution with sea water. Before ultimate sampling the syringes were flushed several times with the geothermal water and sealed with a cap after sampling.
In order to sample the discharging original hydrothermal fluid, undiluted by sea water as much as possible, at two emission points special procedures were applied. In the case of Black Point a 50 cm hole was drilled into the rock formation, at Hot Lake a PTFE lance was penetrated up to 3 m into the sediment (Sieland, 2009).

3.2 Sample preparation

After the dives the gas and water samples were prepared for further analysis and filled into glass or plastic bottles for storage and transportation. This was done in the field laboratory at Panarea Island.

From the 16 L gas bag 300 ml gas bags (previously flushed with N_2) were filled for gas chromatographic analysis at the laboratory in Freiberg. The 300 ml gas bags were made of Tedlar PVF (DuPont)[1] equipped with both an on/off valve and a septum valve. The NaOCl solution with the trapped gas constituents was filled into a 100 ml polyethylene (PE) bottle for analysis with inductively coupled plasma mass spectrometer (ICP-MS) at ACTLABS (Activation Laboratories Ltd., 1336 Sandhill Drive, Ancaster, Ontario, Canada).
Furthermore shares of the sampled gas were piped through washing bottles by means of an electrical diaphragm pump (5002F, Gardner Denver Thomas). In these washing bottles zinc sulphide and barium carbonate were precipitated for $\delta^{34}S$ (H_2S) and $\delta^{13}C$ (CO_2) analysis, respectively (Sieland, 2009).

Water samples were filtered, in order to remove suspended particles and colloids, for the analysis by photometry, ion chromatography (IC), and ICP-MS. It was performed by applying

[1] http://www.coleparmer.com/catalog/0708_pdf_International/KH_0011.pdf (25/06/2009)

cellulose acetate filters with a mesh size of 200 nm (SATORIUS Biolab Products) and a filtration apparatus with a hand pump (NALGENE/MITYRAC).

For analysis of total inorganic carbon (TIC) the water sample was directly filled from the syringe into 50 ml glass flasks. That was done with a short flexible hose plugged at the syringe so that the flask could be filled from the bottom up to avoid too much contact with atmosphere and minimise the loss of dissolved carbon dioxide by degassing. Water sample processing for analysis with ICP-MS and IC as well as for isotopic analysis is reported by (Sieland, 2009).

3.3 Gas analysis

3.3.1 Computation of CO_2

The content of CO_2 in the gas samples was not analysed, but rather calculated.

It is the most abundant specie in the discharging gas phase. Together with H_2S both species account for about 99 vol.% and even more in the gases (Capaccioni et al., 2007, Chiodini et al., 2006, Italiano and Nuccio, 1991). Thus by subtraction of the analysed contents of H_2S, CO, CH_4 and C_2H_6/C_2H_4 from 100 vol.% a quite good estimation of the real CO_2 concentration could be achieved.

3.3.2 Dräger tubes

The determinations of carbon monoxide (CO) and hydrogen sulphide (H_2S) content of the gases were carried out directly from the gas bag in the field laboratory on Panarea Island. It was done by means of DRÄGER tubes (DRÄGER Safety AG & Co. KGaA). Both for determination of CO and H_2S the respective tube was connected to the gas bag through a short flexible hose. The other end of the tube was fixed in the DRÄGER Pumping System (ACCURO pump).

For determination of CO Carbon Monoxide 2/a tubes with a measuring range between 2 and 60 ppm were used (10 times pumping). The standard deviation of the method was quoted in the DRÄGER instruction manual being between ± 10 and 15 %. Basis of the analysis is reaction (3).

$$\mathbf{5\,CO + I_2O_5 \rightarrow I_2 + 5CO_2} \qquad \mathbf{(catalyst: H_2S_2O_7)} \qquad \mathbf{(3)}$$

For the determination of H_2S Hydrogen Sulphide 0.2 %/A tubes with a measuring range between 0.2 and 7 vol.% were used (1 pumping stroke). The standard deviation of the method was quoted to be in the range between ± 5 and 10 % (DRÄGER instruction manual). Following reaction (4) takes place.

$$\mathbf{Cu^{2+} + H_2S \rightarrow CuS + 2H^+} \qquad \mathbf{(4)}$$

3.3.3 Gas chromatography

In the laboratory of the section for Hydrogeology, TU Bergakademie Freiberg the gas samples, which were stored in the 300 ml gas bags, were analysed for methane and ethane by gas chromatography. Therefore, a gas chromatograph HEWLETT PACKARD (HP) GC-FID 5890 with nitrogen (N_2) as carrier gas and make-up gas was applied. During a temperature program methane and ethane were separated in an AT-Q column (30 m long, 0.32 mm in diameter). Detection was realised by a flame ionisation detector (FID) measuring in the split modus. The detection limits for methane and ethane were evaluated to be 0.0002 % and 0.00005 %, respectively (Kummer, pers. comm., 2009).

The sampled gases were inserted from gas bags to the injector through microliter syringes of 25 µl and 50 µl. For calibration a synthetic gas mixture Micro Mat 14 (MATHESON Tri Gas) was used. The 14 L gas bottle contained a mixture of the alkane serial C_1 – C_6 and nitrogen with a concentration of 1000 ppm for all compounds (Appendix 7). The following calibration functions (5 – 8) were determined:

May: methane: area = 25609846000 * c [vol.%], R^2 = 0.9998 **(5)**

ethane/ethene: area = 44450160000 * c [vol.%], R^2 = 0.9997 **(6)**

September: methane: area = 8098916586.538 * c [vol.%], R^2 = 0.9984 **(7)**

ethane/ethene: area = 4297318894.2308 * c [vol.%], R^2 = 0.9969 **(8)**

Due to the fact that in the AT-Q column also ethene can be separated and the peaks of ethane and ethene in a chromatogram are very close to each other, a mixture of both compounds, detected in the executed analysis, can not be excluded (Kummer, 2009, pers. comm.). Thus, the peak at the retention time of about 5.4 minutes will be discussed as the ethane/ethene peak, although calibration was only done with C_1 - C_6 alkane standards.

3.3.4 Volatile trace elements (ICP-MS)

Gases and aerosols (< 25 nm for the samples of September), trapped in 100 ml of a NaOCl solution (1:10 dilution by didest water), as well as the sampled thermal waters were analysed with ICP-MS at ACTLABS for trace element contents. The analysis was performed with High Resolution Magnetic Sector ICP-MS (Finnegan Mat ELEMENT 2)[2]. For the samples of May 2008 the protocol Code 6 MB (for marine water, brines or other aqueous solutions with total dissolved solid contents (TDS) > 0.05 %) was used. Samples taken in September 2008 were previously diluted (in most cases 1 + 41) in the laboratory of Hydrogeology, TU Bergakademie Freiberg. They were then analysed at Actlabs with protocol Code 6 (for natural waters with low TDS < 0.05 %)[2]. The detection limits are listed in (Appendix 5).

The measured element contents in the NaOCl solution have to be processed and converted into the contents related to the sampled gas phase.
It was easy to identify in the original data that the blank of the NaOCl solution was in many cases greater or equal to the respective element concentration of the samples (Appendix 5). These elements were disregarded. The remaining elements results of below detection limit ("< x") were replaced by 0.5 times detection limit for further data processing.
In the case of the gas samples of September 2008, statistical methods were applied. The software program STATGRAPHICS Plus 5.0 (STATPOINT TECHNOLOGIES, Inc.) was used for this purpose. Thereby it was checked whether the measured contents in the six samples are significantly different from the blank of the NaOCl solution. Thus for each element the KRUSKALL-WALLIS test or STUDENT-t test was used, depending on the distribution of the six sample contents, which was previously checked by the KOLMOGOROV-SMIRNOV test. Obvious outliers were identified by the GRUBBS test. After removal of the outlier the residual samples contents were again checked for distribution and significance. For the level of significance $\alpha = 0.05$ was used for each test. Finally, 12 elements were found that show significant concentration in the samples with respect to the blank (Appendix 6). For these elements both the results and the detection limits from the ICP-MS analysis were corrected for the dilution (1 + 41).
For the gas samples of May 2008 the ICP-MS results were not checked for a significant difference between the blank and the samples since only 4 samples were not sufficient for a

[2] http://www.actlabs.com/gg_hydro_can.htm (25/06/2009)

reliable statistical processing. Further calculations were done with these elements for which the blank of the trapping solution was lower than at least on sample.
Now, for the selected elements the blank of the NaOCl solution was subtracted from each sample content. By the recorded time for filling the 16 L gas bag during sampling the gas flow was calculated. This gas flow associated with the recorded time for gas trapping in the NaOCl solution the volume of gas that could be trapped in the solution was computed. By multiplying the elemental concentration in the solution (after subtraction of blank) and the volume of the NaOCl solution one obtain the respective mass. Relating this mass to the volume of dissolved gas in the solution the elemental concentration in the gas phase is obtained.

3.4 Water analysis

3.4.1 On-site parameters

On-site parameters pH-value, specific electrical conductivity (EC), temperature, oxygen content and redox potential were determined immediately after sampling in the field laboratory on Panarea Island. For this purpose the water samples were directly taken from the sampling syringes without filtration.

During the diving campaigns in May and September 2008 the specific electrical conductivity (EC) of the water samples was identified with a WTW LF 320 conductivity meter and a WinLab Data Line Conductivity-Meter from WINDAUS Labortechnik, respectively, together with a WTW TetraCon 325 conductivity electrode. The reference temperature was set to 25 °C with a linear temperature correction of 2% per K. To check the device the electrical conductivity of a 0.5 M KCl standard solution was measured. Thereby a value of 55 mS/cm (in May 2008) and 59.2 mS/cm (in September 2008) resulted at a temperature of 28.3°C (September 2008). Thus, the measured values differ from the exact value of 54.6 mS/cm.

The pH-value, the water temperature and the content of dissolved oxygen were measured with a LDO HQ20 portable dissolved oxygen/pH meter (in May 2008) and a HQ40d multi-parameter meter (in September 2008) by HACH Company. The pH electrode of HQ20 had a 4 M KCl inner electrolyte, for the HQ40d a 3 M KCl inner electrolyte. Calibration for dissolved oxygen for both devices was not necessary since the sensors contain a LED lamp

which acts as internal standard (or reference) for the calibration of the whole optical system[3]. For pH measurements a multipoint calibration was performed with pH standards ranging between pH 2 and pH 10 (Appendix 11). The resulting calibration line of HQ20 pH meter had the following equation (9):

$$\mathbf{pH = -0.0179\ [mV] + 7.1007,\ R^2 = 0.9984} \qquad \mathbf{(9)}$$

For the HQ40d multi-parameter meter calibration yielded the regression line (10) as follows:

$$\mathbf{pH = -0.0175\ [mV] + 7.1783,\ R^2 = 0.999} \qquad \mathbf{(10)}$$

After one week the accuracy of the pH-meter was checked again to ensure good values.

The redox potential was determined using a WinLab Data Line pH-Meter from WINDAUS LABORTECHNIK together with a silver/silver chloride (Ag/AgCl) electrode from PCE. Both electrodes had a 3 mol/L KCl solution as inner electrolyte. During the campaign in September 2008 the procedure of measurement was improved to avoid contact with the atmosphere as much as possible. Immediately after the dives the waters in the sampling syringes were cautiously filled into a titration vessel. After inserting the Ag/AgCl electrode through holes in the cap, latter ones were sealed with Parafilm.

Measured values had to be corrected for the temperature of 25 °C and converted to the potential of a standard hydrogen electrode in order to get the correct redox potential E_h. Correction for the temperature was done by equation 11, whereas E_m is the measured redox potential and T the water temperature.

$$\mathbf{E_{25°C} = Em - 0.198 * (T - 25°C)} \qquad \mathbf{(11)}$$

The conversion to the potential of a standard hydrogen electrode was realised by adding a correction factor (207 mV for the Ag/AgCl electrode with 3 mol/L inner electrolyte at 25 °C (Hölting, 1996)) (equation 12).

$$\mathbf{E_h = E_{25°C} + 207\ mV} \qquad \mathbf{(12)}$$

For varying pH values among different samples the pH-independent rH value is a better quantity for the comparison of redox potentials. It was computed by equation 13, whereas E_N is the Nernst voltage, being 59.16 mV for 25 °C (Hölting, 1996).

$$\mathbf{rH = 2 * E_h/E_N + 2 * pH} \qquad \mathbf{(13)}$$

[3] http://www.hach-lange.de/common/documents/1005/1007/10099_LDO_lab_extern_d.pdf (25/06/2009)

3.4.2 Ion sensitive electrodes (ISE)

The activity of fluoride was determined with WinLab Data Line pH-Meter from WINDAUS, a fluoride electrode F 500 and a reference electrode from WTW. The calibration was performed for standard seawater (SSW) (composition see Sieland (2009)). The following equations for calibration were established for the diving campaigns in May (14) and in September 2008 (15) (Appendix 12).

$$\mathbf{y\ [mV] = -60.225 * lg(c) + 63.117,\ R^2 = 0.9992} \qquad \mathbf{(14)}$$

$$\mathbf{y\ [mV] = -61.333 * lg(c) + 11.067,\ R^2 = 0.9996} \qquad \mathbf{(15)}$$

whereas: y = measured potential and c = fluoride concentration in mg/l

A sample volume of 25 ml was utilised mixed with 10 ml TISAB solution (Total Ionic Strength Adjustment Buffer) in order to adjust the ionic strength and the pH-value. Instead of the sample, for calibration 25 ml of SSW was taken added by 10 ml TISAB and step wise by a 1 g/L fluoride standard solution. The mixture was continuously homogenised by a magnetic stirrer during the measurement that lasted for approximately 20 min.

Beside fluoride also the iodide concentration in the sampled waters was determined by ion sensitive electrodes (Sieland, 2009).

3.4.3 Colorimetry

Filtered water samples were analysed by photometry with respect to sulphide ($H_2S(aq)$, HS^-, S^{2-}), manganese (Mn_{tot}), phosphate (PO_4^{-3}), nitrite (NO_2^-), iron (Fe_{total}, Fe^{2+}) and ammonia (NH_3) (Sieland, 2009). It was realised with a DR/890 Colorimeter (HACH).

Sulphide compounds could be measured in the range between 0 and 0.07 mg/L with a precision of ± 0.02 mg/L. The estimated detection limit (EDL) is 0.01 mg/L (instruction manual by HACH). When measuring range was exceeded the procedure was repeated in higher dilution. Due to interferences with the seawater matrix measured values had to be corrected according to (Rohland, 2007).

3.4.4 Ion chromatography

In the laboratory of Hydrogeology, TU Bergakademie Freiberg water samples were analysed be means of ion chromatography (IC) to determine ionic concentrations of lithium (Li^+), sodium (Na^+), potassium (K^+), calcium (Ca^{2+}), magnesium (Mg^{2+}), manganese (Mn^{2+}), chloride (Cl^-), sulphate (SO_4^{2-}) and bromine (Br^-).

For cations an ion chromatography system 6000 from MERCK/HITACHI was utilised (Sieland, 2009).

Anions were determined with ion chromatograh IC 2001 from Eppendorf/Biotronik with an anion suppressor column (FGC 1AG-P). As the mobile phase an eluent consisting of 2 mM $NaCO_3$ and 4 mM $NaHCO_3$ with a flow rate of 2 ml/min arranged the transport through the column. Samples were measured in two different dilutions, 1+300 (for Cl^-) and 1+20 (for F^- and Br^-). Sulphate could be determined in both solutions. Calibration was performed by measuring series of standards in the respective dilutions (Appendix D1).

3.4.5 TIC determination

Determination of total inorganic carbon (TIC) dissolved in the water samples was performed on the one hand by titration and on the other hand with a TIC analyser.

In order to gain first results titration was performed after sampling in the field laboratory on Panarea Island. Thereby 25 ml of the unfiltered sampled waters were added by NaOH or HCl (0.1 mol/L for the campaign in May, 1.0 mol/L in September 2008) stepwise to reach pH 8.2 or 4.3, respectively. For performance a digital titrator (by HACH) equipped with a cartridge filled with NaOH or HCl was used. With the consumption of NaOH as well as HCl the content of dissolved CO_2 and dissolved HCO_3^- could be calculated. The delivered volume of acid or base by titration was quoted as the amount of revolutions of the titrator, whereas 1 ml equals 800 revolutions. The concentration of dissolved CO_2 (c_{CO2}) and HCO_3^- then could be computed by equation 16 and 17, respectively.

$$\mathbf{c_{CO2} = c_{NaOH} * V_{NaOH} / V_{sample}} \quad \textbf{(16)}$$

$$\mathbf{c_{HCO3^-} = c_{HCl} * V_{HCl} / V_{sample}} \quad \textbf{(17)}$$

whereas: c_x = concentration [mol/L], V_x = volume of acid or base, V_{sample} = 25 ml

The pH-value was measured by WinLab Data Line pH-Meter from WINDAUS. For the diving campaign in May 2008 the device was previously calibrated by a two point calibration

with pH standards of pH 4.0 and 7.0. Therefore the inner calibration stored in the device was used. For the diving campaign in September 2008 calibration was performed by the measurement of pH standards ranging from pH 2 to pH 10. Following calibration function was obtained (equation 18) (Appendix 11):

$$\mathbf{pH = -0.0174 * [mV] + 7.0215,\ R^2 = 0.999} \qquad \mathbf{(18)}$$

Due to the limited volume of the water sample, in most cases it could only performed one titration step either for CO_2 or HCO_3^-. Based on only one specie no TIC could be determined. Furthermore, the results varied between the samples, probably because of different CO_2 degassing during the analysis. Thus, only the TIC results measured by the TIC analyser were used for the evaluation.

This was performed in the laboratory of Hydrogeology of the TU Bergakademie Freiberg. The water samples, stored in 50 ml glass flasks, were analysed by a LiquiTOC elemental analyser (ELEMENTAR ANALYSENSYSTEME GmbH). Depending on the anticipated TIC content sample volumes of 2.38 ml or 1.18 ml (May 2008) and 2.4 ml or 1.4 ml (September 2008) for the respective infrared (IR) range were applied. Due to detection of carbon dioxide (CO_2) all water samples were acidified with phosphoric acid (H_3PO_4) (1.75 mol/L) in order to transform all carbonate species into carbon dioxide.

For the further evaluation the TIC results in C mg/l were converted to hydrogen carbonate (HCO_3^-) and CO_2 in mg/L in relation to their respective pH value (in accordance with Kunze and Schwedt (2002)).

3.5 Depth profiles of TIC and pH

Discharging gaseous CO_2 from fumaroles at the seafloor is dissolving into the seawater during their ascent towards the sea surface. To evaluate the enrichment of dissolved inorganic carbon in seawater due to the emission of hydrothermal fluids both in the liquid and gaseous state water samples were taken at particular depths above seafloor discharges. The water samples were analysed for TIC as mentioned above, including the determination of the pH value. In this way, for five sites in each case a depth profile of the dissolved inorganic carbon content was achieved. The profile was taken at the beginning of a dive while descending at the buoy or while descending within a characteristic exhalation spot (e.g. Point 21 and Bottaro West).

Beside TIC also profiles of pH, EC and water temperature were taken in the investigation area. This was done from a boat, whereas along transect lines 13 and 20 depth profiles were measured in May and September 2008, respectively (Fig. 21 and 22). During the diving campaign in May 2008 the parameters were measured with a multi-parameter probe 650 MDS (YSI Inc.), having a 50 m data cable, coiled up on a cable reel. A Multi-Parameter Water Quality Monitor 6820 (YSI Inc.) was plugged into the cable reel. The logging of data was set to 1 s. In September the pH values were measured with the pH sensor WQ201 by GLOBAL WATER with a data cable of about 30 m length. Water depth, EC and water temperature were measured by a CTD-Diver (VAN ESSEN INSTRUMENTS) fixed at a 30 m rope. The data cable and rope were bond together. Both instruments logged their measurements every second and were synchronised to a computer clock in advance.

Both the multi-parameter probe and WQ201 pH-sensor were previously calibrated. For latter probe pH standards ranging from pH 4.0 and 10.0 were used for an inner calibration that is stored in the software of the sensor. Subsequently, the value of a standard with pH 7.0 was checked (result: pH 6.99). The multi-parameter probe was also calibrated through an inner stored calibration routine with pH standards of pH 4.0 and 7.0. For the EC the multi-parameter probe was checked by use of a 0.5 M KCl solution. The measured value of 57.2 mS/cm differed a little from target value of 54.6 mS/cm. EC measured by the CTD-Diver was automatically calibrated.

The profiles were taken by lowering the instruments slowly to the sea floor and slowly lifting them up again to the sea surface. Both for the lowering and lift up the geographic coordinates were determined by a GPS (GARMIN E-Trex, geodetic date: WGS84). The coordinates were noted every time, no continuos logging of the boat's track were performed. Before lowering the instruments the water depth was determined by a mobile echo sounder (Echotest II, PLASTIMO).

Measured values were stored as ASCII-files (Appendix D2). The parameters of pH (by WQ201 pH-sensor) as well as EC, water temperature and water depth (by CTD-Diver) could join together based on the synchronised time.

Measured GPS data were processed by TRANSDAT 12.04 software (KILLETSOFT, limited version). In order to convert the measured geographic coordinates from [degree. arc minute. arc second] to [degree] it was used location "Italy" and "WGS84 (World wide GPS), geocentric, WGS84" as geodetic datum in the software. The "summands" and "multiplier" for Northing and Easting were set to 0.0 and 1.0, respectively.

Measured depth profiles of pH value, water temperature and EC as well as the corresponding coordinates were displayed by means of the software program Ocean Data View (ODV) (Schlitzer, 2008). Since GPS coordinates were noted for both lowering and lift up of the instruments, both series of measurement were handled as one profile each. For three locations only one profile downward or upward could be measured. Logged data between measurements, e.g. while driving with the boat, were ignored for the display by ODV. For interpolation between the depth profiles in order to create a 2D-face with shading and contouring the DIVA gridding tool of the ODV software was utilised.

The DIVA (Data-Interpolating Variational analysis) gridding tool was developed at the University of Liege[4]. It generally produces better results than the weighted average methods, built into ODV, in case of sparse and heterogeneous data coverage (ODV User's Guide). The software allows spatial analysing and interpolating data in an optimal way, comparable to the optimal interpolation (OI). But unlike OI it also takes coastlines and bathymetry features into account to structure and subdivide the domain where estimation is performed (ODV User's Guide). Calculations are highly optimised and rely on a finite element mesh adapted to the specific gridding domains (ODV User's Guide). DIVA have been successfully performed in various oceanic data analysis[5]. The DIVA software is an implementation of VIM (Variational Inverse Method). VIM was initially designed for climatology, where generally high resolution vertical profiles but irregular horizontal coverage demands for a spatial analysis and horizontal interpolation.

3.6 Gas quantification

In order to quantify the submarine hydrothermal gas output of the investigation area the gas flow rates of all gas exhalations should be determined and summed up. It was restricted to five diving sites (Bottaro West, Bottaro North, Fumarolic Field (close to Hot Lake), Point 21 and Black Point) where quantification was realised during the diving campaign in September 2008.

Measurements were carried out by means of the stainless-steel funnel, which was also used for gas sampling. The funnel (diameter 19.3 cm, height: 45 cm) was placed on seafloor over

[4] http://modb.oce.ulg.ac.be/projects/1/diva (25/06/2009)
[5] http://www.stareso.ulg.ac.be/Stareso/Projets_2_files/Poster%20methodes%20inverses.pdf (25/06/2009)

the gas emission, covering the whole exhalation area. The captured gas was accumulating in a chamber above the funnel until seawater was completely displaced through a bypass. The gas was conducted through the bypass and a short flexible hose directly into an inverted high density polyethylene (HDPE) bottle with a total volume of 1.2 L. Time for complete water displacement in the bottle was noted and based on this, the resulting gas flow rate was calculated (Fig. 7). In most cases the outlet gas temperature was measured additionally by means of a digital thermometer (GMH 3350, GREISINGER ELECTRONICS) which was encapsulated in a home made container. It was performed by inserting the sensor several centimetres into the sediment or rock fractures at the emission point of the fumarole. In order to compensate varying outlet gas temperatures the measured flow rates were converted with respect to a reference temperature. For this purpose the SATP (standard ambient temperature and pressure condition) temperature of 25 °C were applied. The conversion was realised by the ideal gas law for isobaric change of state (law of GAY-LUSSAC) (19):

$$\mathbf{V_m / T_m = V_s / T_s} \qquad \mathbf{(19)}$$

whereas: V_m and T_m are the measured gas flow rate and temperature, respectively; V_s = gas flow rate at the standard temperature (T_s) of 25°C

In this way measurements of the gas output rate of 48 fumaroles were carried out at three different sites (Appendix 13).

Since each site is featured by several hundreds of fumaroles, it was practically impossible to measure all gas flow rates. Therefore, a clustering was established to classify the fumaroles with respect to their intensity of gas release. The established methodology is in accordance with Italiano and Nuccio (1991). It was decided for four classes of gas output rates since all fumaroles could relate to four groups by divers depending on the extent of the formed column of gas bubbles. Based on the measured times for water displacement the range of the gas output rate for each class was defined (Table 4). Furthermore, the respective flow rates of the 48 examined fumaroles were used to compute the average gas flow rate of each class.

Table 4. Classes of gas output based on measurement of 48 fumaroles in September 2008

class	**A**	**B**	**C**	**D**
range of gas flow rate [L/min]	< 2.1	2.1 - 3.6	3.6 - 7.2	> 7.2
number of vents	23	8	6	11
mean [L/min]	1.06	3.04	4.86	9.89
standard deviation [L/min]	0.53	0.47	1.18	2.13

Then, all gas exhalations at the five diving sites were counted and sorted into one of the four classes. The total gas flow rate of each site was obtained by multiplying the number of respective fumaroles and the mean of each class. The result was additionally corrected for the hydrostatic pressure, which is represented by the average water depth of each site. Again the ideal gas law was used for correction, in this case for isothermal change of state (law of BOYLE-MARIOTTE) (20):

$$\mathbf{p_c * V_c = p_s * V_s} \qquad \mathbf{(20)}$$

whereas: V_c and p_c are the computed gas output and average hydrostatic pressure of the site, respectively; V_s = gas output at the sea surface with pressure p_s = 101.325 kPa

Numerous diffuse gas exhalations in the crater of Bottaro West account considerably for the total output of the entire diving site. The field of diffuse exhalations, having an almost circular shape, was examined separately. A diameter of 5.5 m was measured which results in a base area of 23.8 m^2. At six positions within the field the emitting gas rate was measured as mentioned above. Again correction was applied for the gas temperature and hydrostatic pressure. With the mean of the measured gas flow rates Ψ_i, the partial area A_i covered with the gas sampling funnel (293 cm^2) and the whole base area of the field A it was possible to calculate the total gas output of the field (21) (Appendix 14).

$$\mathbf{\Psi = \Psi_i * A / A_i} \qquad \mathbf{(21)}$$

At least 10 fumaroles in the Panarea area discharge greater amounts of gas (> 40 L/min) and can therefore not been determined with the above described technique. It is suggested that at maximum a gas flow rate of about 40 L/min could be detected by the method of water displacement in the 1.2 L bottle which mean a complete water displacement in less than 2 seconds. Furthermore, the more intense gas release makes it dangerous for the diver to handle with the funnel and bottle due to much higher buoyancy. Hence an improved methodology was operated during the diving campaign in September 2008.

For this type of fumaroles a much larger funnel and a flow through cell measurement device was developed, called FSVG (Flowmeter for Submarine Volcanic Gas emission) (Bauer et al., 2009) (Fig. 7). For two large fumaroles at Point 21, defined as “Melanie” and “Claudia” the system was applied to measure the gas flow rates over a period of several hours. It was recorded three series of measurement for the “Melanie” and one serial for the “Claudia” fumarole (Appendix D3). All measured flow rates were again corrected for the respective gas temperature and hydrostatic pressure.

Unfortunately, only two fumaroles at Point 21 were examined by the technique. Based on these results the gas release of further larger fumaroles at Point 21 and Bottaro North were estimated through the comparison of photos (see section 4.2.1).

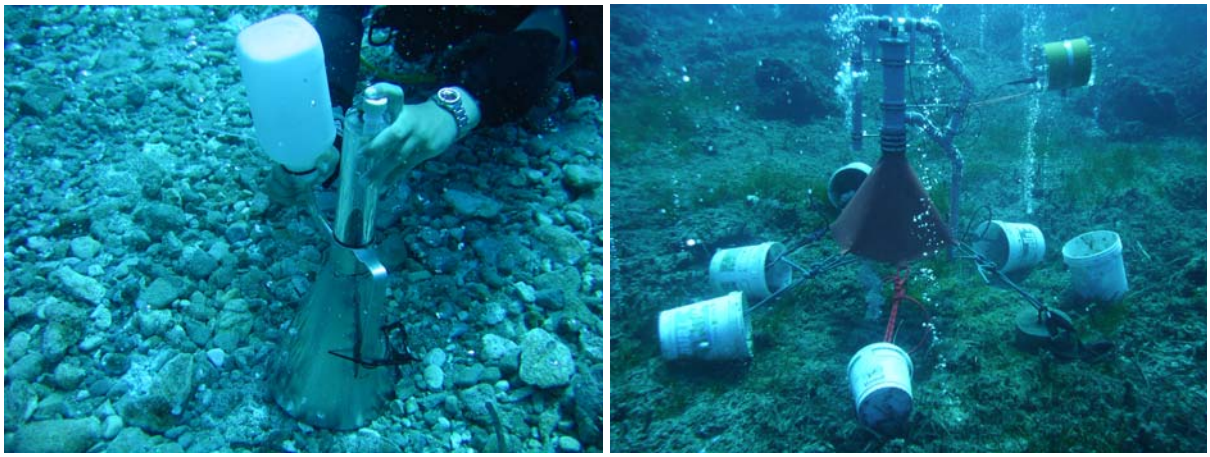

Fig. 7. Determination of gas flow rates of the submarine discharging gases; left: based on time-dependent water displacement in a bottle, gases were captured by a gas sampling funnel; right: the system of the FSVG for intensely gas emitting fumaroles (WISTAU, 2008).

4. Results and evaluation

4.1 Gas composition

4.1.1 Results of compositional analysis

In general the emitting fumarolic gases of the Panarea hydrothermal system predominantly consist of water vapour. However, in this study it was not looked for water vapour in the gases due to lack of an adequate methodology. As water vapour is cooling under the boiling point during the ascent of the gas phase towards the seafloor and the contact with cold seawater steam condenses and is mixing with the ambient seawater. Thus, it is unlikely that a huge content of water vapour can be detected in the vapour phase. But, considering the large and very intense exhaling vents it can not be excluded that these gases contain water vapour.
Measurements of steam concentrations of subaerial fumaroles at La Calcara (on the north-eastern coast of Panarea Island) have yield 93 vol.% in the mid 1980's (Italiano and Nuccio, 1991) and about 95 wt.% in the period between November 2002 and June 2004 (Capaccioni et al., 2007). Latter authors had detected water vapour also in the submarine gas samples. For the Bottaro West and Bottaro North site they determined concentrations in the range between 68.74 and 11.16 wt.% as well as between 61.36 and 17.84 wt.%, respectively. Thereby, steam concentrations showed a decreasing trend from November 2002, the onset of the submarine gas eruption, until June 2004.
In the dry gas fraction analysed carbon dioxide (CO_2) was the most abundant specie, ranging from 96.1 to 99.6 vol.%, as average concentration of the samples from May and September 2008, for the appropriate sites (Fig. 8, Appendix 8). The residual proportion is predominantly defined by the concentration of hydrogen sulphide (H_2S) reaching up to 4.0 vol.% in the sample of Bottaro North in May 2008. Both species show an inverse distribution of the concentrations. Additionally, minor gas species like nitrogen (N_2), methane (CH_4), oxygen (O_2), hydrogen (H_2), carbon monoxide (CO), helium (He) as well as the sum of the hydrocarbons ethane and ethene (C_2H_6/C_2H_4) were detected in the submarine gases in the range between 10^{-1} and 10^{-5} vol.%, respectively (Fig. 9 and 10). Volatile trace elements detected in fumarolic gas flows will mentioned in more detail in section 4.1.3.

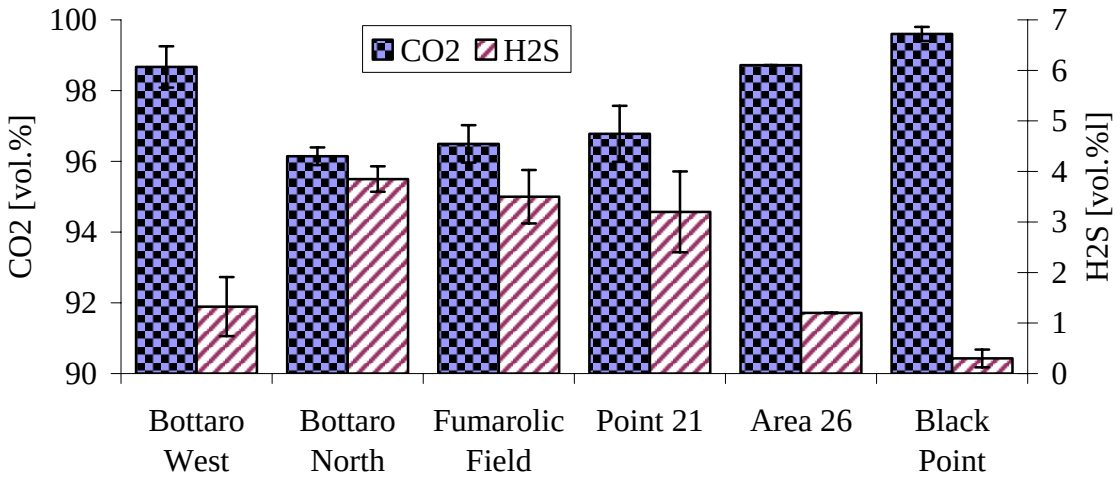

Fig. 8: Average contents of CO_2 and H_2S of the hydrothermal gases sampled in May and September 2008

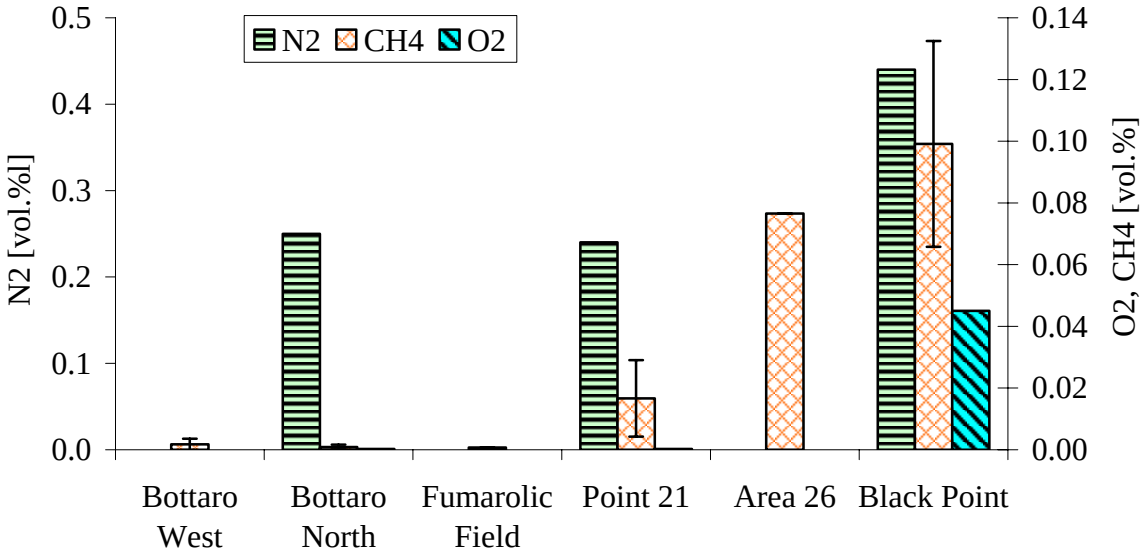

Fig. 9. Average contents of N_2, O_2 and CH_4 of the hydrothermal gases sampled in May and September 2008 as well as from July 2008 (N_2 and O_2) sampled and analysed by Dr. Francesco Italiano (INGV Palermo).

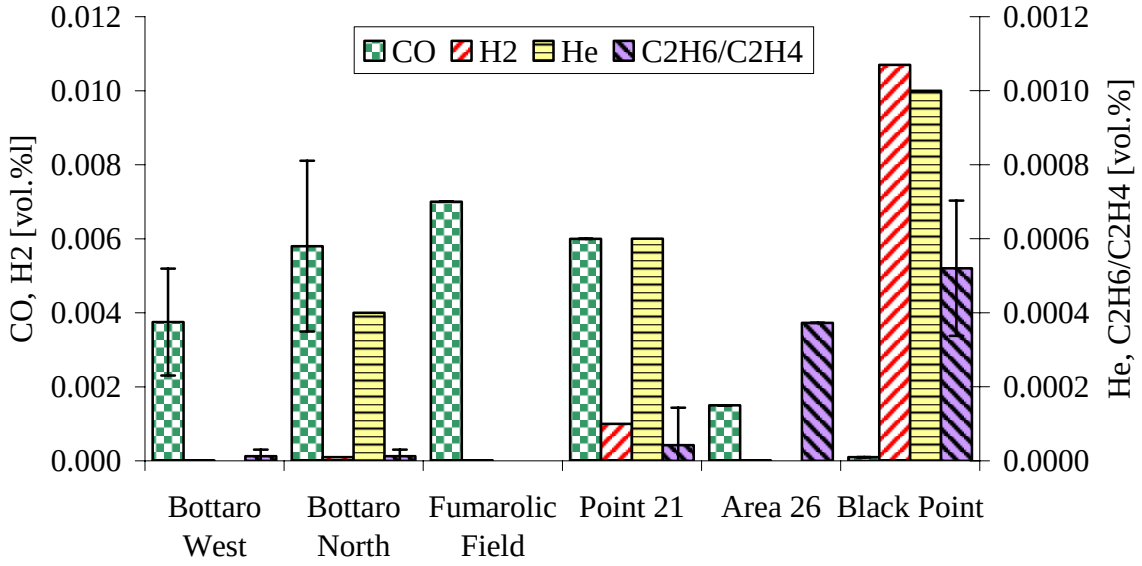

Fig. 10. Average contents of CO, H_2, He and C_2H_6/C_2H_4 of the hydrothermal gases sampled in May and September 2008 as well as from July 2008 (H_2 and He) sampled and analysed by Dr. Francesco Italiano (INGV Palermo).

4.1.2 Evidence for sources and hydrothermal processes affecting the composition of the gas phase

Due to the sparse amount of species analysed in the gas phase of the sampled hydrothermal discharges external data were additionally consulted in order to evaluate the processes that have been affected the composition of the emitted gases.

4.1.2.1 Atmospheric endmember and dissolution processes

The submarine hydrothermal gases were altered on the path towards their emission points. So, the composition analysed for the sampled gases did not represent the composition of the original deep gases. But it could reveal information about the extent of subsurface processes within the hydrothermal system which caused the modification. Two main processes are supposed to affect the composition of the hydrothermal gases through interaction with seawater. One is based on the equilibrium of seawater with the atmosphere (air saturated seawater) which causes an enrichment of atmospheric compounds in the gas phase, such as N_2, O_2 and Ar (Chiodini et al., 2006). These compounds are dissolved in seawater that is permeating beneath the sea floor into the hydrothermal fluids. On the other hand the deep original gas underwent partial dissolution based on the different solubility of the gas species

in water. A further process that influences the physico-chemical conditions of the hydrothermal system might be the input of deep magmatic gases.
In the following the detected gaseous composition of the seafloor discharges will be evaluated with respect to these processes.

The submarine gases sampled in May and September 2008 were CO_2-dominated, and no water vapour was assumed to exist. For the period from November 2002 to June 2004 concentrations of water vapour in the submarine hydrothermal gases were measured by Capaccioni et al. (2007). The authors reported of a progressively decreasing H_2O/CO_2 ratio in the gas phase for the Bottaro West site from about 2.5 in November 2002 to about 0.15 in June 2004. Thereby, the predominance of CO_2 against H_2O was already reached in March 2003. A significant input of deep magmatic gases into the hydrothermal system was expected to cause the degassing crisis in 2002, probably also responsible for the input of magmatic derived water vapour. A debilitated condensation of steam due to high velocity of the ascending deep gases towards the seafloor might result in the detection of high concentrations of water vapour in these gases. After November 2002 the magmatic gas supply from depth was progressively decreasing and the hydrothermal system was shifted back towards a liquid-dominated hydrothermal system with lower temperatures. Thus, less magmatic water vapour was added into the hydrothermal system and the removal of water vapour from the gas phase by condensation was increasing again, resulting in a return towards CO_2-dominated gas emissions at the seafloor since March 2003 (Capaccioni et al., 2007). It may also be possible that the rise of a small magma chamber was prompt boiling the surrounding water causing huge expansion by a factor of about 1000 which finally lead to the explosion and the detection of water vapour even at the sea floor.

The occurrence of oxygen in the submarine discharging gases can indicate an atmospheric endmember to a certain extent at shallow levels (Caracausi et al., 2005a). Also most nitrogen is due to an atmospheric contribution but can also originate from magma (Nicholson, 1993). Additionally, noble gases, typically of atmospheric origin, such as He, Ar and Ne, can be found in hydrothermal gases (Capaccioni et al., 2007, Caracausi et al., 2005a) and confirm an atmospheric contribution either by contamination with ambient air, while sampling procedures beneath or above the sea surface or by dilution of original hydrothermal gas with air saturated seawater. Although, He and Ar can be leached from rocks, too (Nicholson, 1993).

One gas sample from the Black Point taken and analysed in July 2008 by Dr. Francesco Italiano (INGV Palermo) has conspicuous higher concentrations of O_2 and N_2 than sampled gases from other sites (Fig. 9) indicating a higher contribution of air saturated seawater. Two other samples from the Point 21 site and Bottaro North, also sampled in July 2008, were depleted in O_2, which can be explained due to a consumption of oxygen for redox reaction, probably oxidation of sulphides (Caracausi et al., 2005a, Italiano and Nuccio, 1991).
Gases sampled for this study in May and September 2008 might by influenced by air contamination since selective diffusion over longer periods of time was likely (see section 4.1.4). Although, this statement can not be proofed since N_2 or O_2 in the sampled gases were not analysed by the author.

Another tool to evaluate the atmospheric contribution to the hydrothermal gas composition is the $^4He/^{20}Ne$ ratio. Primarily, it is used to correct the measurement of He isotopic ratios. Again, it was measured for the gas samples of July 2008 by Dr. Francesco Italiano (INGV Palermo). For the Bottaro North, Point 21 and Black Point sites ratios of 29.1, 102.1 and 149.4 were determined, respectively. Ratios determined in former times for the submarine hydrothermal field of Panarea ranged between 20 and 630 (Italiano and Nuccio, 1991) for the mid 1980's and between 38 and 389 (Capaccioni et al., 2007, Caracausi et al., 2005a) for the period between November 2002 and June 2004, respectively. Since the $^4He/^{20}Ne$ ratio of air is 0.318, these values suggest a very low air contamination as well as a low atmospheric contribution to the geothermal circulation (Italiano and Nuccio, 1991). The $^4He/^{20}Ne$ ratios, normally 2 to 3 orders of magnitude higher than the typical atmospheric ratio, provide further evidence for the contribution of magmatic fluids (Caracausi et al., 2005a).

Between the most abundant species in the gas phase of our samples, CO_2 and H_2S, there is a correlation, with a Pearson correlation coefficient of R^2 = 99.5 % (SPEARMAN rank correlation coefficients of -1.0 for each specie and P-values = 0.0000 < 0.05) (Fig. 11). The more CO_2 occurred in the dry gas phase, the less H_2S has been detected. By means of this ratio the five investigation sites could be distinguished from each other. The highest concentrations of CO_2 together with the lowest concentrations of H_2S were determined for the Black Point site. In contrast, the lowest CO_2/H_2S ratios were determined for the Bottaro North site, Fumarolic Field and Point 21. The gases of Bottaro West and Area 26 show ratios between both clusters (Fig. 11).

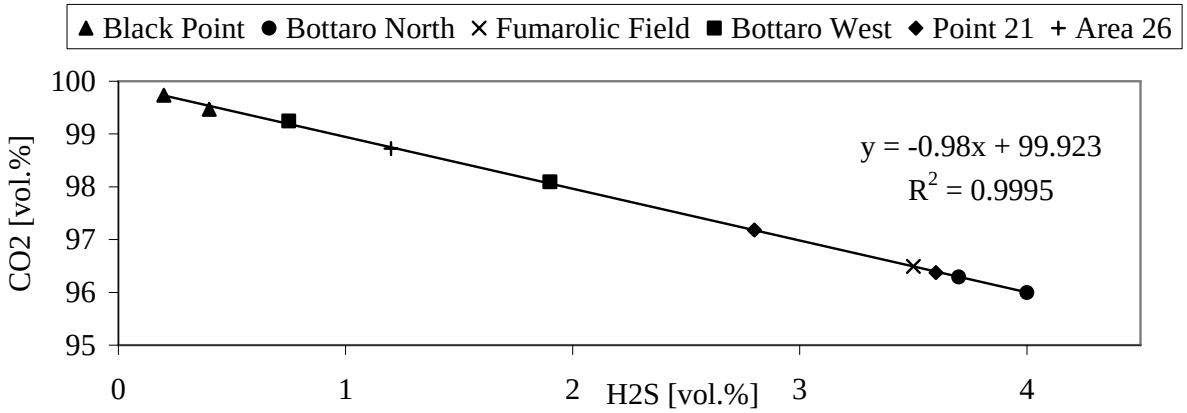

Fig. 11. CO_2 vs. H_2S in the sampled gases from May and September 2008 as well as the linear regression line

The different CO_2/H_2S ratios are likely the result of gas scrubbing effects that took place in different extension between the sites. The process is due to the interaction of deep gases with the thermal modified seawater of the hydrothermal system. The hydrothermal fluids absorb volatiles degassed from shallow magmas, but were also fed through condensation of magmatic gases upon cooling (Symonds et al., 2001). Gas scrubbing mostly affects well soluble acid gases like HCl, HF and the most abundant gaseous S-species (H_2S and SO_2). The process includes dissolution into the aqueous phase (e.g. hydrolysis) and formation of precipitates (e.g. elemental sulphur, sulphides, fluorides, sulphates) from gas-water and gas-water-rock reactions (Symonds et al., 2001).

Since H_2S features an about 3 times higher solubility in water than CO_2 (see Table 2) it is depleted in the gas phase relative to CO_2 in a two-phase hydrothermal fluid at equilibrium. Thus, the emitted gases with high values of H_2S seemed to be exposed to gas scrubbing to a lower extent, probably because of a higher rate of ascent towards the sea bottom. That is particularly quite conceivable for the Bottaro North and Point 21 sites, both having several large vents with intense gas discharges.

Furthermore, dissolved H_2S is oxidised by seawater sulphate (SO_4^{2-}) as well as by dissolved oxygen to form elemental sulphur which is precipitated around the emission point of each fumarole as snow-white deposits (Italiano and Nuccio, 1991) and populated by sulphur reducing micro-organisms.

Finally, the author supposed that the CO_2/H_2S ratio increased with increasing migration of the hydrothermal gases due to more intense gas scrubbing and precipitation of elemental sulphur by oxidation of H_2S.

4.1.2.2 Hydrocarbons

For hydrocarbons only the light alkanes methane and in some cases the sum of ethane and ethene were detected in the gas samples. Peaking values of hydrocarbons were detected for the samples of Black Point and with decreasing concentrations for Area 26 and Point 21 (Fig. 9 and 10).

High methane concentrations are typical for organic-rich sedimentary rocks at depth in low temperature geothermal systems (Nicholson, 1993). An addition of significant amounts of biogenic gases (mainly CH_4) might also be produced at relatively shallow depths (Capaccioni et al., 2007). The most likely methane formation is based on the FISCHER-TROPSCH reaction (Nicholson, 1993) (22):

$$\mathbf{CO_2 + 4H_2 \leftrightarrow CH_4 + 2H_2O} \qquad \mathbf{(22)}$$

On the other hand, CH_4 can be removed by oxidation to CO_2 from the gas phase.

Additionally, light alkanes can originate from thermal decomposition of organic matter as well as bacterial degradation of organic matter at temperatures lower than 50 °C (Capaccioni et al., 2007).

Furthermore, for the first weeks after the onset of the submarine gas burst in November 2002, also light alkenes and isoalkenes were detected by Capaccioni et al. (2007). They used the temperature and redox-dependent ratio of Σalkenes/Σalkanes, being about two orders of magnitude higher in November 2002 than in previous investigations which indicates an increase of temperature or an increase of less reducing conditions or a combination of both within the hydrothermal system (Capaccioni et al., 2007).

4.1.2.3 Temperature and redox-dependent gas species

The reactive gas species H_2S, H_2 and CO in the sampled gas of 2008 differed in their contents between the six investigation sites (Fig. 12). Despite partially high standard deviations it is obvious that high H_2S contents occurred together with high CO contents. Beside very low H_2 concentrations detected for samples from Bottaro North and Point 21 samples, there was detected a high concentration of H_2 of 107 ppm for the Black Point site (data for H_2 from Dr. Francesco Italiano (INGV Palermo)).

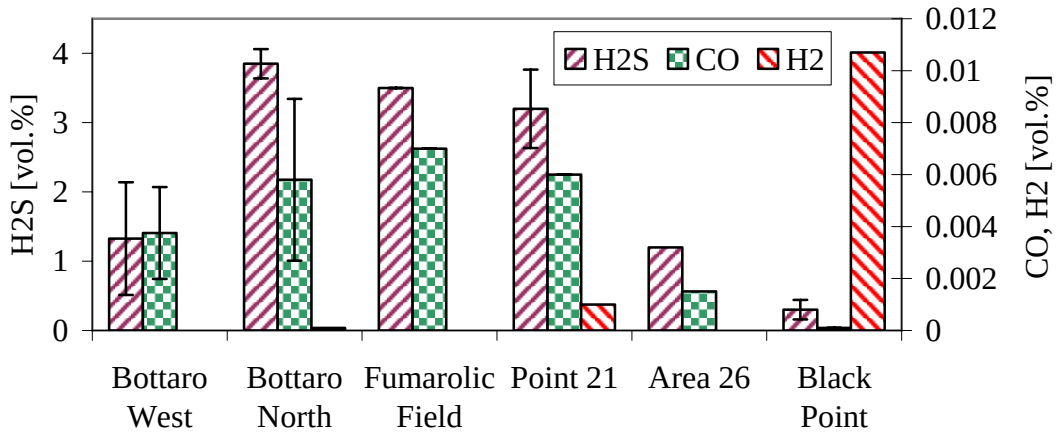

Fig. 12. Average contents of H_2S, CO and H_2 in the sampled gases from 2008 of the Panarea submarine hydrothermal system. Results of H_2 are from Dr. Francesco Italiano (INGV Palermo)

The temperature- and redox-dependent species H_2S, H_2 and CO equilibrate as SO_2/H_2S, H_2/H_2O and CO/CO_2 redox pairs in the gas phase at magmatic conditions. Thereby, H_2S is favoured by decreasing reaction temperature and increasing reducing condition while CO and H_2 are conversely favoured by the increase of both the reaction temperature and reducing condition at their equilibrium (Capaccioni et al., 2007). Despite these contradicting conditions required for high H_2S, CO and H_2 contents, the measured concentrations of H_2S and CO show a correlation (Fig. 12). But the H_2 contents show an absolute different spatial distribution between the sites. Thus, additional processes than different equilibrium temperatures and redox conditions might cause the different concentrations of CO and H_2.

Hydrogen is readily removed in geothermal systems on reaction with wall rocks and is thereby commonly lost over time with increased migration (Nicholson, 1993). Furthermore, H_2 is also a limiting factor for the sulphate reduction by chemolithotrophic microbes to form biologically generated H_2S (Rouxel et al., 2004). Similar to the different degree of gas scrubbing, due to a different velocity of migration towards the seafloor which probably affect the H_2S content, CO could be encountered to equilibrium reactions to different degrees in dependence on its respective gas migration.

Beside others, Capaccioni et al. (2007) used the temporal and spatial variations of the H_2S, CO and H_2 concentrations to reveal temporal changes in the temperature regime and redox condition at different sites of the Panarea hydrothermal system in the period from November 2002 to June 2004.

4.1.2.4 Isotopic ratios of the gas species

The most abundant gas component in geothermal systems is CO_2 (Nicholson, 1993). It can originate from different sources, which can be defined by the isotopic ratio of $^{13}C/^{12}C$ of CO_2. Isotopic ratios of $^{13}C/^{12}C$ of carbon dioxide, expressed as $\delta^{13}C$ (CO_2) notation (versus PDB), were determined by Sieland (2009) for the gas samples of May and September 2008 (Table. 5). The values of $\delta^{13}C$ (CO_2) ranged between -7.30 and +0.3 ‰ PDB, whereas only the Black Point sample of September had a slight enrichment of ^{13}C.

Similar values were reported by Italiano and Nuccio (1991), in the range between -3.20 and -1.06 ‰ (PDB). Capaccioni et al. (2007) determined values of $\delta^{13}C$ (CO_2) ranging between -2.61 and -1.41 ‰ (period from November 2002 to June 2004) for the sites of Bottaro West and Bottaro North, respectively.

Values of $\delta^{13}C$ (CO_2) lower than -3.0 ‰ PDB are suggested to originate both from a decarbonisation process of marine carbonate as well as certainly from degassing of the subducted slab and magma (Capaccioni et al., 2007, Italiano and Nuccio, 1991, Dando et al., 1999). Italiano and Nuccio (1991) assumed more negative $\delta^{13}C$ values in original deep gases altered due to dissolution processes.

Table 5. Isotopic ratios of $^{13}C/^{12}C$ (CO_2), $^{34}S/^{32}S$ (H_2S) (from Sieland (2009)) and $^{3}He/^{4}He$ (by Dr. Francesco Italiano (INGV Palermo)) of the gas samples.

site	date	$\delta^{13}C$ (CO_2) [‰ PDB]	std	$\delta^{34}S$ (H_2S) [‰ VCDT]	std	$^{3}He/^{4}He$ [R/Ra]
Bottaro West	May 08	**-7.30**	*0.06*	**4.19**	*0.16*	
Bottaro West	Sep 08	**-3.20**	*0.00*	**-**	-	
Bottaro North	May 08	**-5.40**	*0.00*	**1.59**	*0.20*	
Bottaro North	Jul 08					**4.35**
Bottaro North	Sep 08	**-2.90**	*0.04*	**5.73**	*0.08*	
Fumarolic Field	Sep 08	**-4.60**	*0.03*	**6.56**	*0.08*	
Point 21	May 08	**-6.50**	*0.08*	**0.78**	*0.20*	
Point 21	Jul 08					**4.39**
Point 21	Sep 08	**-2.50**	*0.04*	**5.00**	*0.08*	
Area 26	Sep 08	**-2.70**	*0.00*	**3.26**	*0.05*	
Black Point	May 08	**-4.00**	*0.05*	-	-	
Black Point	Jul 08					**4.35**
Black Point	Sep 08	**0.30**	*0.04*	**7.73**	*0.06*	
La Calcara (Panarea)	Jul 08					**4.34**

Values for $\delta^{34}S$ of H_2S determined for the 2008 gas samples (from Sieland (2009)) ranged from +0.78 to +7.73 ‰ (VCDT), with the lightest $\delta^{34}S$ (H_2S) value in the gas samples of May

for Point 21 and Bottaro North and the highest $\delta^{34}S$ (H_2S) value for Black Point sampled in September (Table. 5). For the significant lower values of May in contrast to the September samples of Bottaro North and Point 21 it was assumed a higher input of magmatic derived H_2S which is depleted in ^{34}S (Sieland, 2009). The measured values are quite well in the range for hydrothermal fluids, from -0.2 to 7.7 ‰ (VCDT), venting on the seafloor of back arc basins (Yang and Scott, 2006).

Sources for sulphur in hydrothermal systems can be sulphur originating from leaching of igneous rocks and that from reduction of a small amount of admixed seawater-derived sulphate (Rouxel et al., 2004). Thus, the measured $\delta^{34}S$ (H_2S) values in the range of 0.78 to 7.73 ‰ (VCDT) might be explained by mixing of these two components, seawater derived sulphur with $\delta^{34}S$ of about 21 ‰ and rock-derived sulphide with $\delta^{34}S$ of about 0 ‰ indicating that most of the H_2S is derived from leaching of rock (Ono et al., 2007). Beside thermo-chemical reduction of seawater sulphate also microbial sulphate reduction at temperatures below 100 °C is possible (Rouxel et al., 2004). A further supposable process might be the dissolution of a magmatic component containing uncontaminated mantle sulphur with $\delta^{34}S$ ~ 0 ‰ (Cortecci et al., 2005). Moreover, fractionation processes has to be considered.

The $^3He/^4He$ ratio of the submarine gas samples from July 2008 were analysed by Dr. Francesco Italiano (INGV Palermo). The values of the $^3He/^4He$ ratio (R), expressed as R/R_a (R_a = atmospheric $^3He/^4He$ ratio of $1.386 * 10^{-6}$ (Caracausi et al., 2005a)) resulted to 4.35 for Black Point and Point 21, 4.39 for Bottaro North and 4.34 for the subaerial fumaroles of La Calcara on Panarea Island (Table 5). Thus, a ^3He-rich magmatic component in the Panarea gases is suggested by the high R/R_a ratios (Caracausi et al., 2005a, Italiano and Nuccio, 1991). Temporal variations of the R/R_a in the period from November 2002 to June 2004 indicated a varying input of deep magmatic fluids into the hydrothermal system (Capaccioni et al., 2007). The helium isotopic ratio measured at Panarea after November 2002 was in the range of that of the Aeolian Islands, which decreases from 6.2 R/R_a to 3 - 4 R/R_a from Vulcano Island to the Stromboli Island, respectively (Capaccioni et al., 2007).

4.1.3 Volatile trace elements

In the following the wording volatile trace elements is used for elements which occur as gaseous species or aerosols. However, within this study it was not distinguished whether an element formed gaseous species or occurred as aerosol.

In general, the detected elements in the sampled gases from May differ from those of September (Table 6), latter ones were restricted to aerosols < 25 nm. Only five elements (Mg, K, Rb, Co and Pb) were detected in the gases of both sampling periods. In the gases sampled in May 2008 16 elements were detected, for the September ones only 12. This might indicate the removal of aerosols > 25 nm composed of these elements that were detected in May but not in September (Br, Sr, Ba, Zn, Al, Cs, Cu, Zr, Tl, La and Ce). However, there are also some elements detected in the gas samples of September but not in May which is not explainable with this theory (Ni, Cd, Mn, Hf, Nd, Yb and Au). Looking at the concentrations in comparison with the respective elemental abundance in seawater, one can notice that major elements in the oceans, such as Mg, K and Br, are also highest concentrated in the gases and aerosols. But some minor and trace elements of seawater, like Ba, Ni, Al, Zn, Cu, Mn and Pb, were detected in the gases and aerosols of May and/or September in high concentrations, too.
Some elements occurred only in the gases and aerosols of one site (Mg, Zr, Tl, Co, Cd, Mn, Hf, Pb, Yb and Au), in most cases Black Point (e.g. Zr, Tl, Cd, Mn and Hf). Particularly, for the gases and aerosols < 25 nm it is also the site where most volatile elements were detected in the sample. But, the highest concentration varies among the sites from element to element.

Table 6. Volatile elemental concentration in µg/m3 for the hydrothermal gases sampled in May and September 2008 in the order of the respective elemental concentration in seawater (from Brown et al. (1995))

	Bottaro West	Bottaro North	Point 21	Black Point	Bottaro West	Bottaro North	Fumarolic Field	Point 21	Area 26	Black Point	Seawater [mg/L]
	May				September						
Mg	313	0	0	0	0	0	0	0	0	2242	1290
K	2083	2475	547	1583	7688	0	5125	6406	10250	1281	380
Br	4167	4703	629	1978	0	0	0	0	0	0	67
Sr	18.8	2.5	1.9	0	0	0	0	0	0	0	8
Rb	2	0.248	0.164	0	1.54	0.51	1.54	2.88	8.20	1.28	0.12
Ba	688	272	27.3	135	0	0	0	0	0	0	0.02
Zn	94	0	34.2	344	0	0	0	0	0	0	5.0E-04
Ni	0	0	0	0	205	77	359	320	205	525	4.8E-04
Al	208	743	82	0	0	0	0	0	0	0	4.0E-04
Cs	0.417	0	0	0.158	0	0	0	0	0	0	4.0E-04
Cu	125	50	8.2	7.9	0	0	0	0	0	0	1.0E-04
Cd	0	0	0	0	0	0	0	0	0	1.92	1.0E-04
Mn	0	0	0	0	0	0	0	0	0	32	3.0E-05
Zr	0	0	0	0.791	0	0	0	0	0	0	3.0E-05
Tl	0	0	0	0.119	0	0	0	0	0	0	1.0E-05
Hf	0	0	0	0	0	0	0	0	0	0.064	7.0E-06
Co	0	1.11	0	0	1.67	0.64	0	0	1.15	0.58	3.0E-06
La	0.313	0	0.068	0.119	0	0	0	0	0	0	3.0E-06
Nd	0	0	0	0	0	0.51	0.26	0.32	0.77	0.51	3.0E-06
Ce	0.729	0.124	0.096	0.277	0	0	0	0	0	0	2.0E-06
Pb	4.17	2.48	0.55	6.33	0	0	0	0	15.4	0	2.0E-06
Yb	0	0	0	0	0	0	0	0.16	0	0	8.0E-07
Au	0	0	0	0	0	0	0	7.37	0	0	2.0E-08

One possible interpretation of the varying values between the gas samples could be the different gas flow rates as well as the different durations for conducting the gas samples through the washing bottle filled with NaOCl solution. It resulted in total trapped gas volumes in the range between 40 L and 110 L for the gases sampled in May 2008 and between 13 L and 32 L for the samples of September, respectively. Compared to previous analyses of volatile elements in the Panarea submarine gases there were huge differences with respect to detected elements due to a different methodology (Rohland, 2007). Otherwise, because of filtering of the gases before trapping was performed for the first time during the diving campaign in September 2008 in order to remove aerosols and particulates > 25 nm, further data is lacking to verify these results.

Among the detected volatile elements K, Cd, Rb, Zn, Cu, Br, Cs Tl, Au and Pb are reported to be typical elements carried by fumarolic fluids (Fulignati et al., 2006). Moreover, Cd, Br, Au, Cs and Pb are considered to be of magmatic origin (Fulignati et al., 2006). Thereby, most trace elements are volatilised from shallow magma degassing as simple chlorides, although, some elements can occur as sulphides, oxyacids, oxyhalides, hydroxides, hydrides and as native elements (Fulignati et al., 2006).

Due to dissolution processes the characterisation of pure degassed material in discharging hydrothermal fluids is difficult (Rubin, 1997). Furthermore, the representation of the detected volatile elements for a magmatic and/or hydrothermal origin is critical since the high elemental concentration of the trapping solution itself, may perturb the original composition of the discharged gases and aerosols.

The trace element analyses of the water samples revealed a general enrichment of many major, minor and trace elements in the Panarea hydrothermal fluids (Sieland, 2009). Thereby, all elements detected in the gas phase are also enriched over seawater in the hydrothermal fluid discharges except for Mg and Hf.

4.1.4 Critical evaluation of the applied methodology

Sampling was performed by conduction of the seafloor discharging gases towards the sea surface with a Teflon hose. At sea surface the gases were stored in gas bags for transportation and analyses. Until analyses they were exposed to pressure and temperature conditions different to the conditions at their emission point at the sea bottom. Therefore, possible chemical reactions between the gases as well as condensation of vapours and further dissolution processes in the condensates due to decreasing pressure can not be excluded. Slight compositional changes may also occur in the stored gas bags over the period of several hours and days. This may lead to an atmospheric contamination through diffusion of the Tedlar (PVF) gas bags (DuPont)[6] and other possible weak points for leakage of the bags, like the on/off valve and septum valve. Thus, the analysed gas composition might be different from the original composition of the hydrothermal gases emitting from the seafloor.

[6] http://www2.dupont.com/Tedlar_PVF_Film/en_US/assets/downloads/pdf/h49725.pdf (25/06/09)

Another problem was that only few gas constituents could be analysed in the gas samples mainly due to limited instrumentation. Thus, external data had to be used for gas species which are also crucial for an evaluation of the hydrothermal conditions.

The problem of the gas sampling at the sea surface instead directly at the emission and the storage in gas bags may be solved by applying an alternative method.
For submarine application many studies reported of sampling discharging gases directly at the emission point on sea floor with two-way sampling bottles (Pyrex bottles) filled by the dry gases through water displacement (Chiodini et al., 2006, Italiano and Nuccio, 1991, Gugliandolo et al., 2006). The sampled gases were analysed for the common gas composition of the major and minor gas species as well as isotopic ratios of $\delta^{13}C$ (CO_2) and $^{3}He/^{4}He$. Thereby, H_2S and CO_2 were analysed by use of reactive DRÄGER tubes or by gas chromatography (GC) with a thermal conductivity detector (Caracausi et al., 2005a, Gugliandolo et al., 2006, Italiano and Nuccio, 1991). However, the determination of H_2S by Dräger tubes is considered as critical as the analytical tubes are known to provide semi-quantitative concentrations for H_2S in volcanic gases (Capaccioni et al., 2007).
Furthermore, in order to determine acidic gas species (CO_2, SO_2, H_2S, HCl, and HF), which are of very importance indicating variations of the input of deep magmatic gases, the methode described by Giggenbach (1975) has been most widely used. It is based on trapping the acid condensable species in an alkaline solution when sampling fumarolic gases directly at the seafloor emission in Pyrex bottles. However, it is doubtful to assume that no droplet of seawater is carried by the gases into the solution and thus, create a bias. Therefore, the gas sampling directly at the emission on seafloor is only reliable applied in order to determine uncondensable gases (N_2, O_2, CO, H_2, He, Ar, Ne, CH_4, and light hydrocarbons) as well as acidic species like CO_2 and H_2S in a sampling bottle unfilled with a solution for gas trapping. But the major problem is the limited sample volume of about 300 ml got by using the sampling bottles on seafloor. For the determination of ^{34}S (H_2S) a particular amount of sulphur is necessary which cannot get from a 300 ml gas sample. In this case, the applied method for this study had the advantage to obtain a gas sample volume up to 16 L through the gas conduction on the sea surface and storage in a 16 L gas bag.

4.1.5 Traces of magmatic gases in the liquid phase of the hydrothermal fluid discharges

Beside investigations with regard to the submarine hydrothermal gas discharges also thermal waters were sampled at the six diving sites Bottaro West, Bottaro North, Hot Lake, Point 21, Area 26, Black Point as well as Lisca Nera as a reference sample for non- or less influenced seawater by hydrothermal discharges. The water samples from May and September 2008 were analysed for on-site parameters, major, minor and trace constituents as well as isotopic ratios (Sieland, 2009). Some parameters will be evaluated in the following (Appendix 9 and 10) with respect to an impact of deep magmatic gases that may be dissolved in the liquid phase of the hydrothermal fluids in a considerable proportion.

4.1.5.1 On-site parameters

The specific electrical conductivity (EC) varied between 51.3 and 101.1 mS/cm (Fig. 13). Except for much higher values of Hot Lake and Black Point the remaining sites showed values close to 54 mS/cm, the EC of local seawater (Gugliandolo et al., 2006).

The pH ranged between 2.9 and 7.9 for the hydrothermal fluids (Fig. 14), whereas the hot fluids discharging at Black Point featured the lowest pH. The other sites were between 4.75 and 5.9, except Lisca Nera which was slightly below the pH of about 8.1 for local seawater (Gugliandolo et al., 2006).

The redox potential (E_h) ranged between -53.7 and +355.7 mV. Because of the significantly different pH among the different sites the redox potential was converted into the pH-independent rH value (Fig. 15). The average E_h of normal surface seawater is about 500 mV at pH ~ 8.2 (Merkel and Planer-Friedrich, 2002), which conforms a rH value of about 34. This equals the upper boundary for predominantly weak oxidising conditions (Hölting, 1996). The rH of the more or less uninfluenced water of Lisca Nera is in the lower field of predominantly weak oxidising conditions and is therefore much lower than the normal surface seawater redox potential. The samples of the remaining sites except Black Point had rH values between 7.9 and 12.4 and were characterised by strong reducing to predominantly weakly reducing waters. Only the Black Point thermal waters had a higher redox potential with values at the interface of predominantly weak reducing conditions to conditions of an indifferent system (Fig. 15).

Since oxygen is a major oxidising agent in natural solutions the redox potential is largely defined by the content of dissolved oxygen. Thus, the contents of dissolved oxygen show a

similar distribution among the investigated sites (Fig. 16) like the redox potential. High standard deviations are predominantly due to errors in measurement, for example based on different time until analysis as well as different exposure to atmosphere. Dissolved oxygen peaked at Lisca Nera, followed by Black Point. The average oxygen saturation was about 100 % and 74 % for Lisca Nera and the Black Point samples, respectively. On average the samples of Hot Lake were characterised by the lowest saturation of oxygen with about 10 %. At Area 26, Point 21, Bottaro North and Bottaro West oxygen was saturated by about 15, 22, 40 and 43 %, respectively.

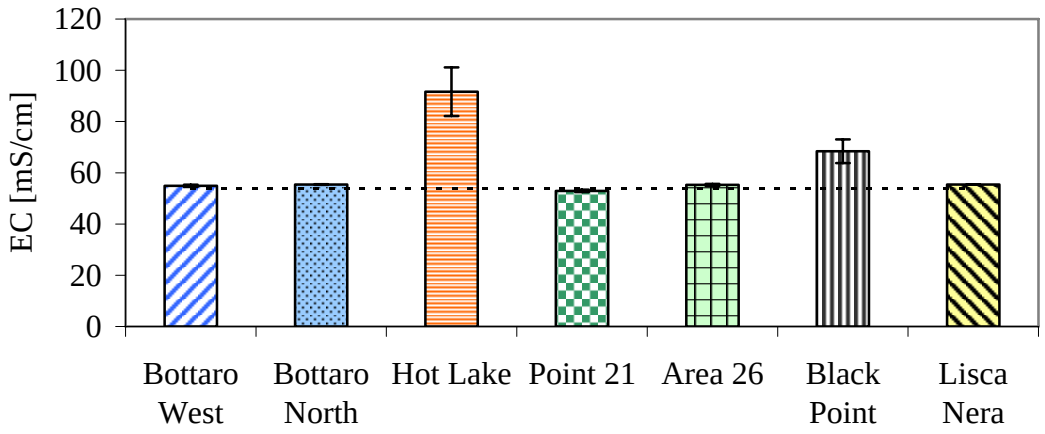

Fig. 13. Average EC values of the thermal water discharges sampled in May and September 2008. As reference the more or less uninfluenced seawater sample of Lisca Nera and the EC of local seawater (dashed line) are displayed.

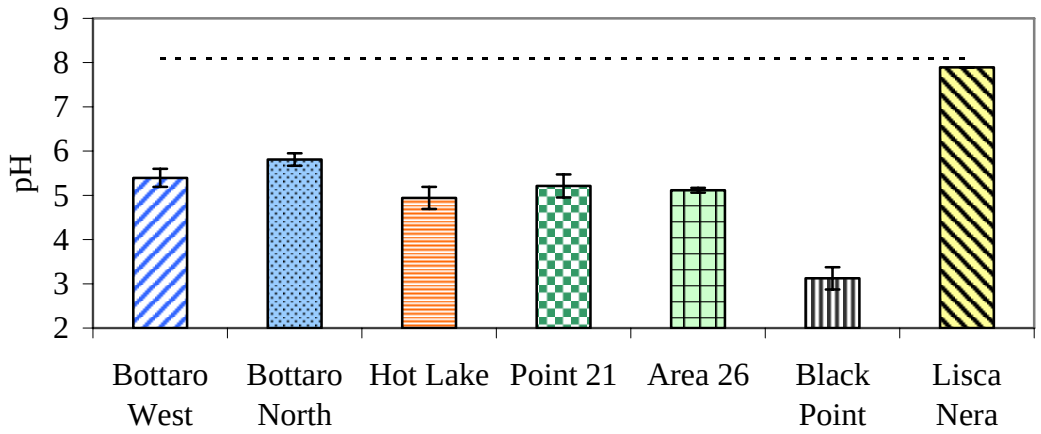

Fig. 14. Average pH of the thermal water discharges sampled in May and September 2008. As reference the more or less uninfluenced seawater sample of Lisca Nera and the pH of local seawater (dashed line) are displayed.

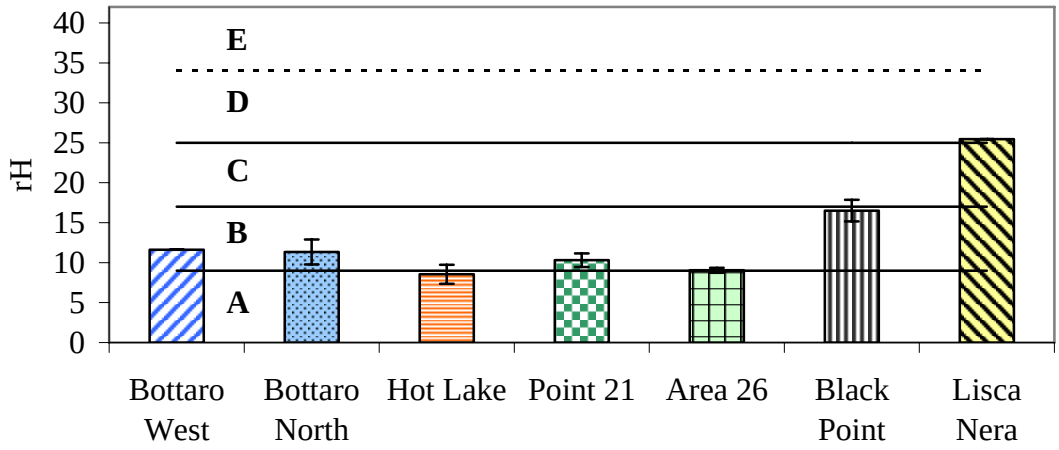

Fig. 15. Average rH values of the thermal water discharges sampled in May and September 2008. As reference the more or less uninfluenced seawater sample of Lisca Nera as well as the rH of normal seawater (dashed line) are displayed. Between the boundaries (solid lines) of rH = 0 and rH = 9 the solution is characterised by strong reducing conditions (sector A). The rH value of 17 is the upper boundary for predominantly weak reducing conditions (sector B), up to rH of 25 for an indifferent system (sector C), 25 to 34 for predominantly weak oxidising (sector D) and up to a rH of 42 for strong oxidising conditions (sector E) (Hölting, 1996).

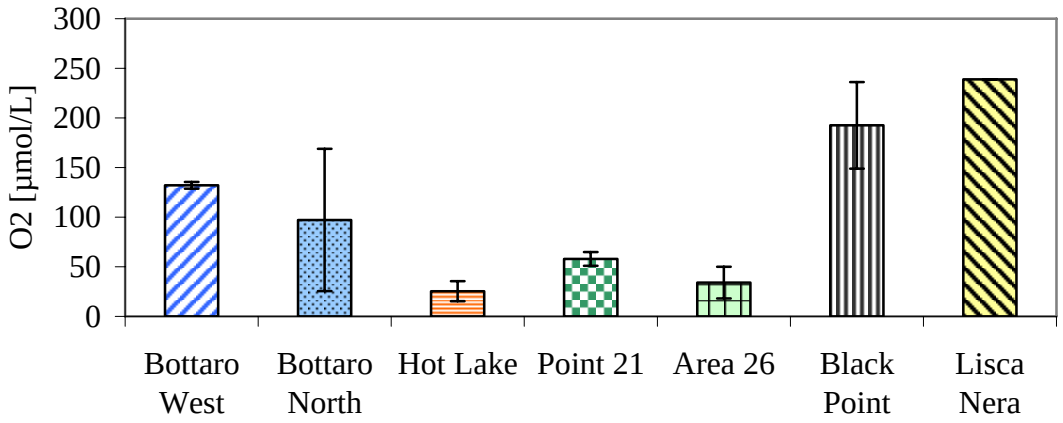

Fig. 16. Average dissolved O_2 concentrations of the thermal water discharges sampled in May and September 2008. As reference the more or less uninfluenced seawater sample of Lisca Nera is displayed.

The on-site parameters reveal different types of sampled waters. Predominantly, with respect to the EC, the thermal waters of Bottaro West, Bottaro North, Point 21 and Area 26 indicate an extensive dilution with ambient seawater. In contrary, the fluids of Hot Lake and Black Point were highly mineralised, thus indicating the emission of hydrothermal altered fluids. A low share of seawater for samples of these both sites were computed by Sieland (2009).

The redox potential (rH) of the Black Point site, including the content of dissolved oxygen, differed distinctively from the remaining sites. Beside the high EC, a very low pH and high fluid temperatures (up to about 135 °C, see Fig. 6) indicate the emission of hardly diluted

original hydrothermal fluid on the one hand. But on the other hand higher redox potentials and higher contents of dissolved oxygen closer to ambient seawater indicate a dilution by seawater. Thus, another process responsible for these values is likely. For example, Capaccioni et al. (2007) reported of more oxidising redox conditions for the Bottaro West site during the onset of the submarine gas eruption in 2002 caused by the input of magmatic fluids into the hydrothermal system. Therefore, it is likely that the Black Point site is fed by a small amount of deep magmatic fluids unlike the other sites.

However, this theory does not explain the high oxygen content also found in the gas phase of the Black Point sample (Fig. 9), which again argue for the input of seawater saturated with atmospheric oxygen.

The mainly reducing behaviour of the discharging hydrothermal waters at the different sites is also expressed by the measured distribution of dissolved redox-sensitive species (Sieland, 2009).

4.1.5.2 Dissolved sulphur and halogen species in the hydrothermal fluids

In this study it was not looked for acidic gases, typical for volcanic degassing like SO_2, HCl, HF and HBr, in the gas phase of the sampled hydrothermal fluids. Their high solubility in seawater causes dissolution into the hydrothermal fluid and depletion in the gas phase. Thus, the measured contents of some particular species dissolved in the sampled hydrothermal fluids will be evaluated in the following.

4.1.5.2.1 Sulphur species

The concentrations of the major dissolved S-species, sulphate (SO_4^{2-}) and sulphide (H_2S, HS^-, S^{2-}) are averaged for all waters sampled in May and September 2008 and displayed in Fig. 17. Sulphides analysed by photometry show strong variations between the samples of May and September 2008 compared to SO_4^{2-} measured by IC. In general, the total dissolved sulphur content of seawater consists predominantly of SO_4^{2-} which is about 29.45 mmol/l in local seawater (Gugliandolo et al., 2006).

The samples of Lisca Nera, Bottaro West and Bottaro North are close to this reference sulphate concentration. Thermal waters of Point 21 and Area 26 were somewhat depleted with sulphate contents of about 26 and 25 mmol/L, respectively. The strongest depletion of

sulphate with respect to local seawater was shown by the water samples from Black Point and Hot Lake. This indicates again the lowest intermixing with seawater.

The distribution of dissolved sulphide is similar to the H_2S distribution in the gas phase (Fig. 8). The average sulphide concentrations ranged between 0.02 and 1.1 mmol/l, whereas for the more or less uninfluenced site of Lisca Nera it was below the estimated detection limit (EDL). High average values of sulphide were determined for the water samples from Bottaro North, Hot Lake, Point 21, and Area 26, the lowest detected average contents were shown by Bottaro West and Black Point (Fig. 17). The high standard deviation of the sulphide contents in the Bottaro North waters is due to the value detected in May 2008, which is with about 1.1 mmol/L more than ten times higher than values measured in September 2008 and in previous campaigns. An explanation might be the sampling of thermal water at a different fumarole, while gas samples were taken always from the same vent in each campaign.

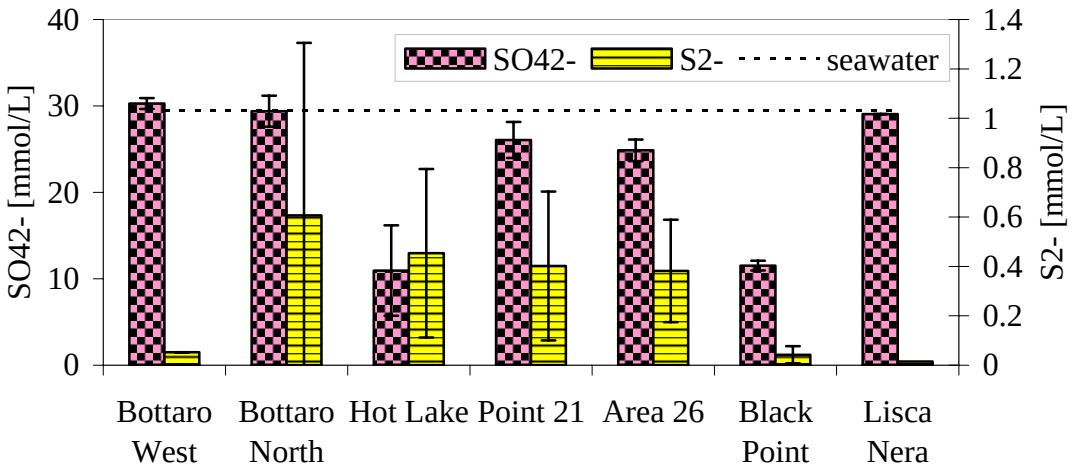

Fig. 17. Dissolved sulphate and sulphide in the water samples taken from the submarine hydrothermal discharges in May and September 2008. As reference the less influenced water of Lisca Nera is displayed, too, as well as the total sulphur content dissolved in local seawater (dashed line).

Sulphate contents are usually low in deep geothermal fluids, but increase with increasing oxidation of hydrogen sulphide (Nicholson, 1993) as well as an increasing input of seawater sulphate. Otherwise, the depletion of sulphate from the hydrothermal liquid phase is probably due to precipitation of anhydrite and partly by thermo-chemical reduction to sulphide.

The occurrence of the reduced sulphur specie sulphide in the sampled waters at all sites confirms reducing conditions with respect to the reference site of Lisca Nera. Higher contents indicate higher reducing conditions as being typical for original hydrothermal fluids (Herzig and Hannington, 2006). Conversely, sulphate concentrations close to those of seawater indicate high contamination by seawater sulphate of the original hydrothermal fluid. Thus, the

less contaminated hydrothermal fluid discharges of Hot Lake and Black Point had lowest sulphate concentrations of all water samples. Of the latter both sites, only Hot Lake had high sulphide contents since the distinctive higher redox potential of the Black Point fluid discharges exclude high contents of sulphide.

Isotopic analyses of $\delta^{34}S$ and partially $\delta^{18}O$ for dissolved sulphate and sulphide, $H_2S_{(g)}$, sulphide minerals as well as native S (S^0) revealed four probable distinct sources of sulphur as well as different processes affecting the different sulphur species (Sieland, 2009).

Finally, the acidic gas specie SO_2, indicating a deep magmatic input of magma degassed SO_2, which dissolves into the hydrothermal fluid can not clearly inferred by the contents of dissolved sulphate and sulphide. However, sulphur isotopic ratios of $H_2S_{(g)}$ indicate a magmatic component. Furthermore, a pH of about 3 measured in the water samples of Black Point indicate a further contribution than the principal hydrothermal acidification processes through water-rock interaction (Herzig and Hannington, 2006) as well as CO_2 that can only achieve values of pH > ~ 4.3. For lower pH a strong acid like H_2SO_4 formed from magmatic SO_2 is necessary.

4.1.5.2.2 Dissolved halogens F, Cl and Br

The detected contents of the halogens fluoride (F^-), chloride (Cl^-) and bromide (Br-) in the sampled thermal waters, as indications for dissolution of the acid magmatic gases HF, HCl and HBr, are displayed in Fig. 18 as average enrichment or depletion factors over the seawater content.

Despite partially high standard deviations, the analysed average contents show an enrichment of fluoride over the normal seawater content of 6.8 µmol/L (Millero, 1996) except for Hot Lake. For chloride only the hydrothermal discharging waters of Black Point and Hot Lake are enriched with a mean of 826 and 1217 mmol/L, respectively, over 655 mmol/L chloride in local seawater (Gugliandolo et al., 2006). At all other sites discharged waters are depleted with respect to the seawater chloride content. A similar distribution is shown for bromide. Beside a strong enrichment for Black Point and Hot Lake the other sites show bromide concentrations close to 0.99 mmol/L of local seawater (Gugliandolo et al., 2006).

With regard to the analysed contents of chloride and bromide the sampled water of Lisca Nera was similar to the composition of normal or local seawater and appears to be less infected by hydrothermal discharges. Only the content of fluoride was slightly enriched over the reference values of normal seawater.

The high chloride and bromide contents of Hot Lake and Black Point identify the water samples of these sites as hydrothermal modified waters, less contaminated by seawater. The evaluation of the different fluoride contents is limited by a high variance of the measured values, in particular for Black Point.

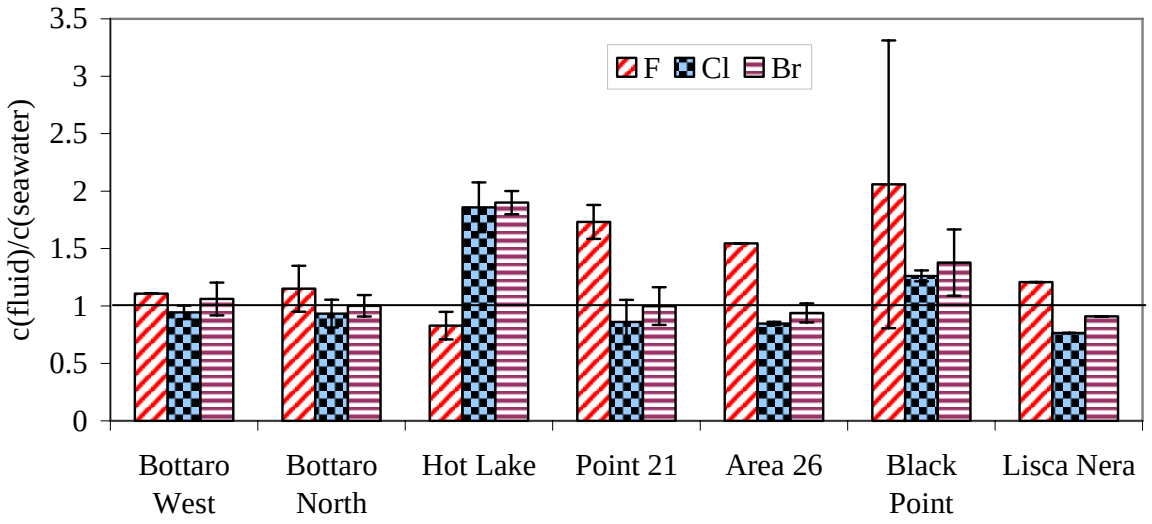

Fig. 18. Average factor of enrichment/depletion over normal or local seawater of fluoride (F^-), chloride (Cl^-) and bromide (Br^-) in the water samples taken from the submarine hydrothermal discharges in May and September 2008. As reference the less influenced water of Lisca Nera is displayed, too.

Geothermal fluids usually have fluoride contents lower than 526 µmol/L (< 10 mg/L, (Nicholson, 1993). High Ca concentrations provide the removal of F by formation of CaF minerals. Unusual high F^- contents, which are accompanied by very high Cl^- and SO_4^{2-} levels, can be produced by the condensation of volcanic gases (HF) into the hydrothermal fluid (Nicholson, 1993). But, all measured fluoride contents were below 526 µmol/L. The highest detected value of about 239 µmol/L was measured for one Black Point sample in September 2008 while another sample some days later only had 99 µmol/L. For the Black Point site fluoride contents of about 916 µmol/l were measured in 2006 while samples from other sites showed contents quite below 526 µmol/L (Tassi et al., 2009).

The strong enrichment of chloride in the Hot Lake and Black Point seafloor hydrothermal fluids (Hot Lake about 118% and Black Point by about 46% enrichment with respect to seawater) may be based on the process of phase separation. Furthermore, supercritical condensation and subsequent remixing of the brine and vapour phase as well as the input of magmatic derived HCl and the dissolution into the thermal modified waters are considered to

cause such high chloride contents in the sampled waters discharging at both sites (Sieland, 2009).

Bromide is usually included at very low levels in geothermal fluids, except were seawater is a component of the geothermal fluid (Nicholson, 1993). Thus, at all sites except for Hot Lake and Black Point the bromide content was close to local seawater, whereas for Hot Lake and Black Point a distinct higher bromide enrichment over seawater was measured.

Finally, considering the very low pH values in the thermal waters of Black Point and the high enrichment of Cl^-, F^- and Br^- over seawater, it is likely that the hydrothermal fluid at the Black Point site is fed by the deep magmatic gases HCl, HF and HBr. These strong acids, as well as the already mentioned H_2SO_4, can cause pH values below about 4.3, which is the maximum acidification can be realised only by CO_2.

4.1.6 Inorganic carbon

The detected content of total dissolved inorganic carbon (TIC) in the sampled waters is displayed in Fig. 19. By means of the respective pH the proportion of HCO_3^- from TIC was computed (see section 3.4.5).

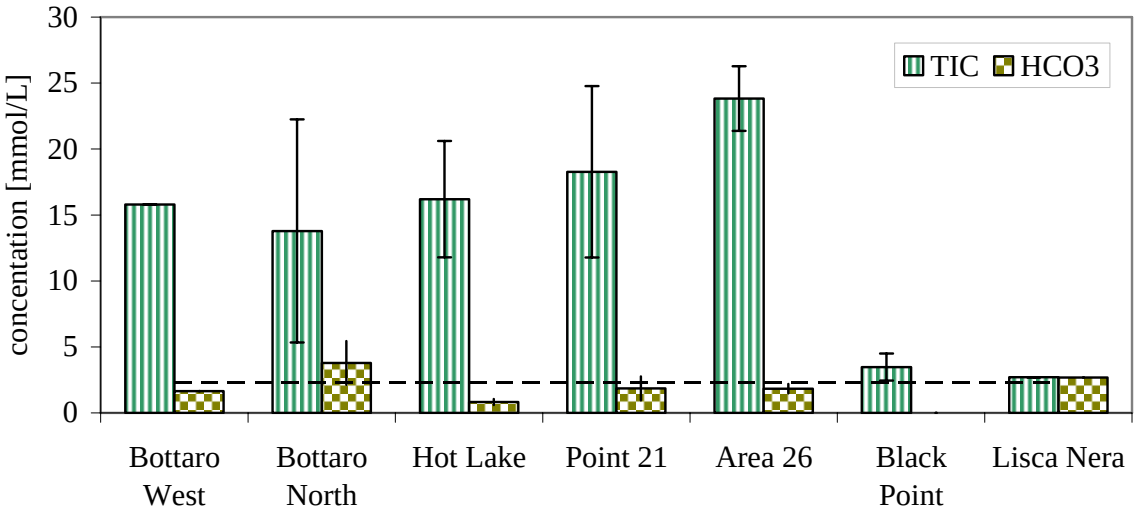

Fig. 19. Concentrations of TIC and HCO_3^- in the water samples taken from the submarine hydrothermal discharges in May and September 2008 compared to the total carbon concentration of normal seawater (dashed line). As reference the less influenced water of Lisca Nera is displayed, too.

The average TIC content in the sampled waters was distinctively enriched at all sites except for Black Point and the more or less uninfluenced site of Lisca Nera. The TIC content of the latter site was close to the total carbon content of normal seawater of 2.33 mmol/L (Brown et al., 1995). For Black Point, the low concentration of inorganic carbon conflicted with the peak CO_2 concentration in the gas phase. But, due to the low pH values of the sampled waters, ranged between 2.9 and 3.4, the predominant species was CO_2(aq) which tends to escape as CO_2(g) into the atmosphere and less TIC was detected in the water sample. Beside the Black Point samples all sites were also depleted or close to the total carbon content of normal seawater.

4.1.6.1 Depth profiles of pH and TIC

Due to the rapid decrease of pressure and temperature affecting the discharging gases condensation and dissolution into seawater take place. Thus the ambient seawater is altered by the dissolution of acidic gases as well as by mixing with discharging acidic hydrothermal waters. Thus, the seawater may predominantly be altered close to the emission spots on the sea floor. To evaluate the extent of influence in the seawater column, depth profiles of TIC as well as of the pH, water temperature and EC were measured. Furthermore, the dissolution process of the ascending CO_2-rich gases will be evaluated in order to derive statements whether the gases are completely dissolving or reaching the sea surface and escaping directly into the atmosphere.

4.1.6.1.1 Depth profiles of TIC at the investigated sites

Since emitted gases consist predominantly of CO_2, water samples were taken from different water depths above a venting area on the sea floor to analyse for the TIC content as well as for the respective pH value (Fig. 20). Comparing both graphs the profiles of TIC and pH show converse variations with increasing depths. The higher the TIC content the lower the pH value indicating that the major carbon specie that cause the variations of both parameters is CO_2 which is predominantly emitted in the gas phase and is subsequently dissolving in seawater.

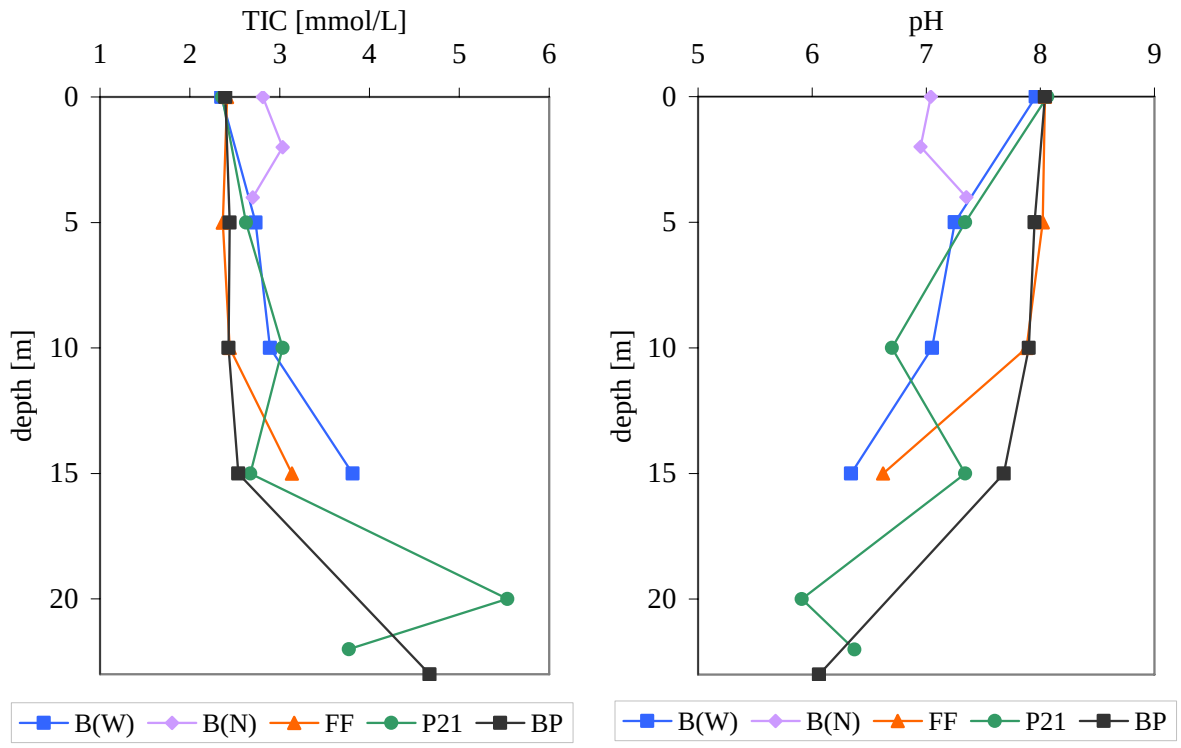

Fig. 20. Depth profiles of TIC and pH above a venting area on the seafloor at the sites of Bottaro West B(W), Bottaro North B(N), Fumarolic Field (FF), Point 21 (P21) and Black Point (BP)

At all five sites, except for Bottaro North, the TIC content and pH value at sea surface is almost equal the TIC content and pH of seawater of about 2.33 mmol/L and 8.1, respectively (Brown et al., 1995, Gugliandolo et al., 2006) (Fig. 20). Thus, at the water surface above these sites no indications for a CO_2-rich gas emission at the seafloor could be detected in the seawater composition with regard to the dissolved carbon content and pH value. With increasing water depth the TIC increases as well as the pH decreases gradually to the highest or lowest value, respectively, which is reached in most cases at the emission centre on the seafloor. Thereby, the increase of TIC or the decrease of pH is stronger for Bottaro West and Point 21 than for Black Point and the Fumarolic Field. This is likely due to sampling above a diffusive exhalation field at Bottaro West and above a large vent at Point 21 with respect to the profiles above less strong emission centres at Black Point and Fumarolic Field. In the latter cases, only the sample at the seafloor was taken close to an emission spot.

The profile of Point 21 and Bottaro North show rather variations than a gradually increase or decrease of the parameters, unlike the other sites. This can be explained by the strong emitting intensity of some large fumaroles which cause the formation of huge gas bubbling columns those rise CO_2-enriched seawater less laminar. Furthermore, at Bottaro North site the large fumaroles are located in a shallow water depth of only about 8 m. The intensity of the rising

plume of gas bubbles can still be seen at the sea surface at calm days and causes a strong mixing of the discharged hydrothermal fluids and the surrounding seawater. Thus, TIC content and pH are higher and lower, respectively, than the values for seawater along the whole depth profile. The highest TIC content was measured at 20 m depth (equals about 2 m above a large fumarole) at Point 21, followed by the seafloor sample of Black Point which was directly taken at the blackish sinter body emitting very hot, acidic and CO_2-rich fluids.

4.1.6.1.2 Depth profiles of pH, T and EC along transects

Beside the depth profiles for TIC dissolved in seawater above the investigated emission sites also depth profiles were taken between these sites within as well as outside the shallow submarine crater surrounded by the outcropping islets. Aim of this investigation was the evaluation of the ambient seawater body affected by hydrothermal gas and water emissions from the seafloor.

By lowering and lifting a multi-parameter probe (or individual probes coupled) depth profiles of pH, water temperature and specific electrical conductivity were measured along line transects. The 2D-face generated by interpolation between the measured profiles (see section 3.5) is displayed in Fig. 21 and 22 for May 2008 and September 2008, respectively. In May the transect crossed the investigation area from the east to the west with a distance of about 3.5 km between the outermost points and including the profiles at Black Point, Point 21 and Hot Lake. In September a shorter distance was covered. Three parallel transects were investigated, with the middle line crossing the sites of Black Point, Point 21 and Hot Lake, the southern one Bottaro North and Bottaro West and the northern one Area 26.

Generally, in September variations of the pH value were larger than in May. Furthermore, the water temperature as well as the EC showed higher values in September than in May. In the graphs of May only the emission field of Point 21 can be identified by slight lower pH values of 6.5 to 7 with respect to the pH of about 8 of the ambient seawater. Certainly, lower pH values were measured in water samples taken directly at the discharging fumaroles. But by lowering and lifting the pH probe at sea surface from a boat measurements directly in or very close to the vents were practically not possible. However, both in May and September it was hit on the submarine depression of Hot Lake which is marked by distinctive high temperature and EC values in Fig. 21 and 22.

In the profiles of May, one can see that the pH of the surrounding seawater was only influenced in the vicinity of Point 21 site up to some meters towards the sea surface, and at Black Point directly at the seafloor. Otherwise the residual profiles along the transect show no influence on the seawater pH within and outside the crater area. Except for the Hot Lake emission point no significant variation can be observed in the T and EC profiles.

In the profiles of September 2008 (Fig. 22) several emission fields at sea floor can be clearly identified with pH values below 6 with respect to pH of about 8 of the ambient seawater. At the northern transect several venting areas are revealed up to a water depth of about 25 m, whereas profile d corresponds the Area 26 site. Distinctive fields between the profiles are probable but cannot be verified because of data lacking. The low pH fields displayed between the depth profiles seems to be the result of the interpolation procedure. Nevertheless, the regions of lower pH than ambient seawater reaches several meters up from the seafloor emission. For profile a and b the influence extents almost over the whole seawater column. Conversely, for the profiles d and e the low pH only reaches up to a particular water depth where it is changed rapidly into the pH of ambient seawater.

Similar different types can be observed for the middle transect, where the emission fields of Black Point and Point 21 are clearly observable. Also at the southern transect the Bottaro North site can be clearly identified, but to a more less extent the Bottaro West site which indicates a lateral uninfluenced profile rather than the measurement directly above the gas emissions of the site. The pH depth profile at Bottaro North shows almost no variations but in general lower pH values with respect to ambient seawater. As already mentioned for the TIC profiles the large fumaroles were exhaling in a very strong intensity forming columns of bubbling gases reaching the seawater surface. Thus, there was a strong mixing of the discharging fluids with seawater along the whole seawater column.

Profiles of T and EC identify again the Hot Lake seafloor emission. The anomalous T and EC values for profiles along the northern transect line cannot be explained. They can be interpreted as artefacts by interpolating slightly different values at the same depths of adjacent profiles.

Finally, for the profiles taken in September 2008 one can infer by the height of lower seawater pH above the seafloor emission the intensity of gas discharge as well as the height of the formed gas bubbling column affecting the water column directly by gas dissolution and indirectly by carrying low-pH water towards the surface. Thus, the measured profiles may indicate the height of the CO_2 bubbles before their complete dissolution. Otherwise, low pH

values restricted to the fumarolic emissions on the sea floor indicate the discharge of acid hydrothermal fluids including only slight degassing activity. By evaluating the trend of seawater pH from the emission point towards the sea surface it has to be considered that it is also affected by the current that forces the rising gas bubbles to a less vertical ascent.

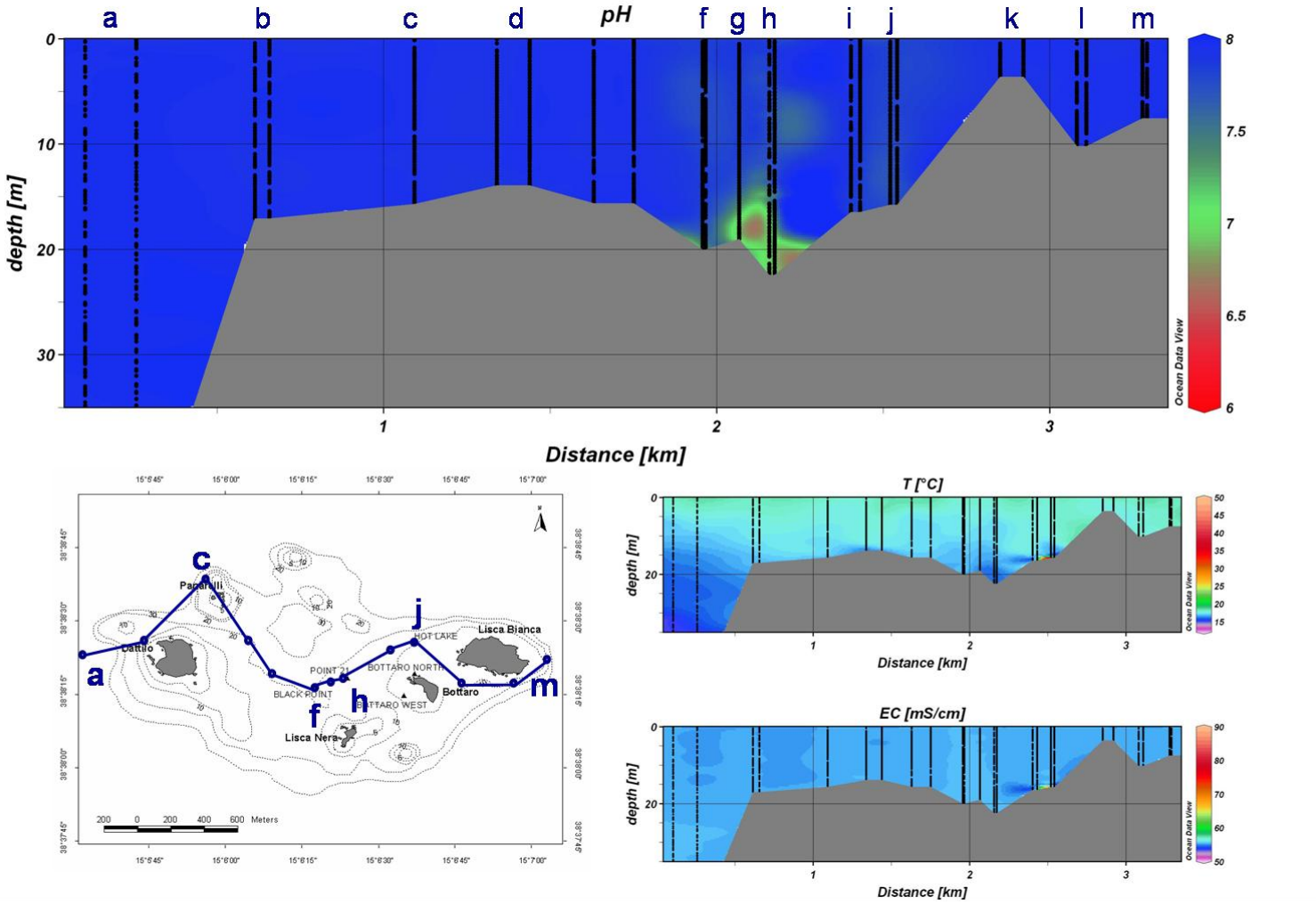

Fig. 21. Depth profiles of pH, water temperature and EC (point a to point m) along a line transect crossing the investigation area between the islets. Most readings from points a to point m consists of both a profile measured in May 2008 while lowering and lifting the probe. Profiles at point f match with the location of Black Point, point h with Point 21 and point j with Hot Lake. 2d-faces of pH, T and EC generated by ODV (Schlitzer, 2008), map modified after Rohland (2007).

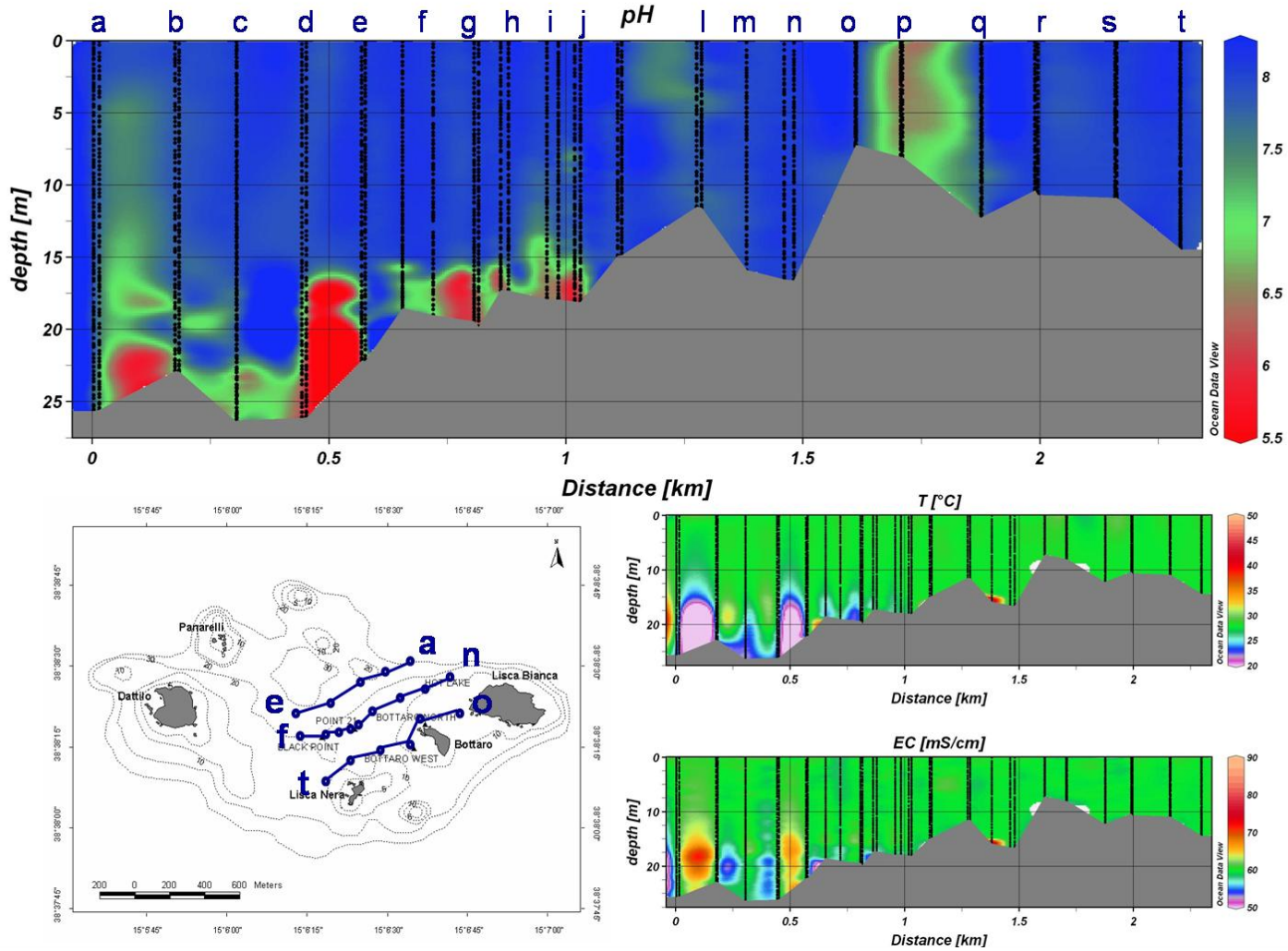

Fig. 22. Depth profiles of pH, water temperature and EC along three line transects. It is displayed as one transect from profile a to t. Most readings from points a to t consists of both a profile measured in September 2008 while lowering and lifting the probes. Profiles at point d match with the location of Area 26, point g with Black Point, point j with Point 21, point m with Hot Lake, point p with Bottaro North and point q with Bottaro West. 2d-faces of pH, T and EC generated by ODV (Schlitzer, 2008), map modified after Rohland (2007).

4.2 Gas quantification

4.2.1 Results of flow rate determinations

Gas flow rates of fumaroles were measured by water displacements in a HDPE bottle of 1.2 L volume (see section 3.6). Based on 48 measurements all fumaroles were classified into four classes of flow rates (Table 4). At each site, except for Hot Lake and Area 26, all gas exhalations were counted and sorted into the respective class A to D (Table 7). Very large fumaroles that showed rates of gas release quite beyond about 40 L/min, the upper limit of that what could be measured by the water displacement methodology, were measured separately by means of a special system called FSVG (see section 3.6). For these few fumaroles located at Bottaro North and Point 21 a class E was established.

Table 7. Number of fumaroles observed at the five investigated sites. Depending on their estimated gas flow rate they were classified into four classes A to D. Class E represents few very large fumaroles that were examined separately.

class	**A**	**B**	**C**	**D**	**E**
range of gas flow rate [L/min]	< 2.1	2.1 - 3.6	3.6 - 7.2	> 7.2	> 40
Bottaro West	591	39	9	2	
Bottaro North	144	11	14	6	5
Fumarolic Field	549	90	37	4	
Point 21	297	61	24	10	5
Black Point	546	36	8	2	

Most gas exhalations occurred at Fumarolic Field, Black Point and Bottaro West with about 600 – 700 observed individual vents as the sum of all classes. For the Bottaro West site the field of numerous diffuse gas exhalations within the crater was thereby not taken into account. Due to the lower extent of Bottaro North site and a quite different morphology in respect to the other locations there were counted only 180 vents.

Fumaroles showed predominantly small degassing activity with gas flow rates less than 2.1 L/min. At all investigation sites fumaroles of this class accounted for about 75 – 92 %. It followed more intense gas exhalations with flow rates in the range of 2.1 – 3.2 L/min, 3.2 – 7.2 L/min and more than 7.2 L/min with decreasing frequencies. Additionally, in each case five very strong exhaling fumaroles were located both at Point 21 and Bottaro North with flow rates clearly exceeding 40 L/min.

Based on the measured average flow rate of each class and the respective number of fumaroles the total gas output of each site was computed. Beforehand, the measured gas flow rates were corrected for the individual outlet gas temperature and finally, for the hydrostatic pressure based on the average water depth of each site (Appendix 15 and 17).
The gas output of the almost circular field of numerous diffusive gas exhalations within the crater of Bottaro West was determined apart and the corrected result was added to the total output of the Bottaro West site (Appendix 14).

Two large fumaroles at Point 21 which have been characterised by a massive gas discharges were measured by means of the special device “FSVG” (Kleutges, 2009). This took place in three series of measurements for the fumarole called “Melanie” and one serial of measurement for the fumarole called “Claudia” (Appendix D3). These results were again corrected for the individual gas release temperature and the hydrostatic pressure affecting the gases at the flow through section on top of the device. After correction the determined series of measurements yield average gas flow rates of about 346 ± 79 L/min and 869 ± 61 L/min for “Melanie” and “Claudia”, respectively.
For the three remaining massive gas exhaling vents at Point 21 as well as five ones located at Bottaro North site no individual measuring was performed during the diving campaign in September 2008. An estimation of their gas flow rates was executed by visually comparison with respect to the two measured fumaroles. The comparison was carried out by means of photos (Appendix 18 and 19).
At the investigation site Point 21 the five big fumaroles are located in a depression in front of a natural wall or in case of “Wanda” escaping directly from a small cavity in the wall (Appendix 18a - e). The vent next to “Melanie” called “Patricia” is approximately half as intense as “Melanie”. The twins in the northern part of the depression called “Claudia” and “Mandy”, are showing an almost equal gas output. From gas bubbling of the vent “Wanda” it is inferred a gas release to a lower extent than the release of “Melanie”, “Mandy” and “Claudia” but comparable with the output of “Patricia”. Thus, based on the measured rates for “Melanie” and “Claudia” (307 L/min and 302 L/min, respectively, for both vents “Patricia” and “Wanda” a gas flow rate of 200 L/min is constituted, while for “Mandy” 350 L/min is assumed. Taking into account the individual gas release temperature and the hydrostatic pressure the corrected gas flow rates range from about 210 to 870 L/min for the five large fumaroles at Point 21(Appendix 16).

Comparing the two measured fumaroles at Point 21 with the five most active gas vents at Bottaro North it is noticeable that vent 5, the strongest gas exhalation at that site, features a gas output comparable with “Melanie” and “Claudia” at Point 21 (Appendix 19a – i)). The remaining vents are less active. Thereby, vents 2, 3 and 4 show equal quantities of gas release, only vent 1, located in the small gravel field, is more less strong, having a gas output comparable with “Patricia” at Point 21. According to that, the individual gas flow rates were estimated for the five massive exhaling vents at Bottaro North. The corrected estimates are in the range between 161 L/min to 630 L/min (Appendix 16).

Finally, all results of gas flow rates were added for each location and finally for the whole investigation area (Appendix 17, Fig. 23).

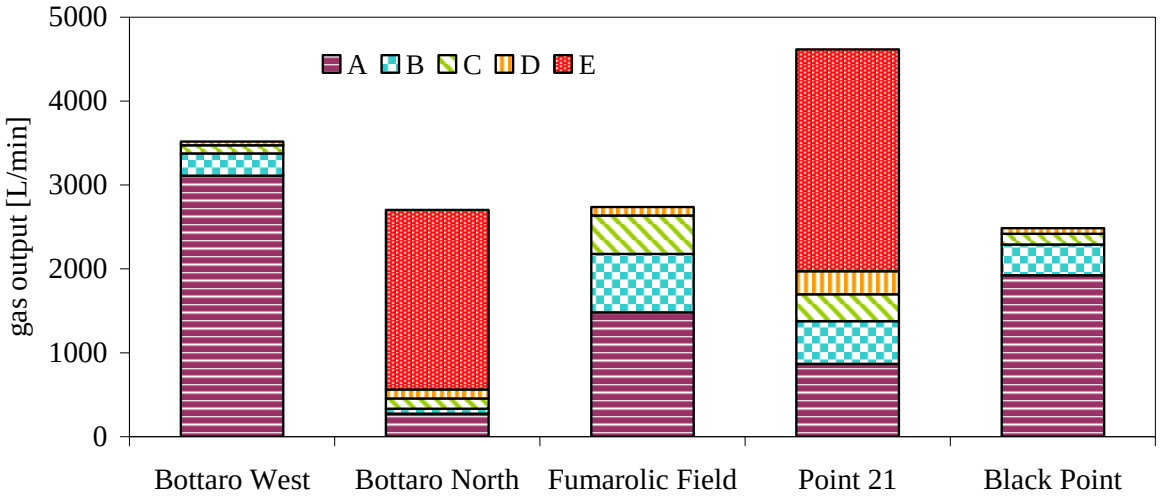

Fig. 23. Total gas output for the five investigated sites and the contribution of the respective classes of gas flow rates (A to E) (see also Appendix 17).

Highest rates of gas release were determined for the Point 21 site with 4617 L/min, followed by the Bottaro West site with 3518 L/min. For the latter site the field of diffusive gas exhalations contributes to the total gas output by approximately 49 %. The locations of Bottaro North, Fumaroles Field and Black Point have nearly equal quantities of gas emission, ranging between 2485 and 2737 L/min.

Thereby, only fumaroles of the classes of weak to moderate flow rates (classes A to D) provide for the determined gas outputs at Bottaro West, Fumaroles Field and Black Point. At Point 21 and Bottaro North the five massive gas exhaling vents of each site (class E), with flow rates up to two orders of magnitude higher than the weak to moderate fumaroles, contribute in a considerable proportion to the total gas output. Particularly, for the Bottaro

North site, where the five large vents along provide for a significant gas emission with about 79 % of the total gas output.
Thus, it results in an individual daily gas output between $3.6 * 10^6 – 6.7 * 10^6$ L/day for the five locations. In sum it is $2.3 * 10^7$ L/day as the total gas output of the whole investigation area assuming that these five investigated sites represent most of the whole submarine crater area of about 2.3 km^2.

The distribution of the submarine gas exhalations reveals a significant gap between the weak to moderate fumaroles (classes A to D) and the more intense gas exhaling fumaroles of Bottaro North and Point 21 (class E). In other words, no gas exhalations were measured having gas flow rates (uncorrected for hydrostatic pressure) more than 16 L/min and less than 302 L/min, whereas for less intense larger fumaroles 200 L/min were estimated as lower limit (Appendix 13 and 16). Possibly there have been few fumaroles, which were counted and sorted into the class D (> 7.2 L/min), but possessed flow rates exceeding 16 L/min and perhaps also 40 L/min, the upper limit for class D. It can also not ruled out that fumaroles occur with gas release in the rate between 16 L/min and 200 L/min at locations apart from the observed submarine investigation sites. But, based on measurements and observations at the investigated locations, the few large fumaroles of class E exhibit outstanding formations with respect to the rate of gas discharge and thus, considerably differ from the predominantly appearing weak and moderate gas emitting fumaroles.

4.2.2 Quality of the quantification

4.2.2.1 Consideration of gas temperature

The rates of submarine gas discharges had to be corrected on the one hand for the hydrostatic pressure due to different water depths of the emission sites and on the other hand for the different temperatures of the gases when they escape from sea floor. Thus, all results of measured gas flow rates, i.e. both by means of water displacement in the HDPE bottle and the special system FSVG, as well as the results of estimation based on the comparison of photos were subsequently corrected for their measured gas temperature. As reference the standard ambient temperature of 25 °C (from SATP conditions) was applied since it differs less strong from the ambient water temperature of about 27 °C in September 2008 than the normal temperature of 0 °C (from STP conditions). Corrections for temperature and also for

hydrostatic pressure were done by the ideal gas law, assuming that gases behave like ideal gases since the absolute pressure at the outlets is only slightly elevated compared to P = 0 bar. Most fumaroles have outlet gas temperatures close to the water temperature of ambient seawater (Appendix 1 - 4). But several ones differ distinctively from the water temperature.

The aim of the temperature correction was to achieve a more precise quantification of the total gas output. But, temperature measurements were carried out only at the fumaroles that were examined for their gas flow rate, all other vents were thus treated as possessing gas temperatures equal to standard ambient temperature of 25 °C, which almost correspond the ambient water temperature of about 27 °C. This constitutes no major problems at the locations of Bottaro North, Bottaro West, Point 21 and Fumaroles Field, where for these few vents characterised by the discharge of warmer gases with respect to ambient seawater, the temperature was measured and taken into account for their gas flow rate. However, for Black Point no measurements were carried out. Here all fumaroles were only counted and sorted into defined classes. Since the Black Point site showed a heterogeneous temperature distribution (Fig. 6) unconsidered elevated gas temperatures of the fumaroles might cause a major uncertainty for the quantification of the total gas output of this site.

A further critical point is the determination of the water temperature rather than the temperature of the discharged gases by means of a digital thermometer. Thus, the temperature measurement some centimetres deep in the sediment or rock fracture of the respective seafloor gas emission led to an underestimation of the temperature of the discharging gases since the temperature of the liquid phase was measured, actually. And discharging gases are cooling faster by mixing with cold seawater based on their lower heat capacity compared to seawater (see section 1.2.3). Enhanced measurement instrumentation will lead to more representative values of the fumarolic gas temperature.

Furthermore, since the discharging hot gases are rapidly cooling the difference in the gas temperature at the seafloor emission and in the measuring system for gas flow determination could be very high, in particular for the FSVG, where the measuring section is located on top of the whole system, about 2 m above the seafloor.

Although, the correction for different gas temperatures should achieve more precise gas quantification, by taking into account the mentioned critical issues of representation of the measured temperatures for the gases that were examined for their flow rate as well as the small number of measured temperatures, this approach seems less successful than it was expected. But, the author suppose that a complete disregard of the individual gas

temperatures, particular for the very intense gas exhaling fumaroles, would lead to a much higher uncertainty of the quantification.

4.2.2.2 Error of the quantification

To evaluate the quality of the quantification some facts have to be considered. To measure the gas flow rates by means of water displacement in a bottle seems to be very accurate in the case the funnel covers the whole fumarolic emission and captures all bubbles. More problematic seems to be the comparison of all fumaroles with regard to their gas bubbling columns in order to classify them with respect to the assumed gas flow rate. Incorrect classification as well as miscounts is likely.

Further challenge was the bordering of the submarine sites, and therefore the decision which gas emanations should be included for the gas output quantification. For crater shaped locations the enclosing slopes could be regarded as the borders, but Bottaro North as well as Point 21 are not entirely enclosed by distinct morphologies. In these cases all fumaroles inside a particular radius from the central structure of the location, i.e. the natural rocky wall at Point 21 and the small gravel field at Bottaro North, were taken into account. At the remaining sites all gas exhalations inside the crater were considered as well as fumaroles located at the slopes and being in field of vision when diving along the crater margin.

For the large fumaroles that were measured by the special system FSVG the obtained values are supposed to be of quite good quality (Johannes Kleutges, 2009, pers. comm.). However, it is likely that the big funnel captured not all discharging gas bubbles of the two large fumaroles measured at Point 21 and, thus, discount a relevant proportion of the released gas. The gas flow rates of the residual large fumaroles at Point 21 and Bottaro North were then estimated by comparison of their bubble columns by means of photographs. Of course these estimations might be very error-prone since the real magnitude of the gas flow rate emerges not explicit from the photos. Errors in the determination of the gas flow rates of these large vents are most serious since these fumaroles contribute to a significant proportion to the total gas output of the respective site.

Furthermore, there are probably numerous fumaroles scattered between the investigated emission sites, but they were not considered. This might led to a higher rate of gas release of the whole submarine hydrothermal area.

Taking into account the mentioned uncertainties as well as the fact that much more gas flow rates were estimated than directly measured, the determination of the submarine gas output

should be deemed as semi-quantitative. That is why influences to the gas output due to different atmospheric pressures, tidal influences and height of waves were neglected.
Finally, the author suppose a possible error up to 100 %, including over- and underestimation, for the determined total gas output of $2.3 * 10^7$ L/day of the whole investigation area. But even in this case the order of magnitude of 10^7 L/day remains the same.

4.2.3 Temporal development of the submarine gas output

The total gas output of $2.3 * 10^7$ L/day determined in September 2008 is more than twice as high as the output occurred before the submarine gas explosion event at November, 3rd 2002 (Fig. 24).
Since the mid 1980's, first results were determined by Italiano and Nuccio (1991). The total gas output of the submarine hydrothermal field east of Panarea remained almost constant at about $9 * 10^6$ L/day, except for a decrease by one-half the rate in 1989 (Caliro et al., 2004). The submarine gas eruption in 2002 caused a gas discharge in a rate about two to three orders of magnitude higher than previous rates (Caracausi et al., 2005b). It was followed by a rapid decrease by one order of magnitude only during two weeks after the onset of the crisis to about $4 * 10^8$ L/day (Caliro et al., 2004, Caracausi et al., 2005b). The total submarine gas output in the investigation area progressively decreased to $2 * 10^7$ L/day in July 2003 (Caliro et al., 2004). About five years later the measured total gas output was in the same order of magnitude indicating that the system has again reached a period of almost constant degassing like before 2002.
However, except for the results of Italiano and Nuccio (1991), it was not definitely declared which exhalation fields were taken into account for the quantification of the entire area by Caliro et al. (2004).

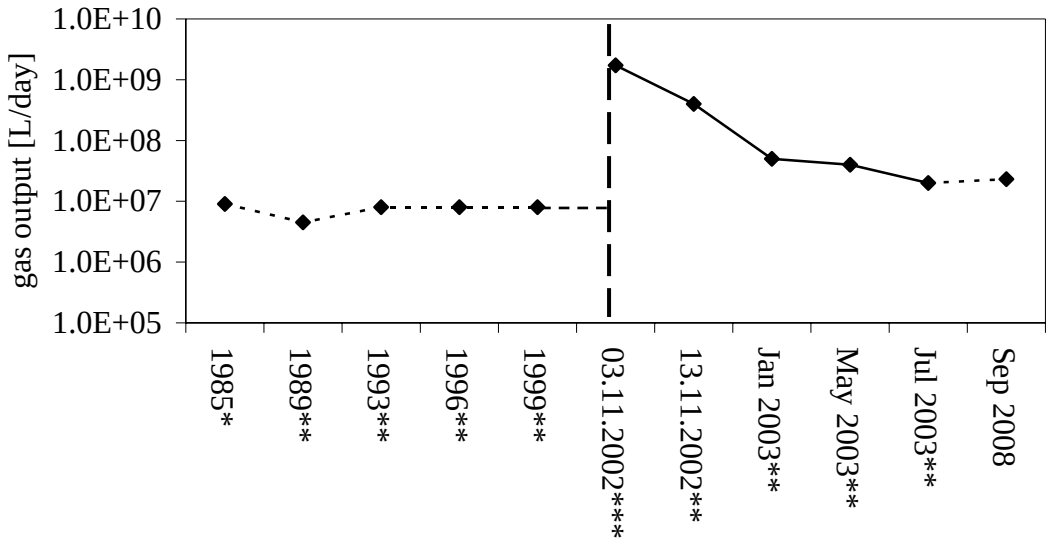

* Italiano and Nuccio (1991), ** Caliro et al. (2004), *** Caracausi et al.

Fig. 24. Temporal development of the total submarine gas output of the Panarea hydrothermal system.

4.2.4 Short-term variations of the gas flow rates

The submarine gas outputs were determined by several dives within several days during the diving campaign in September 2008. Thus, the results depict the state of the Panarea hydrothermal system for this period of time. However, the gas flow rates are not constant over time. Beside the mentioned long-term variations also internal and external factors affect the gas flow rates of the hydrothermal system in shorter periods of time.

By means of the system FSVG three series of measurement were achieved for the “Melanie” fumarole and one serial for the “Claudia” fumarole at Point 21 (Appendix D3). The four series were measured at four consecutive days, having periods ranging from about 30 minutes to almost 10 hours. The “Claudia” fumarole showed an almost constant gas flow rate over the period of measurement apart from normal fluctuations. In contrast to that, the flow rate of the “Melanie” fumarole revealed jumps to about double rates and a subsequent decreasing till the next jump within two series of measurements (Fig. 25). These jumps have varying periodicities in the range of about two hours to almost five hours.

Because errors due to the measurement procedure are unlikely (Johannes Kleutges, 2009, pers. comm.) these variations of gas release may originate from a varying permeability beneath the sea floor. The gas passage seems to clog periodically until the pressure is high enough to remove the blockage and to force a gas release in a much higher rate. No jumps

occur at the serial of gas flow rate of the “Claudia” fumarole, so both vicinal vents probably have different pathways for their fluids towards the sea floor.

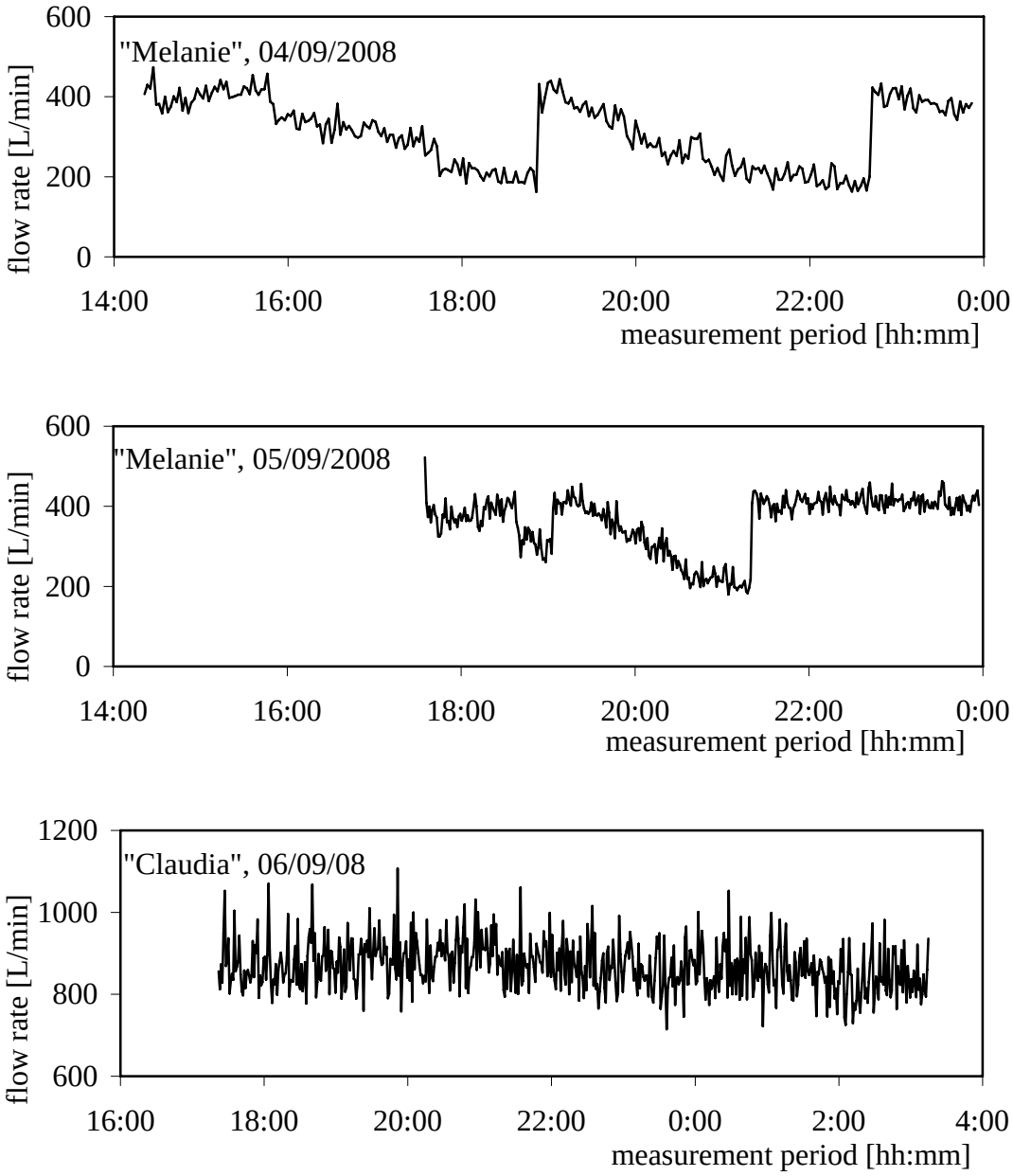

Fig. 25: Times series of measurement for the “Melanie” fumarole (04/09/08 – 05/09/08) as well as for the “Claudia” fumarole (06/09/08) at the Point 21 site. Values are corrected for gas temperature and hydrostatic pressure (data from Kleutges (2009)).

Short-term temporal variations of the gas flow rates may also be caused by changes of both the weight of the water column including atmospheric pressure on the submarine fumaroles and gravity forces of sun and moon on the magma chamber. The local weather situation causes variations of barometric pressure, whereas the water level is affected by earth-tides but

also storms. Tides in general cause amplitudes of water level less than 40 cm typical of the central Mediterranean Sea (Anzidei et al., 2005).

The gas output of the submarine hydrothermal system of Panarea is also affected by seismic events as well as volcanic activity and could therefore treated as an indicator in the case that gas flow rates will be monitored continuously. Heinicke et al. (2009) revealed coincidences of the gas flow rate of a fumarole at Point 21 and seismic events that occurred at the nearby Stromboli volcano. Thus, the authors suggest an interconnection of the gas feeding systems affecting both the submarine hydrothermal fluid discharges of Panarea as well as the Stromboli volcano activity. Thereby, the volcanic fluids are able to interact with the geothermal system of Panarea through a deep tectonic connection.

4.2.5 Output of CO_2 and H_2S

To take into account the different rates of gas emission and the respective relative concentrations of the gas species the output rates of CO_2 and H_2S were computed for each site (Fig. 26). The output for CO_2 ranged between 6.4 and 11.6 tons per day, while the emission of H_2S ranged between 15 and 296 kg per day between the investigated sites. In general, sites characterised by a high gas emission rate had also the highest output of CO_2 since it has been by far the most abundant specie for all submarine gas discharges in the investigation area. So, differences in the CO_2 content between the sites have been of minor consequence for the total output of CO_2. For the output of hydrogen sulphide differences in the gas contents are more substantial. Thus, Black Point emit distinctive less hydrogen sulphide than Bottaro North, although both sites have almost equal total gas flow rates.

The total rate of the seafloor CO_2 output for the entire submarine hydrothermal area east of Panarea accounted for 40.5 ± 0.2 t/day and the H_2S output was about 806 ± 13 kg/day.

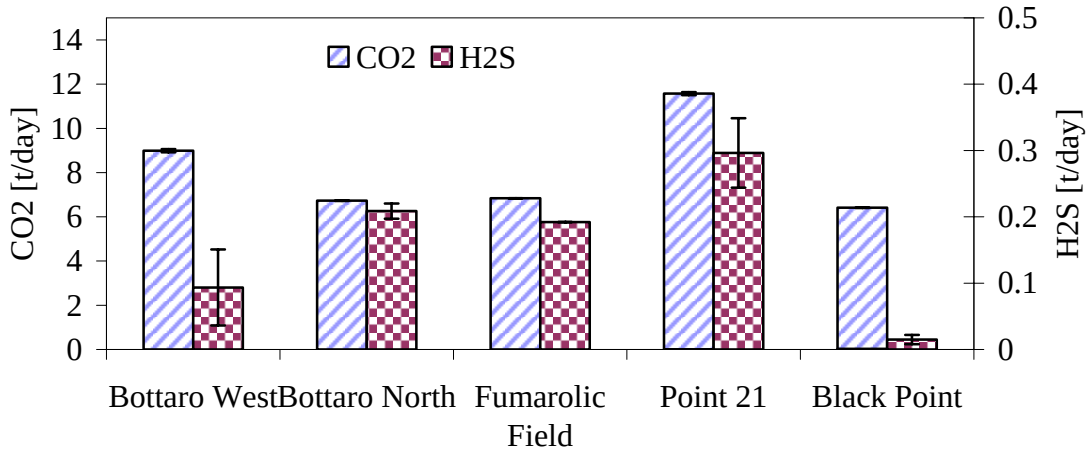

Fig. 26. Total output of the gas species CO_2 and H_2S of the five sites both investigated for their gas composition and gas output.

The abundance of seawater in the shallow subsurface region of the hydrothermal system can be expressed by a gas/water ratio of below 0.2 which was modelled by Caracausi et al. (2005a). This caused a removal of soluble gases like CO_2 and H_2S from the gas phase to a large extent. Based on their model of gas dissolution in seawater the authors ascertained that 20 – 40 % (even up to 60 % at maximum) of CO_2 was generally lost by dissolution in seawater before the gas phase escape from the sea floor. So, they corrected the submarine gas output for this loss to estimate the total CO_2 gas output from the geothermal system.

Taking into account dissolution of CO_2 in the hydrothermal fluid by likely 30 % on average prior the discharge at sea bottom the total emitted CO_2 at seafloor in the investigation area results to 52.7 ± 0.2 t/day.

When the gases escape at the sea floor into the cold ambient seawater further dissolution takes place during ascending to the sea surface due to buoyancy. The dissolved gases influence the original physico-chemical parameters of the seawater (see section 4.1.6). A sink for CO_2 in seawater is the formation of carbonates as well as photosynthesis of marine organisms (see section 1.2.3). If gas bubbles reach the sea surface before they are completely dissolved in seawater they escape directly into the atmosphere. Since the seawater is in equilibrium with the atmosphere an input of CO_2 from a sub-seafloor hydrothermal system will cause the CO_2 release into the atmosphere sooner or later in the course of time.

4.2.6 Comparison with subaerial CO_2 quantifications

Based on the determined output of about 53 tons per day for September 2008 the shallow submarine hydrothermal system of Panarea can be considered as a minor CO_2 emission source with respect to subaerial volcanic emissions (Table 8). The CO_2 degassing of Vulcano and Stromboli, both belonging to the Aeolian volcanic arc, is characterised by CO_2 emission rates of about three times the determined output of Panarea for Vulcano and about 2 orders of magnitude higher than the submarine Panarea output for Stromboli.

Mt. Etna is considered to be one major volcanic gas emitter in the world in the long term (Aiuppa et al., 2006b) with on average 9000 t CO_2/day, more precisely about 2000 t/day during passive degassing and up to 40 times larger emission rate during effusive eruptions (Aiuppa et al., 2006b). Thus, Mt. Etna accounts for about 10 % of world-wide average volcanic emission of CO_2 and, moreover, can also be considered as the world's major point source for the gases of SO_2, HCl and HF (Aiuppa et al., 2006a).

Dando et al. (1999) assumed that the total CO_2 output from all hydrothermal sources in the Mediterranean region (mainly Tyrrhenian and Aegean Seas) could well be of the order of 10,000 – 100,000 t/day, including the submarine hydrothermal system of Panarea.

Submarine volcanic carbon degassing is assumed basically (> 90 %) related to mid-ocean rigdes in divergent plate margins (Morner and Etiope, 2002). Thereby, the CO_2 output rate of the entire 60,000 km long mid-ocean ridge (MOR) volcanic systems was estimated to be in the range between about 80,000 and 180,000 t/day (Gerlach, 1991). So, the CO_2 emission of the entire MOR system is assumed to be in the same order of magnitude as the estimated total Mediterranean hydrothermal CO_2 emissions which indicate a global importance of the Mediterranean sources.

Finally, the global emission rate of CO_2 by all subaerial and submarine volcanoes is uncertain but was firstly estimated to be about 360,000 – 480,000 tons per day (Gerlach, 1991).

Table 8. CO_2 output (in tons per day) of several volcanoes and hydrothermal/volcanic systems for evaluation of the determined submarine CO_2 release of the hydrothermal system of Panarea.

emitter	output [t/day]	reference
Panarea submarine hydrothermal system	52.7 ± 0.2	own data (Sep 2008)
Vulcano	180 ± 10	Baubron et al., 1990
Stromboli	2900 - 5800	Allard et al., 1994
Etna	35,000 ± 8000	Allard et al., 1991
	900 - 67,500	Aiuppa et al., 2006b
Masaya	2800 - 3100	Burton et al., 2000
all Mediterranean hydrothermal sources	10^4 - 10^5	Dando et al., 1999
entire MOR volcanic system	(82 - 178) * 10^3	Gerlach, 1991
global volcanic emissions	(3.6 - 4.8) * 10^5	Gerlach, 1991

Estimates of global subaerial volcanic CO_2 emissions are very uncertain and usually very underestimated since (1) degassing is usually estimated from direct flux observations operating only over a year time-scale and, thus, hardly representing any steady-state degassing, (2) measurements or rough estimates of CO_2 emission rates are only available for less than 20 volcanoes and (3) the principal mode of volcanic CO_2 release by quiescent, non-eruptive diffuse degassing, including the flanks, is strongly underestimated (Morner and Etiope, 2002). Thus, these authors suggested a more realistic global CO_2 emission rate from subaerial volcanoes by at least 820,000 t/day (300 Mt/year), taken into account 500 historically active subaerial volcanoes with an average conservative output of 0.1 - 0.5 Mt/year by plume as well as diffusive degassing.

However, CO_2 is also the most important anthropogenic greenhouse gas (see section 1.2.3). Thereby, the primary sources of the increased atmospheric CO_2 concentration since pre-industrial time results from use of fossil fuel, with an annual average CO_2 emission of 26.4 Gt/year as well as land-use change (about 5.9 Gt/year) (IPCC, 2007). Compared to this, the atmospheric impact from global volcanic CO_2 degassing of about 0.3 * Gt/year is trivial.

5. Final discussion

The submarine discharging gases of the hydrothermal system of Panarea were investigated in respect of their chemical composition as well as their emission rate.

Unfortunately, only few gas compounds could be determined, others were evaluated by means of external data. The most abundant species was CO_2 (> 96 vol.%), followed by H_2S (up to 4 vol.%). For each investigation site both species accounted for more than 99 vol.% of the gas that emits on the seafloor. The occurrence of O_2 and N_2 indicate an atmospheric endmember by subsurface dilution of the hydrothermal fluid with air saturated seawater. However, $^{4}He/^{20}Ne$ ratios in the gases which were more than 100 times the ratio of air suggest a very low atmospheric contribution to the geothermal circulation. The different ratio of CO_2 and H_2S between the sites indicates the occurrence of gas scrubbing, whereas the extent of partial gas dissolution in respect to the different solubility in seawater might be an indicator for the velocity of gas ascent towards the seafloor. Therefore, the gases of large fumaroles which are probably characterised by a rapid gas migration, were least encountered to the dissolution of the more soluble H_2S, which explains the lowest CO_2/H_2S ratio analysed in these gas samples. Thus, such large fumaroles located at Point 21 and Bottaro North may provide the most reliable data on the subsurface composition since through the rapid and direct gas migration there is less time for gas-water-rock interactions.

When the gas phase is ascending and cooling condensation will occur. The condensed water vapour may dilute the hydrothermal fluid. Thus, an open question may be whether the thermal waters associated with the hot gas discharges of the large fumaroles at Bottaro North and Point 21 are only seawater heated by the ascending hot gases, condensed vapours of a biphase hydrothermal fluid, diluted hydrothermal waters, or a mixture of all. The measured EC provide no conclusion since it was close to that of local seawater.

It was not looked for water vapour in the sampled gases but it is not excluded that it could be detected in the discharges of the large fumaroles as well as in the hot gas discharges at Black Point, because in the subaerial fumaroles of La Calcara on Panarea Island water vapour was detected with about 93 vol.% (Italiano and Nuccio, 1991). Here, a reliable method to analyse for water vapour in the discharging gases has to be designed.

Regarding the analysed elements in the sampled gases and aerosols some differences of the elemental composition is noticeable, particular between the gas and aerosols sampled in May 2008 and the gases and aerosols restricted to the size < 25 nm (September 2008). Most elements were detected in the sample of Black Point. Some of the elements are considered to

be of magmatic origin, other ones might originated from gas-water-rock interaction. However, an evaluation of the detected elemental compositions is difficult since the trapping solution had high elemental concentrations itself and comparable data of previous studies are lacking.

One aim of this study was the detection of an input of magmatic gases to the hydrothermal fluid based on the feeding of the system by of deep magmatic fluids. The chemical composition of the sampled gases provided no evidence. However, isotopic ratios of $^{13}C/^{12}C$ (CO_2), $^{34}S/^{32}S$ (H_2S) and $^{3}He/^{4}He$ argued for a magmatic contribution for the contents of these gases.

When looking to the results of hydrothermal water samples it is obvious that Black Point deserve special attention. It had the second highest EC, indicating a low dilution of the original hydrothermal fluid with seawater, the lowest pH (mean of 3.1) and highest redox potential and oxygen concentration, compared to all other investigation sites. The more oxidising redox conditions unlike the typical hydrothermal fluid redox state might also caused by the input of small amount of magmatic fluids as it was reported by Capaccioni et al. (2007) for the submarine gas eruption in 2002. The enrichment of Cl^-, F^- and Br^- over seawater might also indicate for a contribution of magmatic derived acid gases, such like HCl, HF and HBr, in order to decrease the pH of the fluid more than the typical hydrothermal acidification as well as CO_2 can provide for. Another strong acid, H_2SO_4 derived from magmatic SO_2, might be also be reasonable for low pH in the fluid, although the fluid samples of Black Point were depleted in total dissolved sulphur over seawater.

Based on all mentioned geochemical parameters for the Black Point fluids one could infer that Black Point was significantly more affected by the input of deep magmatic fluids than the fluids at the other sites.

The highest gas output of five investigated sites provided Point 21, followed by the site of Bottaro West. Together they account for a total submarine gas emission of $2.3 * 10^7$ L/day of the investigation area, assuming that the five sites represent most of the entire submarine crater area of about 2.3 km^2. A maximum error of ± 100 % was estimated for this semi-quantitative determination.

All fumaroles, up to 600 – 700 in the case for Fumarolic Field, Bottaro West and Black Point site, were therefore classified with regard to their gas flow rate. Most of them (75 – 92 %) were weak discharging fumaroles. At least 10 fumaroles were found that are characterised by a very intense gas release. These fumaroles, located at Point 21 and Bottaro North, contributed significantly to the total gas emission of the respective site. Thus, for a correct

quantification it is very important that the gas flow rates of these vents are determined as precise as possible.

After a period of nearly constant degassing before November, 3rd 2002, when the activity of Panarea volcanic complex was considered to be quiescent, the submarine gas eruption caused an increase of gas release by 2 to 3 orders of magnitude. Since July 2003 it can assume that the hydrothermal system of Panarea has again reached a state of constant degassing, still more than twice the rate than the period before 2002.

With regard to CO_2 the system is emitting 52.7 t/day, including the subsurface dissolution of 30 % prior the discharge on seafloor. Although, at first the discharged CO_2 predominantly dissolve in the seawater sometime it will be degassed into the atmosphere. Through the CO_2 input in the ambient seawater the TIC increases and the pH decreases, particularly over intense gas discharges, revealed by measured depth profiles. For the very shallow site of Bottaro North the pH was decrease as well as the TIC was increased along the entire water column of about 8 m. Over deeper emissions there is a region of the lower pH up to a particular water depth where the pH equals again the ambient seawater pH. The height over the emission might be depending on the intensity of gas release.

In comparison with subaerial volcanoes like Vulcano, Stromboli and Etna the determined CO_2 emission rate is trivial. A global CO_2 emission by subaerial volcanoes is estimated to be least 0.3 Gt/year (Morner and Etiope, 2002). This is again trivial against the average CO_2 emission caused by burning of fossil fuel of about 26.4 Gt/year (IPCC, 2007).

What might be a future scenario? All researchers agree that a gas eruption like the one in 2002 may occur again in the future. The system seems to be capable of gathering and transferring a particular amount of magmatic fluids towards the seafloor emissions. Will there be a strong and rapid increase of the feeding rate, e.g. induced by seismic events, then a new gas eruption can not be excluded. This poses hazards for inhabitants and tourists on the sea as well as on Panarea Island, e.g. by the exposure of huge amounts of toxic gases. Thus, by monitoring of the geochemical parameters of the hydrothermal gas and water discharges as well as of the gas output rate it might be possible to identify significant variations that make forewarnings possible.

6. References

AIUPPA, A., BELLOMO, S., BRUSCA, L., D'ALESSANDRO, W., DI PAOLA, R. & LONGO, M. (2006a) Major-ion bulk deposition around an active volcano (Mt. Etna, Italy). *Bulletin of Volcanology,* 68**,** 255-265.

AIUPPA, A., FEDERICO, C., GIUDICE, G., GURRIERI, S., LIUZZO, M., SHINOHARA, H., FAVARA, R. & VALENZA, M. (2006b) Rates of carbon dioxide plume degassing from Mount Etna volcano. *Journal of Geophysical Research-Solid Earth,* 111**,** -.

ALLEN, A. G., BAXTER, P. J. & OTTLEY, C. J. (2000) Gas and particle emissions from Soufriere Hills Volcano, Montserrat, West Indies: characterization and health hazard assessment. *Bulletin of Volcanology,* 62**,** 8-19.

ANZIDEI, M., ESPOSITO, A., BORTOLUZZI, G. & DE GIOSA, F. (2005) The high resolution bathymetric map of the exhalative area of Panarea (Aeolian Islands, Italy). *Annals of Geophysics,* 48**,** 899-921.

BAHLBURG, H. & BREITKREUZ, C. (2004) *Grundlagen der Geologie,* München, Heidelberg, Spektrum Akademischer Verlag.

BAUER, K., BAUER, D. & BARTH, G. (2009) Flow rate measurements at submarine volcanic gas emissions. IN MERKEL, B. & SCHIPEK, M. (Eds.) *Research in Shallow Marine and Fresh Water Systems: 1st International Workshop – Proceedings.* Freiberg Online Geology, 22.

BECKE, R. (2009) Mineralogische & Geochemische Untersuchung von submarinen, vulkanogen-hydrothermalen Mineralpräzipitaten im back-arc-basin des Tyrrhenischen Meeres am Beispiel von Panarea, Äolischer Inselbogen, Italien. *Fakultät für Physik und Geowissenschaften Institut für Geophysik und Geologie - Universität Leipzig*.

BECKER, F.-M., BOORTZ, G., DIETRICH, V., ENGELMANN, L., ERNST, C., FANGHÄNEL, G., HÖHNE, H., LENERTAT, R., LIESENBERG, G., MEYER, L., PEWS-HOCKE, C., SCHMIDT, G.-D., STAMM, R. & WEBER, K. (1994) *Formeln und Tabellen für die Sekundarstufen I und II,* Berlin, paetec Gesellschaft für Bildung und Technik mbH.

BERNER, R. A. (2004) *The Phanerozoic Carbon Cycle: CO2 and O2,* Oxford, Oxford University Press.

BROWN, E., COLLING, A., PARK, D., PHILLIPS, J., ROTHERY, D. & WRIGHT, J. (1995) *Seawater: Its Composition, Properties And Behaviour,* Kidlington, Pergamon.

BURTON, M. R., OPPENHEIMER, C., HORROCKS, L. A. & FRANCIS, P. W. (2000) Remote sensing of CO2 and H2O emission rates from Masaya volcano, Nicaragua. *Geology,* 28**,** 915-918.

CALANCHI, N., PECCERILLO, A., TRANNE, C. A., LUCCHINI, F., ROSSI, P. L., KEMPTON, P., BARBIERI, M. & WU, T. W. (2002) Petrology and geochemistry of volcanic rocks from the island of Panarea: implications for mantle evolution beneath the Aeolian island arc (southern Tyrrhenian sea). *Journal of Volcanology and Geothermal Research,* 115**,** 367-395.

CALIRO, S., CARACAUSI, A., CHIODINI, G., DITTA, M., ITALIANO, F., LONGO, M., MINOPOLI, C., NUCCIO, P. M., PAONITA, A. & RIZZO, A. (2004) Evidence of a recent input of magmatic gases into the quiescent volcanic edifice of Panarea, Aeolian Islands, Italy. *Geophysical Research Letters,* 31**,** 1-5.

CAPACCIONI, B., TASSI, F., VASELLI, O., TEDESCO, D. & POREDA, R. (2007) Submarine gas burst at Panarea Island (southern Italy) on 3 November 2002: A magmatic versus hydrothermal episode. *Journal of Geophysical Research-Solid Earth,* 112**,** -.

CAPACCIONI, B., TASSI, F., VASELLI, O., TEDESCO, D. & ROSSI, P. L. (2005) The November 2002 degassing event at Panarea Island (Italy): five months of geochemical monitoring. *Annals of Geophysics,* 48**,** 755-765.

CARACAUSI, A., DITTA, M., ITALIANO, F., LONGO, M., NUCCIO, P. M. & PAONITA, A. (2005a) Changes in fluid geochemistry and physico-chemical conditions of geothermal systems caused by magmatic input: The recent abrupt outgassing off the island of Panarea (Aeolian Islands, Italy). *Geochimica Et Cosmochimica Acta,* 69**,** 3045-3059.

CARACAUSI, A., DITTA, M., ITALIANO, F., LONGO, M., NUCCIO, P. M. & PAONITA, A. (2005b) Massive submarine gas output during the volcanic unrest off Panarea Island (Aeolian arc, Italy): Inferences for explosive conditions. *Geochemical Journal,* 39**,** 459-467.

CHESTER, R. (2003) *Marine Geochemistry,* Malden, Mass., Blackwell-Publishing.

CHIODINI, G., CALIRO, S., CARAMANNA, G., GRANIERI, D., MINOPOLI, C., MORETTI, R., PEROTTA, L. & VENTURA, G. (2006) Geochemistry of the submarine gaseous emissions of panarea (Aeolian Islands, Southern Italy): Magmatic vs. hydrothermal origin and implications for volcanic surveillance. *Pure and Applied Geophysics,* 163**,** 759-780.

CORTECCI, G., BOSCHETTI, T., MUSSI, M., LAMELI, C. H., MUCCHINO, C. & BARBIERI, M. (2005) New chemical and original isotopic data on waters from El Tatio geothermal field, nothern Chile. *Geochemical Journal,* 39**,** 547-571.

DANDO, P. R., STUBEN, D. & VARNAVAS, S. P. (1999) Hydrothermalism in the Mediterranean Sea. *Progress in Oceanography,* 44**,** 333-367.

DE ROSA, M., GAGLIARDI, G., ROCCO, A., SOMMA, R., DE NATALE, P. & DE NATALE, G. (2007) Continuous in situ measurements of volcanic gases with a diode-laser-based spectrometer: CO2 and H2O concentration and soil degassing at Vulcano (Aeolian islands: Italy). *Geochemical Transactions,* 8**,** -.

DOLFI, D., DE RITA, D., CIMARELLI, C., MOLLO, S., SOLIGO, M. & FABBRI, M. (2007) Dome growth rates, eruption frequency and assessment of volcanic hazard: Insights from new U/Th dating of the Panarea and Basiluzzo dome lavas and pyroclastics, Aeolian Islands, Italy. *Quaternary International,* 162**,** 182-194.

EMERSON, S. R. & HEDGES, J. I. (2008) *Chemical Oceanography and the Marine Carbon Cycle,* Cambridge, Cambridge University Press.

ESPOSITO, A., GIORDANO, G. & ANZIDEI, M. (2006) The 2002-2003 submarine gas eruption at Panarea volcano (Aeolian Islands, Italy): Volcanology of the seafloor and implications for the hazard scenario. *Marine Geology,* 227**,** 119-134.

FABRY, V. J., SEIBEL, B. A., FEELY, R. A. & ORR, J. C. (2008) Impacts of ocean acidification on marine fauna and ecosystem processes. *Ices Journal of Marine Science,* 65**,** 414-432.

FAVALLIM, M., KARATSON, D., MAZZUOLI, R., PARESCHI, M. T. & VENTURA, G. (2005) Volcanic geomorphology and tectonics of the Aeolian archipelago (Southern Italy) based on integrated DEM data. *Bulletin of Volcanology,* 68**,** 157-170.

FULIGNATI, P., SBRANA, A., CLOCCHIATTI, R. & LUPERINI, W. (2006) Environmental impact of the acid fumarolic plume of a passively degassing volcano (Vulcano Island, Italy). *Environmental Geology,* 49**,** 1139-1155.

GABBIANELLI, G., GILLOT, P. Y., LANZAFAME, G., ROMAGNOLI, C. & ROSSI, P. L. (1990) Tectonic and Volcanic Evolution of Panarea (Aeolian Islands, Italy). *Marine Geology,* 92**,** 313-326.

GAMO, T., ISHIBASHI, J., TSUNOGAI, U., OKAMURA, K. & CHIBA, H. (2006) Unique Geochemistry of Submarine Hydrothermal Fluids From Arc-Back-Arc Settings of the Western Pacific. IN CHRISTIE, D. M., FISHER, C. R., LEE, S.-M. & GIVENS, S. (Eds.) *Back-Arc Spreading Systems: Geological, Biological, Chemical and Physical Interactions.* American Geophysical Union.

GERLACH, T. (1991) Volcanology - Etnas Greenhouse Pump. *Nature,* 351**,** 352-353.

GIGGENBACH, W. F. (1975) A simple method for the collection and analysis of volcanic gas samples. *Bulletin of Volcanology,* 39**,** 132-145.

GRAEDEL, T. E. & CRUTZEN, P. J. (1994) *Chemie der Atmosphäre: Bedeutung für Klima und Umwelt,* Spektrum Akademischer Verlag.

GUGLIANDOLO, C., ITALIANO, F. & MAUGERI, T. L. (2006) The submarine hydrothermal system of Panarea (Southern Italy): biogeochemical processes at the thermal fluids-sea bottom interface. *Annals of Geophysics,* 49**,** 783-792.

HALL-SPENCER, J. M., RODOLFO-METALPA, R., MARTIN, S., RANSOME, E., FINE, M., TURNER, S. M., ROWLEY, S. J., TEDESCO, D. & BUIA, M. C. (2008) Volcanic carbon dioxide vents show ecosystem effects of ocean acidification. *Nature,* 454**,** 96-99.

HEINICKE, J., ITALIANO, F., MAUGERI, R., MERKEL, B., POHL, T., SCHIPEK, M. & BRAUN, T. (2009) Evidence of tectonic control on active arc volcanism: The Panarea-Stromboli tectonic link inferred by submarine hydrothermal vents monitoring (Aeolian arc, Italy). *Geophysical Research Letters,* 36**,** -.

HERZIG, P. M. & HANNINGTON, M. D. (2006) Input from the Deep: Hot Vents and Cold Seeps. IN SCHULZ, H. D. & ZABEL, M. (Eds.) *Marine Geochemistry.* Berlin Heidelberg, Springer-Verlag.

HIGHWOOD, E. J. & STEVENSON, D. S. (2003) Atmospheric impact of the 1783-1784 Laki Eruption: Part II - Climatic effect of sulphate aerosol. *Atmospheric Chemistry and Physics,* 3**,** 1177-1189.

HILL, M. N. (1971) *The Sea: v.4,* John Wiley & Sons INC.

HÖLTING, B. (1996) *Hydrogeologie: Einführung in die allgemeine und angewandte Hydrogeologie,* Stuttgart, Ferdinand-Enke Verlag.

IPCC (2007) Summary for Policymakers. IN SOLOMON, S., QIN, D., MANNING, M., CHEN, Z., MARQUIS, M., AVERYT, K. B., TIGNOR, M. & MILLER, H. L. (Eds.) *Climate Change 2007: The Physical Science Basis. Contribution of Working Group I to the Fourth Assessment Report of the Intergovernmental Panel on Climate Change.* Cambridge University Press, Cambridge, United Kingdom and New York, NY, USA.

ITALIANO, F. & NUCCIO, P. M. (1991) Geochemical Investigations of Submarine Volcanic Exhalations to the East of Panarea, Aeolian Islands, Italy. *Journal of Volcanology and Geothermal Research,* 46**,** 125-141.

KLEUTGES, J. (2009) Gasvolumenstrommessung an submarinen Gasaustritten. *Department of Mechanics and Fluid Dymanic (imfd) - TU Bergakademie Freiberg***,** unpublished.

KUNZE, U. R. & SCHWEDT, G. (2002) *Grundlagen der qualitativen und quantitativen Analyse,* Weinheim, Wiley-VCH.

LANGMUIR, D. (1997) *Aqueous environmental geochemistry,* London, Prentice-Hall.

LUCCHI, F., TRANNE, C. A., CALANCHI, N. & ROSSI, P. L. (2007) Late Quaternary deformation history of the volcanic edifice of Panarea, Aeolian Arc, Italy. *Bulletin of Volcanology,* 69**,** 239-257.

MCGONIGLE, A. J. S., AIUPPA, A., GIUDICE, G., TAMBURELLO, G., HODSON, A. J. & GURRIERI, S. (2008) Unmanned aerial vehicle measurements of volcanic carbon dioxide fluxes. *Geophysical Research Letters,* 35**,** -.

MERKEL, B. & PLANER-FRIEDRICH, B. (2002) *Grundwasserchemie - Praxisorientierter Leitfaden zur numerischen Modellierung von Beschaffenheit, Kontamination und Sanierung aquatischer Systeme,* Berlin, Springer Verlag.

MILLERO, J. (1996) *Chemical Oceanography - Second Edition,* Boca Raton, CRC Press.

MORNER, N. A. & ETIOPE, G. (2002) Carbon degassing from the lithosphere. *Global and Planetary Change,* 33**,** 185-203.

NICHOLSON, K. (1993) *Geothermal Fluids: Chemistry and Exploration Techniques,* Heidelberg, Springer-Verlag.

ONO, S., SHANKS, W. C., ROUXEL, O. J. & RUMBLE, D. (2007) S-33 constraints on the seawater sulfate contribution in modern seafloor hydrothermal vent sulfides. *Geochimica Et Cosmochimica Acta,* 71**,** 1170-1182.

ORR, J. C., FABRY, V. J., AUMONT, O., BOPP, L., DONEY, S. C., FEELY, R. A., GNANADESIKAN, A., GRUBER, N., ISHIDA, A., JOOS, F., KEY, R. M., LINDSAY, K., MAIER-REIMER, E., MATEAR, R., MONFRAY, P., MOUCHET, A., NAJJAR, R. G., PLATTNER, G. K., RODGERS, K. B., SABINE, C. L., SARMIENTO, J. L., SCHLITZER, R., SLATER, R. D., TOTTERDELL, I. J., WEIRIG, M. F., YAMANAKA, Y. & YOOL, A. (2005) Anthropogenic ocean acidification over the twenty-first century and its impact on calcifying organisms. *Nature,* 437**,** 681-686.

PICHLER, T. (2005) Stable and radiogenic isotopes as tracers for the origin, mixing and subsurface history of fluids in submarine shallow-water hydrothermal systems. *Journal of Volcanology and Geothermal Research,* 139**,** 211-226.

POSCHL, U. (2005) Atmospheric aerosols: Composition, transformation, climate and health effects. *Angewandte Chemie-International Edition,* 44**,** 7520-7540.

ROHLAND, K. (2007) Investigation in submarine water and gas chemistry at Panarea, Aeolian Islands, Italy. *Department of Geology, Section for Hydrogeology - TU Bergakademie Freiberg***,** unpublished.

ROUXEL, O., FOUQUET, Y. & LUDDEN, J. N. (2004) Subsurface processes at the Lucky Strike hydrothermal field, Mid-Atlantic Ridge: Evidence from sulfur, selenium, and iron isotopes. *Geochimica Et Cosmochimica Acta,* 68**,** 2295-2311.

RUBIN, K. (1997) Degassing of metals and metalloids from erupting seamount and mid-ocean ridge volcanoes: Observations and predictions. *Geochimica Et Cosmochimica Acta,* 61**,** 3525-3542.

SCHLITZER, R. (2008) Ocean Data View. 3.4.0 ed., http://odv.awi.de.

SIELAND, R. (2009) Chemical and isotopic investigations of submarine hydrothermal fluid discharges from Panarea, Aeolian Island, Italy. *Freiberg Online Geology,* 21.

SYMONDS, R. B., GERLACH, T. M. & REED, M. H. (2001) Magmatic gas scrubbing: implications for volcano monitoring. *Journal of Volcanology and Geothermal Research,* 108**,** 303-341.

TASSI, F., CAPACCIONI, B., CARAMANNA, G., CINTI, D., MONTEGROSSI, G., PIZZINO, L., QUATTROCCHI, F. & VASELLI, O. (2009) Low-pH waters discharging from submarine vents at Panarea Island (Aeolian Islands, southern Italy) after the 2002 gas blast: Origin of hydrothermal fluids and implications for volcanic surveillance. *Apllied Geochemistry,* 24**,** 246-254.

TINTI, S., MANUCCI, A., PAGNONI, G., ARMIGLIATO, A. & ZANIBONI, R. (2005) The 30 December 2002 landslide-induced tsunamis in Stromboli: sequence of the events reconstructed from the eyewitness accounts. *Natural Hazards and Earth System Sciences,* 5**,** 763-775.

WEI, G. J., MCCULLOCH, M. T., MORTIMER, G., DENG, W. F. & XIE, L. H. (2009) Evidence for ocean acidification in the Great Barrier Reef of Australia. *Geochimica Et Cosmochimica Acta,* 73**,** 2332-2346.

WISTAU (2007) Scientific Diving Excursion on Panarea 2007 - Final reports of participants. *Department of Geology, Section for Hydrogeology - TU Bergakademie Freiberg***,** unpublished.

WISTAU (2008) Scientific Diving Excursion on Panarea 2008 - Final reports of participants. *Department of Geology, Section for Hydrogeology - TU Bergakademie Freiberg***,** unpublished.

YANG, K. & SCOTT, D. (2006) Magmatic Fluids as a Source of Metals in Seafloor Hydrothermal Systems. IN CHRISTIE, D. M., FISHER, C. R., LEE, S.-M. & GIVENS, S. (Eds.) *Back-Arc Spreading Systems: Geological, Biological, Chemical, and Physical Interactions.* American Geophysical Union.

ZEEBE, R. E. & WOLF-GLADROW, D. (2001) *CO2 In Seawater: Equilibrium, Kinetics, Isotopes,* Amsterdam, Elsevier.

Appendix

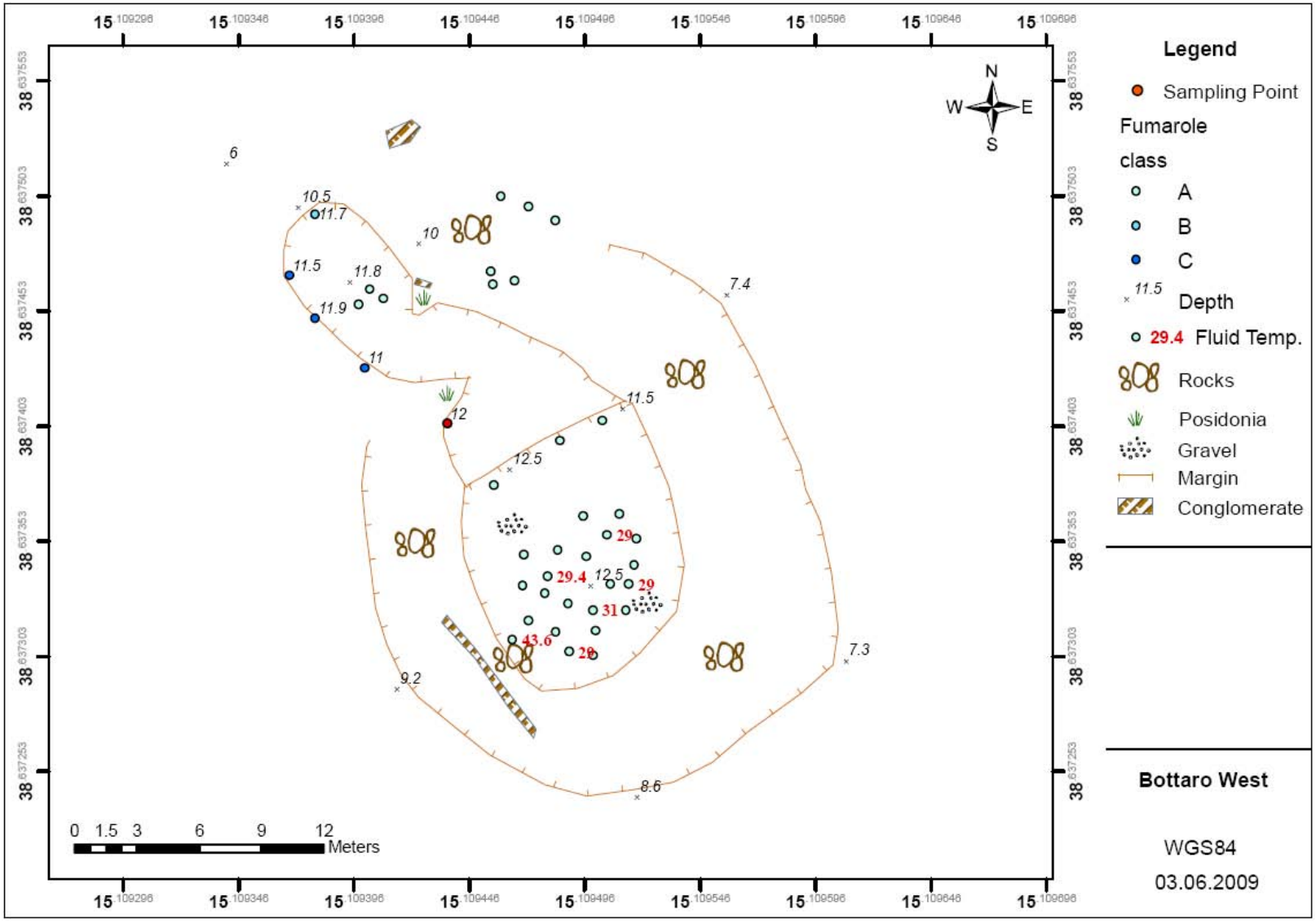

Appendix 1. **Map of Bottaro West, including the classification of the examined fumaroles with regard to their measured gas flow rate (map modified from Rohland (2007)). The respective fluid temperature is displayed, too. The temperature of ambient seawater was 27.3 °C.**

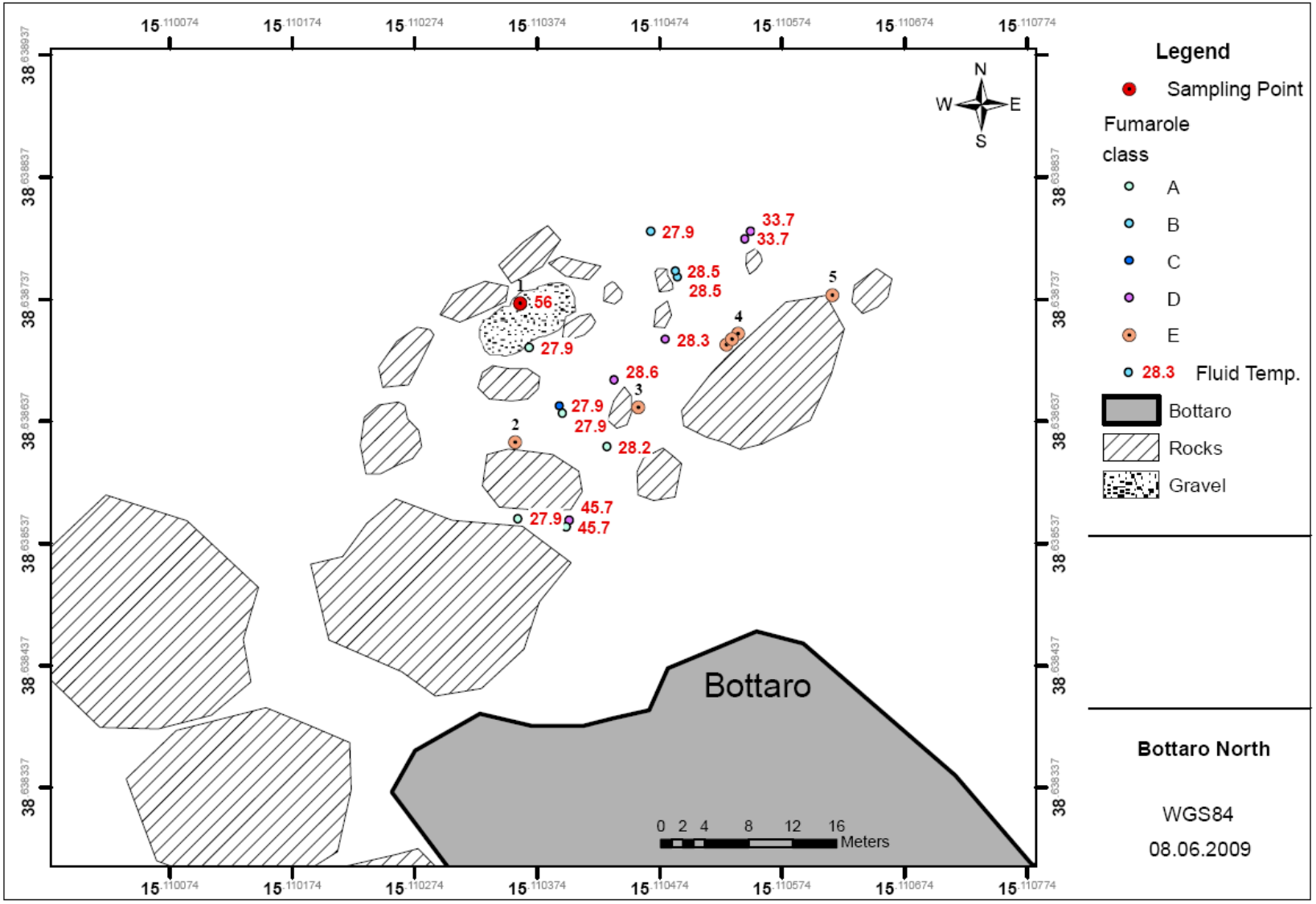

Appendix 2: **Map of Bottaro North, including the classification of the examined fumaroles with regard to their measured gas flow rate (map modified from Rohland (2007)). The respective fluid temperature is displayed, too. The temperature of ambient seawater was 27.9 °C.**

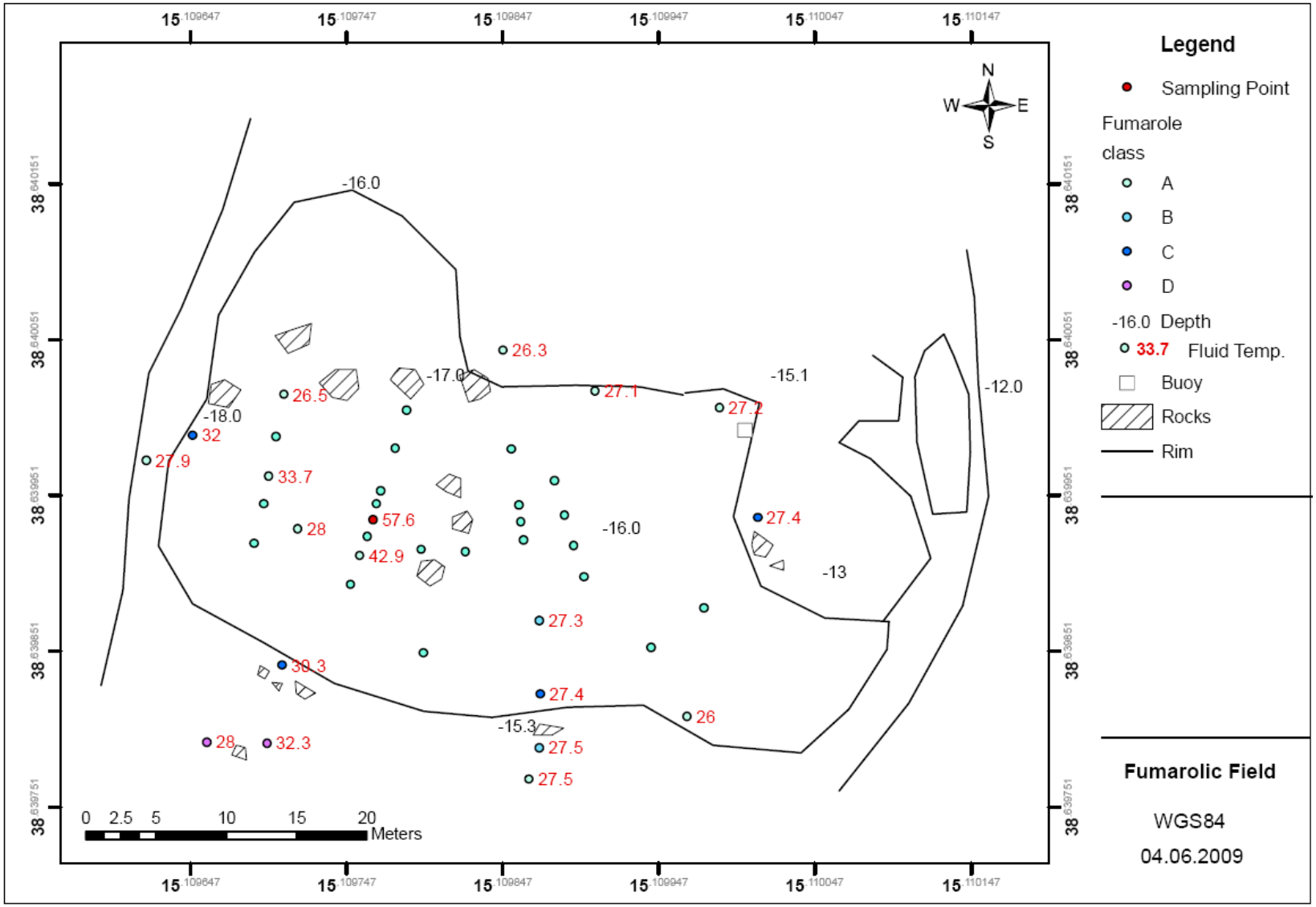

Appendix 3. **Map of Fumarolic Field, including the classification of the examined fumaroles with regard to their measured gas flow rate (map modified from Rohland (2007)). The respective fluid temperature is displayed, too. The temperature of ambient seawater was 27 °C.**

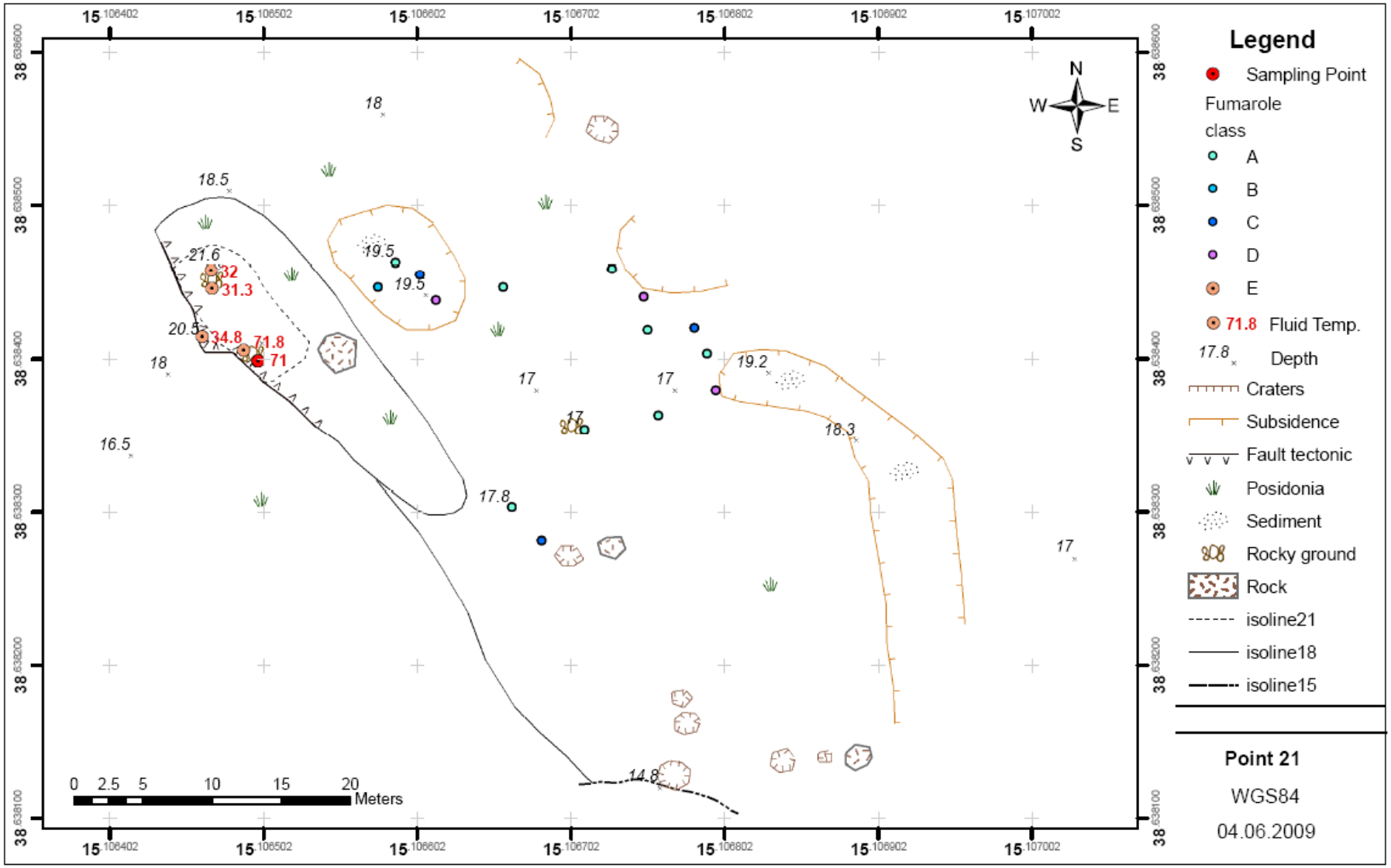

Appendix 4. **Map of Point 21, including the classification of the examined fumaroles with regard to their measured gas flow rate (map modified from Rohland (2007)). The respective fluid temperature is displayed, too. The temperature of ambient seawater was 24.6 °C.**

Appendix 5a. ICP-MS results for the gas samples trapped in NaOCl solution (1:10) from May and September 2008 (analysis by Actlab, Canada)

Site		Dilution	Filling gas bag [s]	Trapping in NaOCl	Analyte Unit	B µg/L	Na µg/L	Li µg/L	Be µg/L	Mg µg/L	Al µg/L	Si µg/L	K µg/L	Ca µg/L	Sc µg/L	Ti µg/L	V µg/L	Cr µg/L	Mn µg/L	Fe µg/L
					Detection Limit	3	5	1	0.1	1	2	200	30	700	1	0.1	0.1	0.5	0.1	10
Bottaro West	May 08		75	225		< 300	3500000	< 100	< 10	200	200	20000	7000	70000	< 100	< 10	< 10	< 50	< 10	1000
Point 21	May 08		35	240		< 300	3500000	< 100	< 10	< 100	400	20000	8000	70000	< 100	< 10	< 10	< 50	< 10	1000
Bottaro North	May 08		95	240		< 300	3500000	< 100	< 10	< 100	400	20000	7000	70000	< 100	< 10	< 10	< 50	< 10	1000
Black Point	May 08		38	240		< 300	3500000	< 100	< 10	< 100	< 200	20000	8000	70000	< 100	< 10	< 10	< 50	< 10	1000
Blank NaOCl (1:10)	May 08					< 300	3500000	< 100	< 10	< 100	< 200	20000	6000	70000	< 100	< 10	< 10	< 50	< 10	1000
Black Point	Sep 08	1:41	180	360		< 3	> 35000	< 1	< 0.1	18	< 2	< 200	150	< 700	< 1	< 0.1	< 0.1	< 0.5	0.3	< 10
Bottaro North	Sep 08	1:41	240	240		< 3	> 35000	< 1	< 0.1	2	< 2	< 200	140	< 700	< 1	< 0.1	< 0.1	< 0.5	< 0.1	< 10
Bottaro West	Sep 08	1:41	300	300		< 3	> 35000	< 1	< 0.1	2	< 2	< 200	170	< 700	< 1	< 0.1	< 0.1	< 0.5	< 0.1	< 10
Fumarolic Field	Sep 08	1:41	240	240		< 3	> 35000	< 1	< 0.1	< 1	< 2	< 200	160	< 700	< 1	< 0.1	< 0.1	< 0.5	< 0.1	< 10
Point 21	Sep 08	1:41	240	240		< 3	> 35000	< 1	< 0.1	< 1	< 2	< 200	160	< 700	< 1	< 0.1	< 0.1	< 0.5	< 0.1	< 10
Area 26	Sep 08	1:41	240	240		< 3	> 35000	< 1	< 0.1	2	< 2	< 200	180	< 700	< 1	< 0.1	< 0.1	< 0.5	0.1	< 10
Blank NaOCL (1:10)	Sep 08	1:41				< 3	> 35000	< 1	< 0.1	< 1	< 2	< 200	140	< 700	< 1	< 0.1	< 0.1	< 0.5	< 0.1	< 10

Appendix 5b. ICP-MS results (continuation)

Site		Dilution	Filling gas bag [s]	Trapping in NaOCl	Analyte Unit	Co µg/L	Ni µg/L	Cu µg/L	Zn µg/L	Ga µg/L	Ge µg/L	As µg/L	Se µg/L	Br µg/L	Rb µg/L	Sr µg/L	Y µg/L	Zr µg/L	Nb µg/L	Mo µg/L
					Detection Limit	0.005	0.3	0.2	0.5	0.01	0.01	0.03	0.2	3	0.005	0.04	0.003	0.01	0.005	0.1
Bottaro West	May 08		75	225		< 0.5	< 30	190	70	< 1	< 1	< 3	< 20	2300	2.1	46	< 0.3	2	< 0.5	< 10
Point 21	May 08		35	240		< 0.5	< 30	160	150	< 1	< 1	< 3	< 20	2600	1.7	44	< 0.3	2	< 0.5	10
Bottaro North	May 08		95	240		0.7	< 30	150	< 50	< 1	< 1	< 3	< 20	2200	1.2	38	< 0.3	2	< 0.5	< 10
Black Point	May 08		38	240		< 0.5	< 30	140	460	< 1	< 1	< 3	< 20	2800	< 0.5	35	< 0.3	3	< 0.5	< 10
Blank NaOCl (1:10)	May 08					< 0.5	< 30	130	< 50	< 1	< 1	< 3	< 20	300	1.1	37	< 0.3	2	< 0.5	10
Black Point	Sep 08	1:41	180	360		0.007	4.6	3.7	1.2	< 0.01	< 0.01	< 0.03	< 0.2	52	0.04	1.25	0.01	0.02	0.005	< 0.1
Bottaro North	Sep 08	1:41	240	240		0.005	0.8	3.4	< 0.5	< 0.01	< 0.01	< 0.03	< 0.2	51	0.03	0.73	0.01	0.01	0.005	< 0.1
Bottaro West	Sep 08	1:41	300	300		0.009	1.3	4.7	< 0.5	< 0.01	< 0.01	< 0.03	< 0.2	63	0.04	1.01	0.01	0.02	0.005	0.1
Fumarolic Field	Sep 08	1:41	240	240		< 0.005	1.9	3.9	0.8	< 0.01	< 0.01	< 0.03	< 0.2	58	0.04	0.87	0.01	0.02	0.005	< 0.1
Point 21	Sep 08	1:41	240	240		< 0.005	1.5	3.9	0.7	< 0.01	< 0.01	< 0.03	< 0.2	56	0.04	0.81	0.01	0.02	0.005	0.1
Area 26	Sep 08	1:41	240	240		0.007	1.3	3.9	1.1	< 0.01	< 0.01	< 0.03	< 0.2	54	0.06	0.79	0.01	0.02	0.005	< 0.1
Blank NaOCL (1:10)	Sep 08	1:41				< 0.005	0.5	3.5	1.6	< 0.01	< 0.01	< 0.03	< 0.2	64	0.03	0.84	0.01	< 0.01	0.005	< 0.1

Appendix 5c. ICP-MS results (continuation)

Site		Dilution	Filling gas bag [s]	Trapping in NaOCl	Analyte Unit	Ru µg/L	Pd µg/L	Ag µg/L	Cd µg/L	In µg/L	Sn µg/L	Sb µg/L	Te µg/L	I µg/L	Cs µg/L	Ba µg/L	La µg/L	Ce µg/L	Pr µg/L	Nd µg/L	Sm µg/L
					Detection Limit	0.01	0.01	0.2	0.01	0.001	0.1	0.01	0.1	1	0.001	0.1	0.001	0.001	0.001	0.001	0.001
Bottaro West	May 08		75	225		< 1	< 1	< 20	< 1	< 0.1	< 10	< 1	< 10	< 100	0.4	350	0.2	0.4	< 0.1	< 0.1	< 0.1
Point 21	May 08		35	240		< 1	< 1	< 20	< 1	< 0.1	< 10	< 1	< 10	< 100	0.2	120	0.3	0.4	< 0.1	< 0.1	< 0.1
Bottaro North	May 08		95	240		< 1	< 1	< 20	< 1	< 0.1	< 10	< 1	< 10	< 100	0.2	130	< 0.1	0.1	< 0.1	< 0.1	< 0.1
Black Point	May 08		38	240		< 1	< 1	< 20	< 1	< 0.1	< 10	< 1	< 10	< 100	0.4	190	0.2	0.4	< 0.1	< 0.1	< 0.1
Blank NaOCl (1:10)	May 08					< 1	< 1	< 20	< 1	< 0.1	< 10	< 1	< 10	< 100	0.2	20	< 0.1	< 0.1	< 0.1	< 0.1	< 0.1
Black Point	Sep 08	1:41	180	360		< 0.01	0.01	< 0.2	0.02	0.001	< 0.1	< 0.01	< 0.1	< 1	0.01	1.6	0.01	0.01	0.001	0.01	0.001
Bottaro North	Sep 08	1:41	240	240		< 0.01	0.02	< 0.2	< 0.01	0.001	< 0.1	< 0.01	< 0.1	< 1	0.01	0.5	0.01	0.01	0.001	0	0.001
Bottaro West	Sep 08	1:41	300	300		< 0.01	0.01	< 0.2	< 0.01	0.001	< 0.1	< 0.01	< 0.1	< 1	0.01	0.6	0.01	0.01	0.001	0	0
Fumarolic Field	Sep 08	1:41	240	240		< 0.01	0.02	< 0.2	< 0.01	0.001	< 0.1	< 0.01	< 0.1	< 1	0.01	0.5	0.01	0.01	0.001	0	0
Point 21	Sep 08	1:41	240	240		< 0.01	0.06	< 0.2	< 0.01	0.001	< 0.1	< 0.01	< 0.1	< 1	0.01	0.8	0.01	0.01	0.001	0	0
Area 26	Sep 08	1:41	240	240		< 0.01	0.07	< 0.2	< 0.01	0.001	< 0.1	< 0.01	< 0.1	< 1	0.01	18.8	0.01	0.01	0.001	0.01	0.001
Blank NaOCL (1:10)	Sep 08	1:41				< 0.01	< 0.01	0.2	< 0.01	0.001	< 0.1	< 0.01	< 0.1	< 1	0	139	0.01	0	0.001	0	0.001

Appendix 5d. ICP-MS results (continuation)

Site		Dilution	Filling gas bag [s]	Trapping in NaOCl	Analyte Unit	Eu µg/L	Gd µg/L	Tb µg/L	Dy µg/L	Ho µg/L	Er µg/L	Tm µg/L	Yb µg/L	Lu µg/L	Hf µg/L	Ta µg/L	W µg/L	Re µg/L	Os µg/L	Pt µg/L
					Detection Limit	0.001	0.001	0.001	0.001	0.001	0.001	0.001	0.001	0.001	0.001	0.001	0.02	0.001	0.002	0.3
Bottaro West	May 08		75	225		< 0.1	< 0.1	< 0.1	< 0.1	< 0.1	< 0.1	< 0.1	< 0.1	< 0.1	< 0.1	< 0.1	< 2	< 0.1	< 0.2	< 30
Point 21	May 08		35	240		< 0.1	< 0.1	< 0.1	< 0.1	< 0.1	< 0.1	< 0.1	< 0.1	< 0.1	< 0.1	< 0.1	< 2	< 0.1	< 0.2	< 30
Bottaro North	May 08		95	240		< 0.1	< 0.1	< 0.1	< 0.1	< 0.1	< 0.1	< 0.1	< 0.1	< 0.1	< 0.1	< 0.1	< 2	< 0.1	< 0.2	< 30
Black Point	May 08		38	240		< 0.1	< 0.1	< 0.1	< 0.1	< 0.1	< 0.1	< 0.1	< 0.1	< 0.1	< 0.1	< 0.1	< 2	< 0.1	< 0.2	< 30
Blank NaOCl (1:10)	May 08					< 0.1	< 0.1	< 0.1	< 0.1	< 0.1	< 0.1	< 0.1	< 0.1	< 0.1	< 0.1	< 0.1	< 2	< 0.1	< 0.2	< 30
Black Point	Sep 08	1:41	180	360		< 0.001	0.001	0.001	0.001	0.001	0.001	0.001	0.001	0.001	0	0.001	< 0.02	0.001	0.002	< 0.3
Bottaro North	Sep 08	1:41	240	240		< 0.001	0	0.001	0.001	0.001	0.001	0.001	0.001	0.001	0.001	0.001	< 0.02	0.001	0.002	< 0.3
Bottaro West	Sep 08	1:41	300	300		< 0.001	0.001	0.001	0.001	0.001	0.001	0.001	0.001	0.001	0.001	0.001	< 0.02	0.001	0.002	< 0.3
Fumarolic Field	Sep 08	1:41	240	240		< 0.001	0.001	0.001	0.001	0.001	0.001	0.001	0.001	0.001	0.001	0.001	< 0.02	0.001	0.002	< 0.3
Point 21	Sep 08	1:41	240	240		< 0.001	0	0.001	0	0.001	0.001	0.001	0	0.001	0.001	0.001	< 0.02	0.001	0.002	< 0.3
Area 26	Sep 08	1:41	240	240		< 0.001	0.001	0.001	0	0.001	0.001	0.001	0.001	0.001	0.001	0.001	< 0.02	0.001	0.002	< 0.3
Blank NaOCL (1:10)	Sep 08	1:41				0.005	0	0.001	0.001	0.001	0.001	0.001	0.001	0.001	0.001	0.001	< 0.02	0.001	0.002	< 0.3

Appendix 5e. ICP-MS results (continuation)

Site		Dilution	Filling gas bag [s]	Trapping in NaOCl	Analyte Unit Detection Limit	Au µg/L 0.002	Hg µg/L 0.2	Tl µg/L 0.001	Pb µg/L 0.01	Bi µg/L 0.3	Th µg/L 0.001	U µg/L 0.001
Bottaro West	May 08		75	225		< 0.2	< 20	< 0.1	3	< 30	< 0.1	< 0.1
Point 21	May 08		35	240		< 0.2	< 20	< 0.1	3	< 30	< 0.1	< 0.1
Bottaro North	May 08		95	240		< 0.2	< 20	< 0.1	2	< 30	< 0.1	< 0.1
Black Point	May 08		38	240		< 0.2	< 20	0.2	9	< 30	< 0.1	< 0.1
Blank NaOCl (1:10)	May 08					< 0.2	< 20	< 0.1	1	< 30	< 0.1	< 0.1
Black Point	Sep 08	1:41	180	360		0.003	< 0.2	0.001	0.09	< 0.3	0.001	0.01
Bottaro North	Sep 08	1:41	240	240		0.01	< 0.2	0.001	0.06	< 0.3	0.001	0.001
Bottaro West	Sep 08	1:41	300	300		0.003	< 0.2	0.001	0.05	< 0.3	0.001	0.01
Fumarolic Field	Sep 08	1:41	240	240		0.009	< 0.2	0.001	0.06	< 0.3	0.001	0.001
Point 21	Sep 08	1:41	240	240		0.027	< 0.2	0.001	0.08	< 0.3	0.001	0
Area 26	Sep 08	1:41	240	240		0.005	< 0.2	0.001	0.16	< 0.3	0.001	0
Blank NaOCL (1:10)	Sep 08	1:41				0.004	< 0.2	0.001	0.1	< 0.3	0.001	0

Appendix 6. Statistical analysis for significant difference of the ICP-MS results of September 2008 gas samples against the blank of NaOCl solution (1:10), values "< dection limit" were replaced by 0.5 times detection limit, bold values represent significance.

Site		Mg	K	Mn	Co	Ni	Cu	Rb	Sr	Zr	Mo	Pd	Cd	Cs	La	Ce	Nd	Sm	Dy	Yb	Hf	Au	Pb	U
Black Point		**18**	**150**	**0.3**	**0.01**	**4.6**	3.7	**0.04**	1.25	0.02	0.05	0.01	**0.02**	0	0.01	0.01	**0.01**	0	0	0	**0**	0	0.09	0.01
Bottaro North		2	**140**	0.05	**0.01**	**0.8**	3.4	**0.03**	0.73	0.01	0.05	0.02	0.01	0	0.01	0.01	**0**	0	0	0	0	0.01	0.06	0
Bottaro West		2	**170**	0.05	**0.01**	**1.3**	4.7	**0.04**	1.01	0.02	0.1	0.01	0.01	0	0.01	0.01	**0**	0	0	0	0	0	0.05	0.01
Fumarolic Field		0.5	**160**	0.05	**0**	**1.9**	3.9	**0.04**	0.87	0.02	0.05	0.02	0.01	0	0.01	0.01	**0**	0	0	0	0	0.01	0.06	0
Point 21		0.5	**160**	0.05	**0**	**1.5**	3.9	**0.04**	0.81	0.02	0.1	0.06	0.01	0	0.01	0.01	**0**	0	0	**0**	0	**0.03**	0.08	0
Area 26		2	**180**	0.1	**0.01**	**1.3**	3.9	**0.06**	0.79	0.02	0.05	0.07	0.01	0	0.01	0.01	**0.01**	0	0	0	0	0.01	**0.16**	0
Blank NaOCl (1:10)		0.5	140	0.05	0	0.5	3.5	0.03	0.84	0.01	0.05	0.01	0.01	0	0.01	0	0	0	0	0	0	0	0.1	0
statistical processing ($\alpha = 0.5$)																								
KOLMOGOROV-SMIRNOV	p-value	< 0.01	≥ 0.10	< 0.05	≥ 0.10	< 0.05	< 0.05	< 0.05	≥ 0.10	< 0.01	< 0.01	< 0.05	< 0.01	< 0.01	< 0.01	< 0.05	≥ 0.10	≥ 0.10	< 0.01	< 0.01	< 0.01	< 0.10	≥ 0.10	≥ 0.10
KRUSKALL-WALLIS	p-value	0.28		0.53		0.13	0.30	0.13		0.06	0.53	0.13	0.68	0.09	0.09	0.10			0.53	0.68	0.68	0.61		
STUDENT-t test	p-value		**0.02**		**0.04**				0.41								**0.03**	0.09					0.36	0.81
GRUBBS test	p-value	**0.00**	0.76	**0.00**	0.98	**0.01**	0.10	**0.01**	0.15	1	1	0.68	**0**	1	1	0.42	0.63	1	1	**0**	**0**	**0.03**	**0.04**	1
outlier:		**"18"**		**"0.3"**		**"4.6"**		**"0.061"**														**"0.027**	**"0.16"**	
without outlier:																								
KOLMOGOROV-SMIRNOV	p-value	< 0.05		< 0.01		≥ 0.10		≥ 0.10												-	-	≥ 0.10	≥ 0.10	
KRUSKALL-WALLIS	p-value	0.32		0.65																-	-			
STUDENT-t test	p-value					**0.01**		**0.01**												-	-	0.25	**0.01**	

Appendix 7. GC analysis of the gases sampled from May and September 2008

May 2008		Area		Volume	Concentration [vol.%]		
		methane	ethane/ethene	[µl]	methane	ethane/ethene	methane (corrected)
Std. Mix C1-C6, 14l Flasche, 1000 ppm	*standard*	5190146	9073608	50	0.020%	0.020%	
Std. Mix C1-C6, 14l Flasche, 1000 ppm	*standard*	10127294	17441376	100	0.040%	0.040%	
Std. Mix C1-C6, 14l Flasche, 1000 ppm	*standard*	15276450	26563048	150	0.060%	0.060%	
Std. Mix C1-C6, 14l Flasche, 1000 ppm	*standard*	20391308	35494024	200	0.080%	0.080%	
Std. Mix C1-C6, 14l Flasche, 1000 ppm	*standard*	25773798	44666032	250	0.100%	0.100%	
blank 250 µl	*blank*	147788	0	250	0.0006%	0.000%	0.000%
PAN_150508BP_G1	Black Point	17091012	173186	250	0.067%	0.00039%	0.066%
PAN_130508_B(W)_G1	Bottaro West	159942	0	250	0.001%	0.00000%	0.000%
PAN_150508_B(N)_G1	Bottaro North	142642	0	250	0.001%	0.00000%	0.000%
PAN_140508_P21_G1	Point 21	5376500	37995	250	0.021%	0.000085%	0.020%
Sep 08		**Area**		**Volume**	**Concentration [vol.%]**		
		methane	**ethane/ethene**	**[µl]**	**methane**	**ethane/ethene**	**methane (corrected)**
Std. Mix C1-C6, 14l Flasche, 1000 ppm	*standard*	1589936	2769662	50	0.020%	0.020%	
Std. Mix C1-C6, 14l Flasche, 1000 ppm	*standard*	1606052	2822819	50	0.020%	0.020%	
Std. Mix C1-C6, 14l Flasche, 1000 ppm	*standard*	3125458	5459445	100	0.040%	0.040%	
Std. Mix C1-C6, 14l Flasche, 1000 ppm	*standard*	4800654	8494337	150	0.060%	0.060%	
Std. Mix C1-C6, 14l Flasche, 1000 ppm	*standard*	6317298	11222992	200	0.080%	0.080%	
Std. Mix C1-C6, 14l Flasche, 1000 ppm	*standard*	7642058	13542552	250	0.100%	0.100%	
blank 250 µl	*blank*	41238	0	250	0.0005%	0.00000%	
PAN_310808_B(N)_G1	Bottaro North	175699	0	250	0.0022%	0.00000%	0.0022%
* PAN_040908_B(W)_G1	Bottaro West	315300	0	250	0.0039%	0.00000%	0.0039%
PAN_080908_Area26_G1	Area 26	6240142	53322	250	0.0770%	0.00037%	0.0770%
blank 250 µl	*blank*	45771	0	250	0.0006%	0.00000%	
PAN_290808_P21_G1	Point 21	1116213	0	250	0.0138%	0.00000%	0.0138%
PAN_040908_HL(F)_G1	Fumarolic Field	100353	0	250	0.0012%	0.00000%	0.0012%
blank 250 µl	*blank*	32944	0	250	0.0004%	0.00000%	
PAN_040908_HL(F)_G1	Fumarolic Field	100483	0	250	0.0012%	0.00000%	0.0012%
PAN_280808_BP_G1	Black Point	10752447	93033	250	0.1328%	0.00065%	0.1328%
PAN_280808_BP_G1	Black Point	4142664	32357	100	0.1279%	0.00057%	0.1279%
Std. Mix C1-C6, 14l Flasche, 1000 ppm	*standard*	8001785	13858208	250	0.100%	0.100%	
Std. Mix C1-C6, 14l Flasche, 1000 ppm	*standard*	8584873	15191009	250	0.100%	0.100%	
Std. Mix C1-C6, 14l Flasche, 1000 ppm	*standard*	11562362	20575666	350	0.140%	0.140%	
Std. Mix C1-C6, 14l Flasche, 1000 ppm	*standard*	15479699	26969568	500	0.200%	0.200%	
mean blank	*blank*	39984.333	0		0.0005%	0.00000%	0.0005%

Appendix 8. Composition of the sampled gases from May and September 2008. Additionally, external data were used

Sample-ID	Date	Site	CO2 [mol.%]	H2S [vol.%]	CO [mol.%]	CH4 [vol.%]	C2H6/C2H4 [vol.%]	N2 [mol.%]	O2 [mol.%]	H2 [mol.%]	He [mol.%]
PAN-150508-BP-G1	May 08	Black Point	99.7	0.2	0.0001	0.0660	3.9E-04				
PAN-280808-BP-G1	Sep 08	Black Point	99.5	0.4	0.0001	0.1323	6.5E-04				
PAN-150508-B(N)-G1	May 08	Bottaro North	96.0	4.0	0.0036	0.0001	2.5E-05				
PAN-310808-B(N)-G1	Sep 08	Bottaro North	96.3	3.7	0.0080	0.0017	0.0E+00				
PAN-130508-B(W)-G1	May 08	Bottaro West	98.1	1.9	0.0050	0.0001	2.5E-05				
PAN-040908-B(W)-G1	Sep 08	Bottaro West	99.2	0.8	0.0025	0.0034	0.0E+00				
PAN-040908-HL(F)-G1	Sep 08	Fumarolic Field	96.5	3.5	0.0070	0.0007	0.0E+00				
PAN-140508-P21-G1	May 08	Point 21	96.4	3.6	0.0060	0.0200	8.5E-05				
PAN-290808-P21-G1	Sep 08	Point 21	97.2	2.8	0.0060	0.0133	0.0E+00				
PAN-080908-Area 26-G1	Sep 08	Area 26	98.7	1.2	0.0015	0.0766	3.7E-04				
external data*											
	Jul 08	Black Point	97.9	0.6	0.0002	0.0898		0.44	0.045	0.0107	0.001
	Jul 08	Point 21	96.5	1.8	0.0007	0.0195		0.24	bdl	0.001	0.0006
	Jul 08	Bottaro West		1.5							
	Jul 08	Bottaro North	95.4	2.6	0.0001	0.0002		0.25	bdl	bdl	0.0008

** data from Dr. Francesco Italiano (INGV, Palermo), bdl – below detection limit*

Appendix 9. On-site parameters of the sampled waters from May and September 2008

sample ID	location	pH	Eh [mV]	rH	LF [mS/cm]	O2 [mmol/L]	O2 [%]	T [°C]
PAN-130508-BW-W1	Bottaro West	5.54			54.6	0.135	30	k.A.
PAN-040908-BW-W1	Bottaro West	5.25	33.0	18.6	55.2	0.130	55	29.4
PAN-150508-BN-W1	Bottaro North	5.71	-35.3	17.2	55.5	0.047	17.4	21.7
PAN-310808-B(N)-W1	Bottaro North	5.91	18.5	19.4	55.3	0.148	63.3	30.1
PAN-160508-HL-W1	Hot Lake	5.37	-12.7	17.3	75.6	0.010	3.5	19.9
PAN-310808-HL-W1 (1m)	Hot Lake	4.75	-49.1	14.8	92	0.025	10.6	28.7
PAN-310808-HL-W2 (2m)	Hot Lake	4.79	-42.6	15.1	100	0.038	15.1	26.7
PAN-070908-HL(80 cm)-W3	Hot Lake	4.95	217.3	24.2	93.4	0.026	10.9	29
PAN-080908-HL(80 cm)-W4	Hot Lake	4.85	-53.7	14.9	97.2	0.029	12.2	29.2
PAN-140508-P21-W1	Point 21	5.11	4.0	17.4	52.5	0.065	23	19.7
PAN-150508-P21-W1	Point 21	5.51	3.5	18.2	52.9	0.057	20.6	22.3
PAN-290808-P21-W1	Point 21	5.02	-18.2	16.4	53.4	0.052	21.6	28.5
PAN-070908-Area 26-W1	Area 26	5.17	-47.3	15.7	54.8	0.016	6.7	30.4
PAN-080908-Area 26-W2a (BM)	Area 26	5.06	-32.2	16.0	55.5	0.042	18.8	32.8
PAN-080908-Area 26-W2b (MS)	Area 26	5.12	-26.0	16.3	55.5	0.044	19.7	32.2
PAN-150508-BP-W1	Black Point	3.02	355.7	25.1	66	0.238	85.1	20.7
PAN-280808-BP-W1	Black Point	2.94	293.9	22.8	73.7	0.151	61.6	27.4
PAN-030908-BP-W2	Black Point	3.41	261.4	22.6	65.5	0.189	75.4	26.1
PAN-060908-BP(N)-W3	Black Point North	5.74	n.d.	n.d.	54	0.180	75.6	28
PAN-030908-BP-EX	Black Point	n.d.	n.d.	n.d.	n.d.	n.d.	n.d.	n.d.
PAN-070908-BP(N)-EX1	Black Point North	5.28	n.d.	n.d.	51.3	0.070	32.4	34
PAN-060908-BW(LB)-Ref	Lisca Nera	7.89	286.2	32.4	55.4	0.239	101.8	29.5
Panarea Hafen_120508	Hafen	8.10	n.d.	n.d.	49.4	n.d.	n.d.	n.d.

n.d. – not determined

Appendix 10. Chemical parameters of the sampled waters from May and September 2008

sample ID	location	S^{2-} [mmol/L]	F- [mmol/L]	Cl- [mmol/L]	SO42- [mmol/L]	Br- [mmol/L]	TIC [mmol/L]	HCO3- [mmol/l]	CO2 [mmol/l]
PAN-130508-BW-W1	Bottaro West	n.d.	n.d.	644.8	29.84	1.15	n.d.	n.d.	n.d.
PAN-040908-BW-W1	Bottaro West	0.052	0.076	590.8	30.72	0.95	15.79	1.65	14.14
PAN-150508-BN-W1	Bottaro North	1.101	0.069	666.6	28.11	1.06	19.78	4.96	14.81
PAN-310808-B(N)-W1	Bottaro North	0.112	0.088	554.6	30.65	0.93	7.81	2.61	5.19
PAN-160508-HL-W1	Hot Lake	0.112	n.d.	976.3	20.18	1.79	8.38	1.16	7.22
PAN-310808-HL-W1 (1m)	Hot Lake	0.262	0.049	1283.0	9.20	1.85	19.12	0.63	18.49
PAN-310808-HL-W2 (2m)	Hot Lake	1.011	0.068	1346.4	7.13	2.01	18.08	0.65	17.43
PAN-070908-HL(80 cm)-W3	Hot Lake	0.412	0.053	1229.3	9.12	1.79	17.81	0.98	16.83
PAN-080908-HL(80 cm)-W4	Hot Lake	0.472	0.056	1250.0	9.12	1.96	17.61	0.75	16.86
PAN-140508-P21-W1	Point 21	0.681	0.111	635.0	27.18	0.93	13.31	1.06	12.24
PAN-150508-P21-W1	Point 21	0.442	0.114	636.6	27.35	1.17	15.89	2.86	13.03
PAN-290808-P21-W1	Point 21	0.082	0.130	417.6	23.66	0.86	25.63	1.66	23.96
PAN-070908-Area 26-W1	Area 26	0.621	n.d.	n.d.	n.d.	n.d.	n.d.	n.d.	n.d.
PAN-080908-Area 26-W2a (BM)	Area 26	0.262	0.106	547.5	23.98	0.99	25.55	2.09	23.46
PAN-080908-Area 26-W2b (MS)	Area 26	0.262	n.d.	561.3	25.75	0.87	22.09	1.58	20.51
PAN-150508-BP-W1	Black Point	0.022	0.084	855.3	12.17	1.65	2.50	0.00	2.50
PAN-280808-BP-W1	Black Point	0.082	0.239	828.3	11.23	1.36	4.55	0.00	4.55
PAN-030908-BP-W2	Black Point	0.022	0.099	793.7	11.16	1.08	3.39	0.00	3.39
PAN-060908-BP(N)-W3	Black Point North	-0.007	0.085	550.3	31.05	0.82	8.41	2.21	6.20
PAN-030908-BP-EX	Black Point	n.d.	0.082	560.9	30.51	0.97	6.96	n.d.	n.d.
PAN-070908-BP(N)-EX1	Black Point North	n.d.	0.104	551.4	26.82	0.95	13.27	n.d.	n.d.
PAN-060908-BW(LB)-Ref	Lisca Nera	n.d.	n.d.	520.8	26.41	0.98	12.89	1.49	11.39
Panarea Hafen_120508	Hafen	<EDL	0.083	500.6	29.05	0.90	2.71	2.67	0.04

n.d. - not determined, <EDL - below estimated detection limit

Appendix 11. Calibration of pH meter HQ20 (May) and HQ40d (September) from HACH, as well as WinLab Data Line (September) from WINDAUS

pH	HQ 20	HQ 40d	WinLab Data Line
		potential [mV]	
2.0	290.6	296.4	288.0
3.0	233.6	242.5	230.7
4.0	175.3	184.7	173.3
5.0	107.8	120.0	116.0
6.0	58.0	60.2	58.6
7.0	-1.2	5.1	1.3
8.0	-48.4	-46.3	-56.1
9.0	-108.2	-105.5	-113.4
10.0	-152.7	-152.6	-170.8

Appendix 12. Calibration for fluoride determination (by ISE) in seawater with a 1 g/L fluoride solution

Addition step	Total addition	Concentration	log concentration	Seawater [mV]	
[10^{-6} L]	[L]	[mg/L]		May	September
pure + 10 mL TISAB					
10	1.0E-05	0.400	-0.398	84.4	36
15	2.5E-05	0.999	0.000	63	11.6
25	5.0E-05	1.996	0.300	45.7	-10.1
50	1.0E-04	3.984	0.600	27.9	-25.2
150	2.5E-04	9.901	0.996	4.4	-50.1
250	5.0E-04	19.608	1.292	-13.5	-67.5
500	1.0E-03	38.462	1.585	-30.7	-84.8
1500	2.5E-03	90.909	1.959	-54.1	-108.3
2500	5.0E-03	166.667	2.222	-71.4	-125.3
5000	1.0E-02	285.714	2.456	-87.7	-141

Appendix 13a. Measurements of the flow rate of fumaroles at Point 21 and Fumarolic Field. Based on the time for water displacement and fluid temperature the flow rate was determined

nr.	depth [m]	T [°C]	time [s]	flow rate [L/min]	flow rate (corrected for T) [L/min]	class
Point 21 (29.08.08)						
1	17.8		20	3.60	3.60	B
2	18.0		8	9.00	9.00	D
3	17.5		15	4.80	4.80	C
4	17.8		7	10.29	10.29	D
5	17.6		57	1.26	1.26	A
6	18.8		64	1.13	1.13	A
7	18.4		8	9.00	9.00	D
8	18.0		53	1.36	1.36	A
9	18.7		17	4.24	4.24	C
10	17.8		37	1.95	1.95	A
11	18.5		8	9.00	9.00	D
12	16.7		123	0.59	0.59	A
13	16.3		73	0.99	0.99	A
14	16.0		63	1.14	1.14	A
15	15.5		12	6.00	6.00	C
sea water:		24.6				
Fumarolic Field (30.08.08)						
1	15.0	27.4	10	7.20	6.57	C
3	14.9	26.0	232	0.31	0.30	A
4	15.8	27.3	30	2.40	2.20	B
5	15.7	27.4	20	3.60	3.28	B
6	14.9	27.5	33	2.18	1.98	A
7	14.3	27.5	181	0.40	0.36	A
8	14.5	30.3	18	4.00	3.30	B
9	13.2	32.3	5	14.40	11.15	D
10	13.9	28.0	7	10.29	9.18	D
44	15.4	27.2	50	1.44	1.32	A
48	16.5	27.1	100	0.72	0.66	A
41	17.2	26.3	225	0.32	0.30	A
60	16.3	57.6	11	6.55	2.84	B
15	15.7	42.9	42	1.71	1.00	A
42	15.9	28.0	80	0.90	0.80	A
59	16.6	33.7	55	1.31	0.97	A
56	17.2	26.5	90	0.80	0.75	A
62	16.2	32.0	15	4.80	3.75	C
31	15.0	27.9	36	2.00	1.79	A
sea water:		27.0				

Appendix 13b. Flow rate measurements at Bottaro North (continuation)

Botaro North (31.08.08)						
nr.	depth [m]	T [°C]	time [s]	flow rate [L/min]	flow rate (corrected for T) [L/min]	class
60a	8.2	33.7	7	10.29	7.63	D
60b	8.2	33.7	6	12.00	8.90	D
62	8.7	27.9	24	3.00	2.69	B
42a	8.1	28.5	18	4.00	3.51	B
42b	8.1	28.5	22	3.27	2.87	B
31	8.0	28.3	7	10.29	9.09	D
56	7.9	28.6	4	18.00	15.73	D
15	7.6	28.2	178	0.40	0.36	A
44a	8.1	45.7	4	18.00	9.85	D
44b	8.1	45.7	20	3.60	1.97	A
41	7.6	27.9	45	1.60	1.43	A
59a	6.9	27.9	17	4.24	3.80	C
59b	6.9	27.9	60	1.20	1.08	A
48	8.6	27.9	75	0.96	0.86	A
sea water:		27.9				

Appendix 14. Gas flow rates measurements and determination of the total gas output of the diffusive fumarolic field within the crater of Bottaro West

Bottaro West (field of diffusive exhalations) (06.09.08)						
nr.	depth [m]	T [°C]	time [s]	flow rate [L/min]	flow rate (corected for T and P) [L/min]	class
1	12.2	43.6	27	2.87	3.65	A
2	12.1	29.0	88	0.82	1.55	A
3	12.2	31.0	103	0.70	1.24	A
4	12.3	29.0	213	0.34	0.64	A
5	12.3	29.4	33	2.20	4.17	A
6	12.3	29.0	96	0.74	1.43	A
sea water		27.3				
mean:					2.11 ± 1.43	
area(entire field)/area(funnel):					812.1	
total gas flow rate [L/min]:					**1717**	

Appendix 15. The average gas flow rate for each class as well as the classified fumaroles observed at the five sites

	A	B	C	D
measured flow rates (corrected for T)				
mean [L/min]	1.06	3.04	4.86	9.89
std [L/min]	0.53	0.47	1.18	2.13
observed fumaroles				
Bottaro West	2	9	39	591
Bottaro North	6	14	11	144
Fumarolic Field	4	37	90	549
Point 21	10	24	61	297
Black Point	2	8	36	546

Appendix 16. Estimated gas flow rates of the large fumaroles at Point 21 and Bottaro North

Large fumaroles		gas flow rate [L/min]	T [°C]	depth [m]	flow rate (corrected for T and P) [L/min]
Point 21					
#1	"Melanie"	345.6*	71	20	345.6
#2	"Patricia"	200	71.8	20	208.9
#3	"Wanda"	200	34.8	18	402.3
#4	"Claudia"	868.8*	31.3	20	868.8
#5	"Mandy"	350	32	20	820.3
Bottaro North					
#1		200	56	8	160.7
#2		250		8	450
#3		250		8	450
#4		250		8	450
#5		350		8	630

** data from Kleutges (2009)*

Appendix 17. Calculation of the respective gas outputs (corrected for the average hydrostatic pressure of each site)

site	average water depth [m]	gas flow rate [L/min]						total gas output (Σ (A to E))	
		A	B	C	D	Σ (A to D)	E	[L/min]	L/day]
Bottaro West	12.3	1395.9	264.1	97.5	44.1	3518		3518	5.07E+06
Bottaro West (diffuse field)		1716.8							
Bottaro North	7.9	273.4	59.9	121.9	106.4	562	2141	2702	3.89E+06
Fumarolic Field	15.5	1481.8	696.4	458.1	100.8	2737		2737	3.94E+06
Point 21	17.6	866.9	510.5	321.3	272.6	1971	2646	4617	6.65E+06
Black Point	23.3	1925.7	364.0	129.4	65.9	2485		2485	3.58E+06

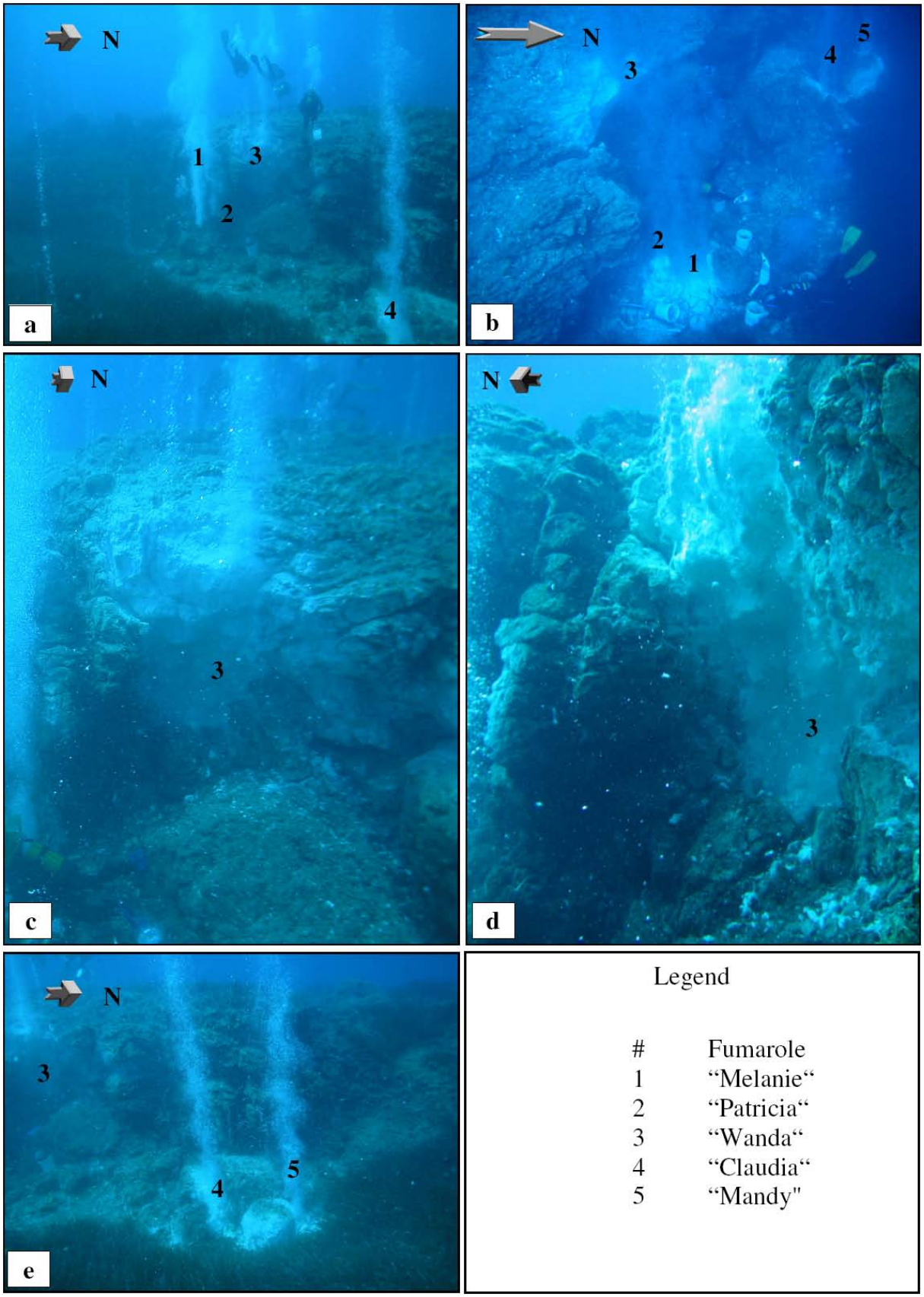

Appendix 18a - e. **Photos of the five large fumaroles (1 - 5) located at Point 21 site for comparison of the gas flow rates (modified from WISTAU (2008)).**

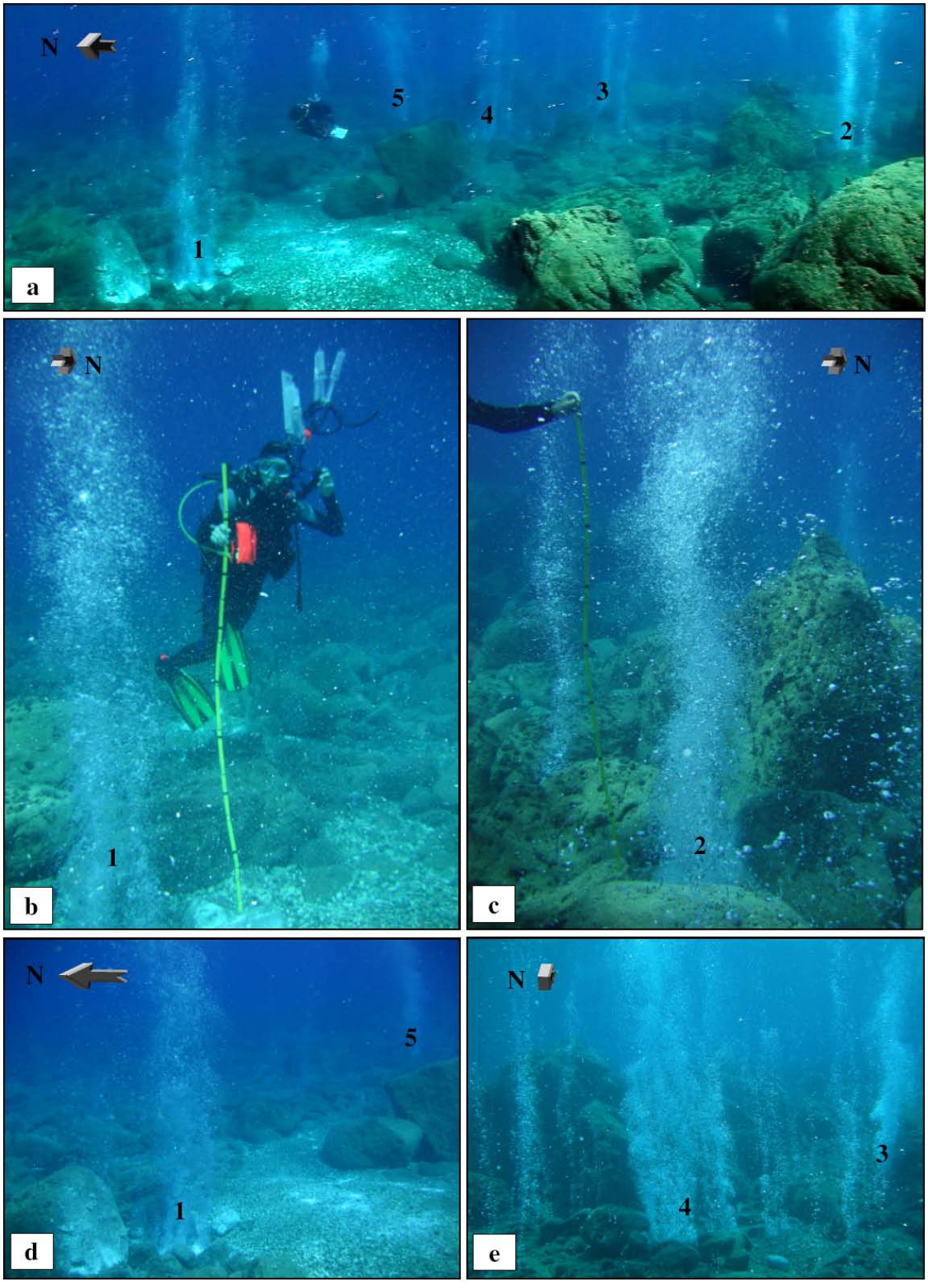
N
5
4
3
2
1
a
N
1
b
N
2
c
N
5
1
d
N
3
4
e

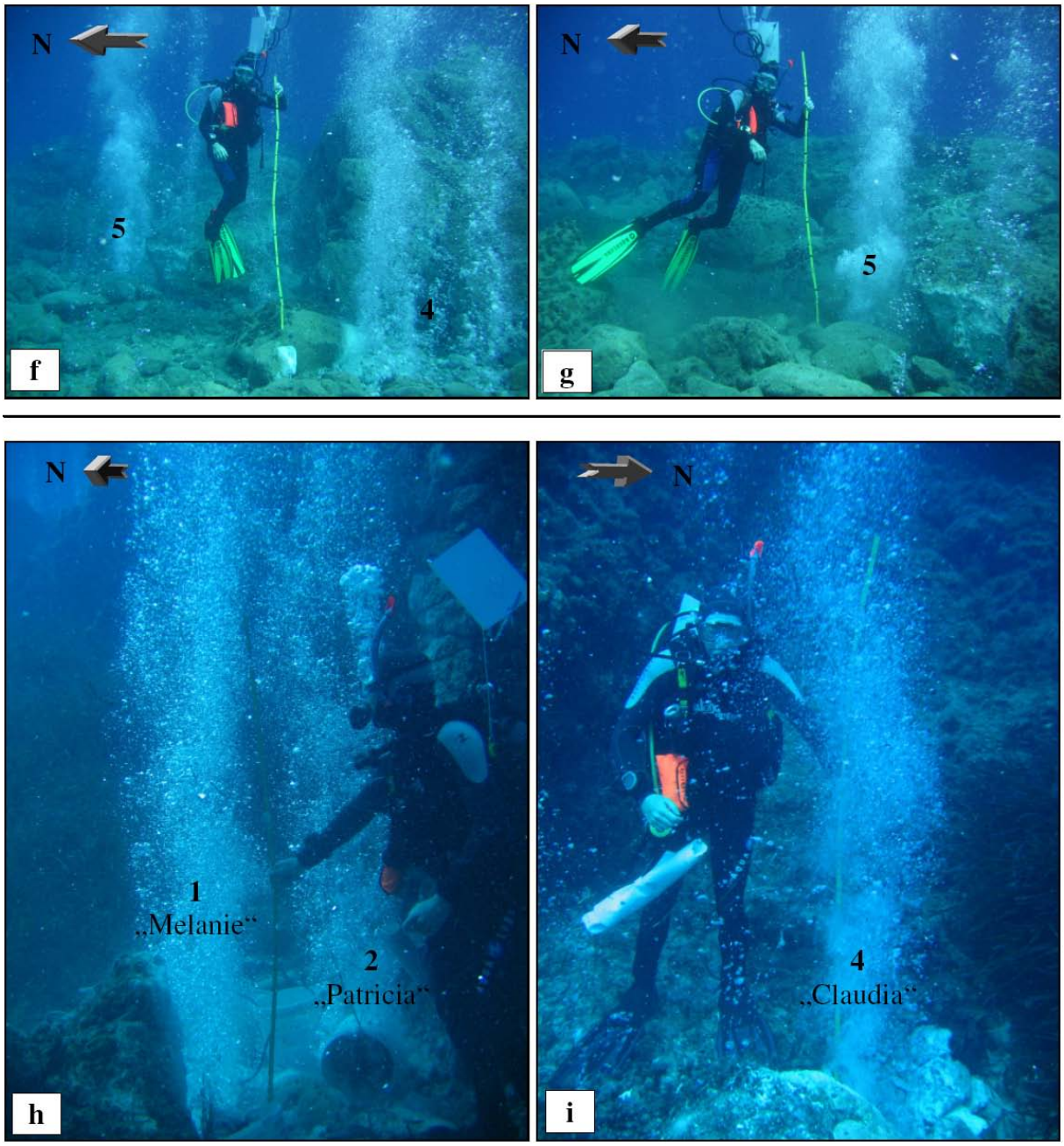

Appendix 19a - i. **Photos of the five large fumaroles (1 - 5) located at Bottaro North site (photo a – g) for comparison of the gas flow rates with respect to the measured fumaroles “Melanie” and “Claudia” (photo h and i) at Point 21 (modified from WISTAU (2008)).**